SAPIENZA
UNIVERSITÀ DI ROMA

Facoltà di Scienze Matematiche Fisiche e Naturali

DOTTORATO DI RICERCA
IN GENETICA E BIOLOGIA MOLECOLARE

XXXVII Ciclo
(A.A. 2024/2025)

The role of RNA-RNA interactions in the post-transcriptional control of cancer-related genes: the case of circHIPK3/*BRCA1* mRNA pairing

Dottoranda
Chiara Grelloni

Docente guida
Prof. Irene Bozzoni

Coordinatrice
Prof.ssa Isabella Saggio

INDEX

SUMMARY AND AIM

Circular RNAs are covalently-closed RNA molecules involved in gene-expression regulation at different levels.
These peculiar molecules have recently attracted the attention of the scientific community especially due to their deregulation in different pathological conditions and
recent technologies advances have allowed to better define their role in the cell.

The work I carried out during my PhD aimed at elucidating the molecular mechanism through which the circular RNA circHIPK3, which results deregulated in different tumoral contexts, can influence cancer progression. While many studies describe circHIPK3 as a sponge of miRNAs, we looked for possible direct interactions with ubiquitously expressed mRNAs which could represent functional mechanisms conserved in different cancer types, regardless to specific miRNA signatures.

We showed that circHIPK3 regulates the levels of BRCA1 protein, an essential DNA-repair factor, through a direct interaction between the circRNA back-splicing-junction (BSJ) and the last coding exon of *BRCA1* mRNA. This interaction prevents the binding on the *BRCA1* transcript of FMRP protein, which we identified as a BRCA1 translational repressor. We discovered this competitive model at first in embryonal rhabdomyosarcoma cell line (RD), we validated it in other tumoral contexts and we modulated it in different conditions to study phenotypic effects and possible therapeutic applications. We demonstrated that the disruption of circHIPK3/*BRCA1* interaction causes BRCA1 protein down-regulation and consequent DNA-damage accumulation, strengthening the effects of DNA damage-inducing drugs and sensitizing BRCA1 wild-type tumour cells to PARP inhibitors

by synthetic lethality. On the other hand, the inhibition of FMRP/*BRCA1* interaction with locked-nucleic acids restores physiological BRCA1 levels and prevents DNA-damage accumulation in BRCA1 hemizygous breast cancer cells.

INTRODUCTION

Circular RNAs

CircRNAs characteristics

According to the ENCODE (ENCyclopedia Of DNA Elements) Project Consortium[1], despite only 1,5% of human DNA encodes proteins, more than 80% of our genome results actively transcribed and functional in the cell.

What for many years was considered as 'junk' transcriptional products, turned out to be essential functional regulatory molecules[2], classified as non-coding RNAs. Non-coding RNAs include ribosomal RNAs (rRNAs), structural and functional components of ribosomal subunits, transfer RNAs (tRNAs), essential for protein synthesis, small nuclear RNAs (snRNAs), with an important role in splicing, snoRNAs (small nucleolar RNAs), involved in rRNA processing and RNA modification, microRNAs (miRNAs), which generally regulate gene expression by targeting mRNAs and long-non-coding RNAs (lncRNAs), transcripts longer than 200 nt which can regulate gene expression at different levels. Long-non-coding RNAs include a peculiar class of transcripts called circular RNAs.

Circular RNAs (CircRNAs) are single-strand covalently closed transcripts without free 5' and 3' ends which originates through a non-canonical splicing event called back-splicing in which a 5' splice site is joined to an upstream 3' splice site in the pre-mRNA. The formation of this phosphodiester bond induces the circularization of one or more exons and sometimes even of introns and the formation of a peculiar sequence not present in the linear transcript, called back-splicing junction, which allows to specifically distinguish a

circRNA from the linear transcript produced by the canonical splicing from the same locus. (Figure 1).

Fig. 1

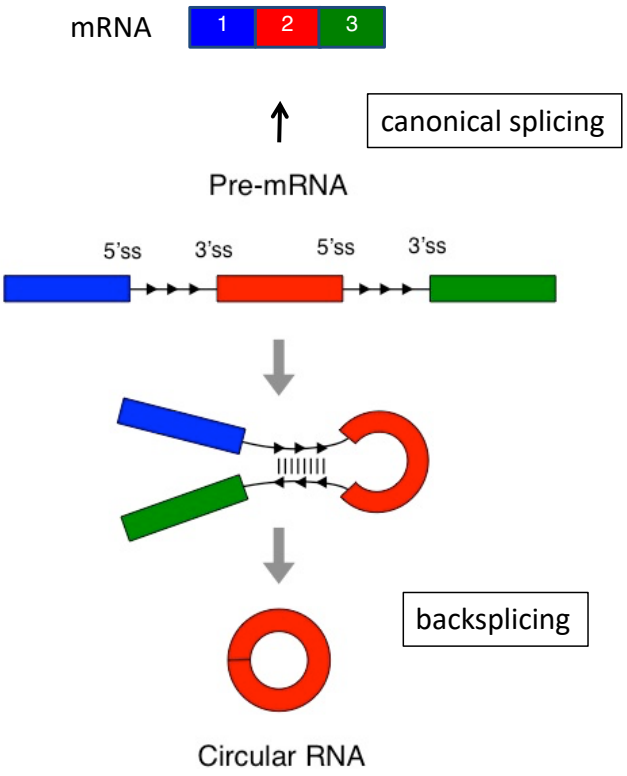

Fig. 1
Schematic representation of canonical splicing and back-splicing (Adapted from Liang *et al.,* 2014[3])

CircRNAs discovery

The first observation of circular RNA molecules dates back to the 1970s. In 1976, Sanger *et al*. described viroids containing "single-stranded and covalently closed circular RNA molecules". In 1979, thanks to electron microscopy, circular transcripts, with an unknown role, were observed in eukaryotic cells for the first time[4].

In 1991 and 1992, two studies described RNAs produced through non-canonical splicing, characterized by an inverted exon order compared to the reference genome, that originated respectively from the human DCC and EST-1 gene[5,6].In the following years, these non-polyadenylated RNAs with "scrambled exons" were firstly classified as covalently closed circular RNAs[7,8].

In the early 2000s, circular RNA intermediates were identified during intron self-splicing from mitochondrial RNAs, ribosomal RNAs, and transfer RNAs[9–11].

Even though between 1970s and 2000s many studies documented the existence of circular RNA molecules, their relevance remained underappreciated and their functional role was not fully deepened for a long time. The lack of evidence of their translation into proteins made scientists believe, for a long time, that such RNAs were not functional molecules, but mis-splicing artifacts or by-products of pre-mRNA processing[7].

In the last 15 years, advancement of Next Generation Sequencing techniques and the invention of specific bioinformatics scripts have allowed the recognition of many circRNAs, that were previously missed in transcriptomic profiling studies of polyadenylated mRNAs[12–16].

These technological advances have allowed to discover important and peculiar features that characterize circRNAs and that make them interesting molecules to be studied. CircRNAs commonly have tissue- and developmental stage-specific expression, result conserved between organisms and their expression is deregulated in many pathological conditions[14].

CircRNAs biogenesis

In eukaryotic cells, circular RNAs are produced through a non-canonical splicing process known as back-splicing, in which a downstream splice donor (5′ splice site) is joined to an upstream splice acceptor (3′ splice site), forming a head-to-tail junction and leading to the circularization of one or more exons. In some cases, introns may also be retained within the circular molecule[17]. The exons that compose circRNAs appear in reverse order compared to the reference transcriptome, and this reorganization of genomic information provides an additional mechanism for diversifying gene expression in eukaryotes. The back-splicing junction is the unique region that distinguishes circularized exons in circRNAs from their linear counterparts in mRNA transcribed from the same genomic region[12,14].

The production of circRNAs is a strongly regulated process typically involving the same spliceosome machinery engaged in canonical splicing, but recruited in a different order[18]. The fact that canonical splicing and back-splicing can be differently affected could depend on differences in exon definition mechanisms and on the requirement of a different set of splicing regulators[19,20]. Ashwal-Fluss *et al.*[21] show that when the linear splicing is enhanced, the back-splicing is disadvantaged and vice versa, suggesting a competition between the two mechanisms. Back-splicing is generally a

less common and efficient event compared to canonical splicing[22], hence circRNAs are commonly expressed at lower levels than linear counterparts[23]. However, in certain tissues and in some conditions, such as pathological ones, circRNAs production may increase and their levels could overcome the ones of the linear RNAs, also thanks to their higher stability[24,25]. Due to the lack of free ends, in fact, circRNAs, unlike linear transcripts, cannot be degraded by exonucleases.

Two models have been proposed to explain how back-splicing is coupled with splicing at the same locus: the “direct back-splicing” and the “lariat intermediate” models.
In the “lariat intermediate” model, canonical splicing happens first, producing a linear mRNA with skipped exons and a long intron lariat containing the skipped exons, which is subsequently processed to generate a mature circRNA.
In the “direct back-splicing” model, instead, back-splicing happens first and generates a circRNA together with a linear lariat containing both exons and introns, which can be further spliced to produce a linear mRNA with one or more skipped exon(s) or be degraded[26]. (Figure 2)

Fig. 2

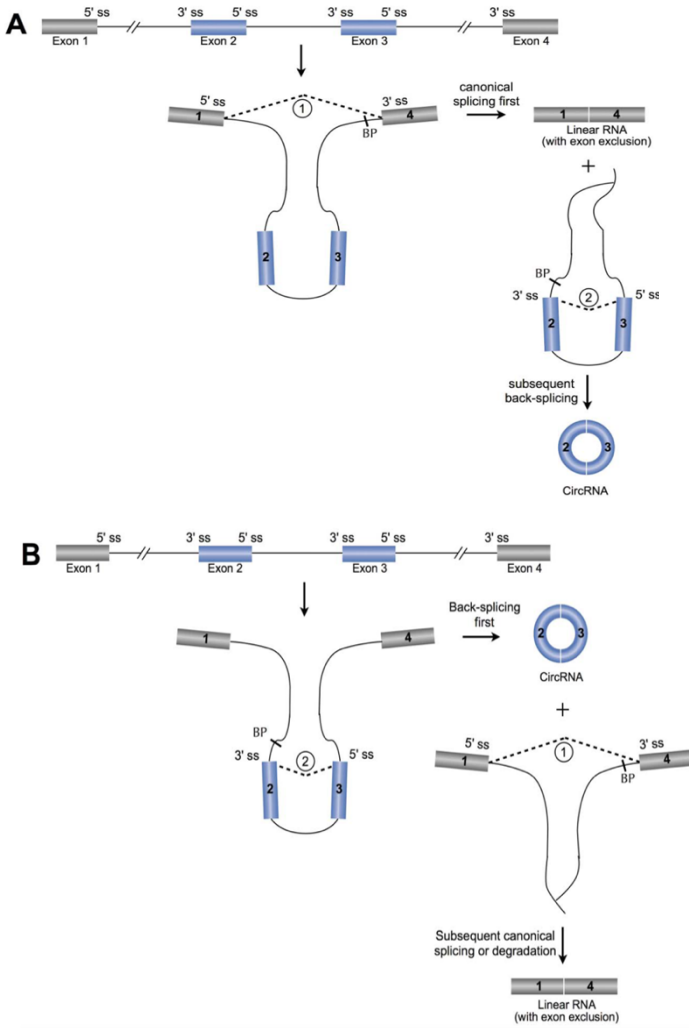

Fig. 2
“Lariate intermediate” (A) and “Direct” (B) models for circularRNAs biogenesis **(**Chen and Yang, 2015)

Many factors can modulate circRNA production and this regulation can happen both in *cis* and in *trans.* (Figure 3)

Cis factors that strongly promote the back-splicing reaction are the existence of very long exons and the presence of inverted repeated sequences in the introns flanking the exons that circularize. The pairing between repeated sequences, such ALU elements, for sequence complementary, in fact, brings the two splice sites into close proximity and the resulting secondary structure facilitates back-splicing[13,27,28]. In some cases, even very short intronic inverted repeats (30 or 40 nucleotide-long) are sufficient to promote back-splicing[29].

Among the back-splicing regulators in *trans*, RNA-binding proteins play a crucial role in promoting or preventing the circularizazion. Several RBPs, including QKI[30], NF90/NF110[31], MBL/ MBNL1[32], FUS[33] and hnRNPs[34] bind intronic sequences flanking the circularising exons and, by dimerization, bring the splice sites closer, promoting circRNA production.

The double-strand RNA binding protein ADAR1, an adenosine-deaminase involved in RNA editing, also plays a crucial role in time-dependent and tissue-dependent regulation of circRNAs production. The ADAR1-mediated adenosine-to-inosine modification, in fact, can prevent base pairing and, consequently, circRNA biogenesis[15].

More recently, other RNA modifications have been discovered to regulate circRNAs biogenesis. In particular, for a specific subset of circRNAs, N6-methyladenosine (m6A) modification at specific sites on primary transcripts can direct the splicing machinery towards the back-splicing reaction[35,36].

Fig. 3

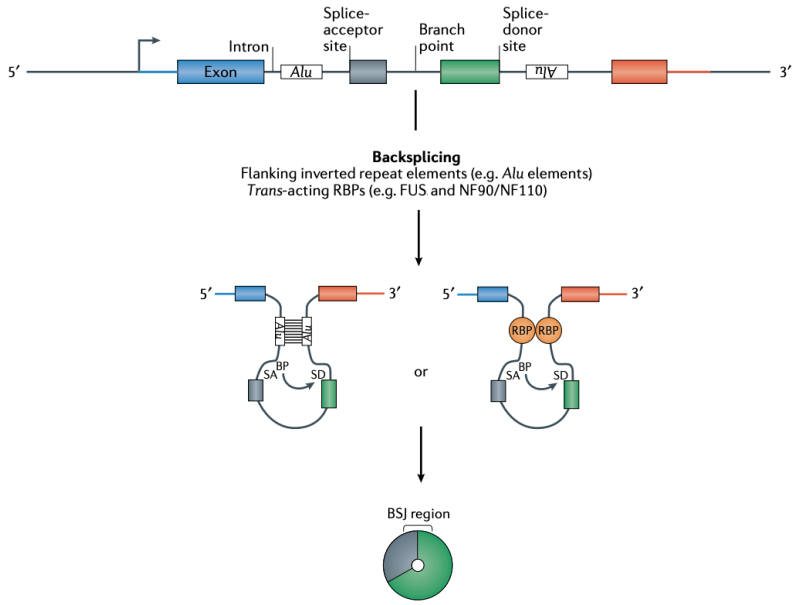

Fig. 3
CircularRNA biogenesis, regulated by *cis*- and *trans*-acting factors *(*Adapted from Kristensen *et al*., 2019)

CircRNAs molecular functions

The tissue- and developmental-stage specific regulation of circRNAs, together with their conservation among different species, are characteristics associated to molecules with a functional relevance in the cell[37,38]. In the last years it has been discovered that circRNAs can localize both in the nucleus and in the cytoplasm, where they can regulate gene expression at different levels. (Figure 4)

In the nucleus, the interaction of circRNAs with DNA, pre-mRNAs or protein factors can influence the **regulation of crucial processes such as transcription and splicing** both in *cis* and in *trans.* Some circular RNAs can form R-loops with their producing locus to impact transcription, as in the case of Ci-ankrd52 which forms an R-loop with the second intron of the ANKRD52 locus, blocking its transcription[39]. On the other hand, some nuclear circRNAs can regulate transcription by interacting with RNA Pol II[40] or transcriptional factors as in the case of circPOK and circIPO11, which respectively recruit IL2/3 on Il6 promoter[41] and TOP1 on GLI1 promoter[42].
In the nucleus, circRNAs can also promote exon skipping of circle-forming exons at the parental gene locus. As an example, in *Arabidopsis thaliana*, the circRNA circSEP3, which originates from the back-splicing of *SEP3* exon 6, can form an R-loop with its parental DNA locus, inducing the skipping of exon 6 in *SEP3* mRNA[43].

Both nuclear and cytoplasmatic circRNAs can act as **scaffolds or decoys of proteins**. Two known examples are circANRIL, which sequesters PES1 protein and affects rRNA processing[44] and circFOXO3 which can bind both p21 and CDK2 proteins favouring the inhibition of CDK2 by p21 and impacting cell cycle progression[45]. CircRNAs can also interact with acid nucleic-binding protein with a role in immune surveillance and, hence, influence the innate immune response of cells. Cia-cGAS binds to the DNA sensor cGAS through an interaction stronger than the ones with self-DNA, thus preventing cGAS activation in presence of self-DNA[46]. CircRNAs with intermolecular RNA-RNA interactions can bind to RNA sensors such as PKR and NF90/NF110, keeping them in an inactive status, and reduced expression of those circular transcripts is generally associated to autoimmune diseases[47].

For many cytoplasmatic circRNAs a competing endogenous role has been proposed. The competing endogenous RNAs (ceRNAs) are transcripts which can indirectly regulate post-transcriptional gene expression by **binding microRNAs** and preventing their interaction with mRNAs[48]. Examples of circRNAs with a competing endogenous role are circSRY that contains different miR-7 binding sites in mouse testis[49], circHIPK2 that contains one miR124-2HG binding site and modulates astrocyte activation [50] and circBIRC6 that contains miR-34a and miR-145 binding sites to modulate human cell pluripotency and differentiation[51].
Not all miRNA-binding circRNAs act as miRNA sponges, as in the case of CDR1as, the first functional circRNA ever described[49]. CDR1as was initially considered to act as a ceRNA for miR-7, preventing it from targeting mRNAs [14], but, in a more recent work[52], it has been discovered that CDR1as may, instead, stabilize miR-7 and translocate it towards neuronal synapses, where the miRNA is released from the circRNA and can target mRNAs related to synaptic transmission.

Though circRNAs are commonly classified as non-coding RNAs, it has been discovered that some circular transcripts containing an Open Reading Frame (ORF) and an Internal Ribosomal Entry Site (IRES) can be recognized by the polysome machinery and be **translated** in a cap-independent way[53,54]. The typical circRNA-specific ORF passes through the back-splicing junction, finally encountering a downstream stop-codon. Typically, the circRNA-encoded protein coincides to a truncated version of the corresponding full-length protein encoded by the linear mRNA, with the addition of a new aminoacidic sequence due to the codons downstream the back-splicing junction.
The first two circular RNAs observed to be translated into peptides are circZNF609, which controls cell proliferation in

human primary myoblasts[53] and circMBL, the most abundant circRNA in *Drosophila*, highly conserved through evolution [54]. Different studies have demonstrated that circular RNA translation can be enhanced by the m6A RNA modification [36,55].

For some circRNAs-encoded peptides, an antagonistic role in respect to the full full-length protein has been discovered. CircFGFR1 encodes for a peptide that corresponds to a truncated form of FGFR1 and interacts with FGFR1 through a dominant-negative effect resulting in suppressed cell proliferation[56]. CircARHGAP35 encodes for a peptide that, contrary to the corresponding full-length protein which acts as a tumour suppressor in HCC, promotes cancer progression[57].

More recently, it has been showed that cytoplasmatic circRNAs can regulate gene expression at post-transcriptional level by **directly interacting with messenger RNAs**. A work carried out in our laboratory suggested this mechanism for the first time, showing that circZNF609 can impact cancer cells cycle progression by directly interacting with the *CKAP5* mRNA, promoting the binding of the RBP HuR on the transcript and, hence, enhancing the production of CKAP5 protein, essential for cell mitotic division[58]. Another example is the circRNA circHOMER1 which reduces synaptic translation of the *Homer1b* mRNA by binding its 3' untranslated region (UTR)[59].

A direct interaction with a ubiquitously expressed mRNA could represent a more general mechanism though which a circRNA regulates gene expression, since it does not depend on specific microRNA signatures that vary among different contexts, and it is less affected by stoichiometry issues respect to a competing endogenous role.

Fig. 4

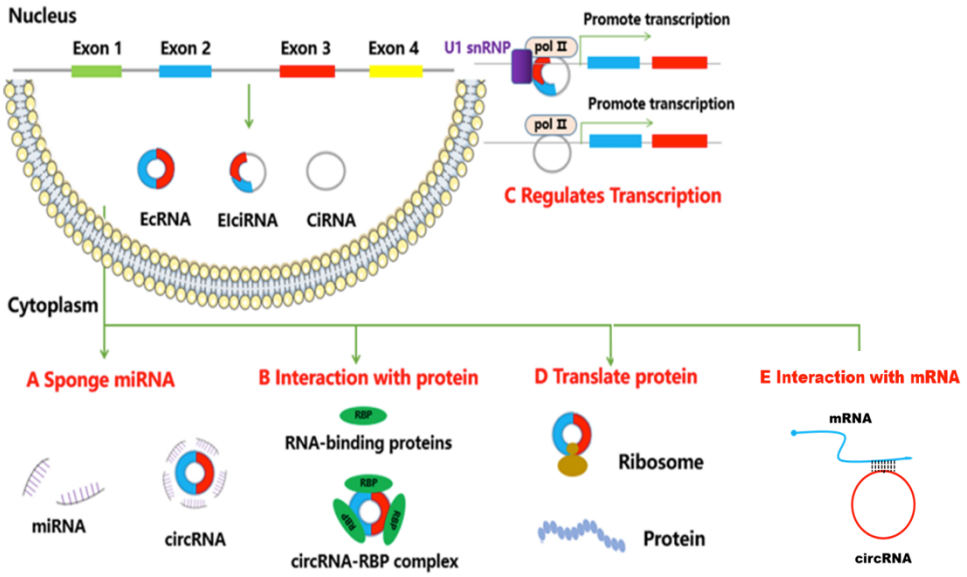

Fig. 4
CircularRNA molecular functions in the cell.
(Adapted from Zhang *et al*., 2020)[60]

CircRNAs in cancer

The main characteristic of circRNAs that has attracted the interest of many researchers in the last years is their common de-regulation in many pathological conditions, such as Alzheimer, diabetes, and cancer[61–63]. To date, thousands of circRNAs have been discovered to be differentially expressed among normal and cancer tissues, and to be involved in cancer onset and progression.

Overall, differentiated cells that have left the cell cycle tend to accumulate more circRNAs, than cells that continuously divide and dilute these molecules[64]. For this reason, some circular RNAs appear downregulated in cancer cells, compared to normal cells, as in the case of hsa_circ_0014717, deregulated in colon cancer cells, which can suppress tumorigenesis[65]. However, there are also several examples of circular RNAs that promote tumour progression and that result up-regulated in tumoral contexts, such as circ-PRKCI, which originates from genomic aberrations in many tumors, and stimulate proliferation and tumorigenesis[66].

CircRNAs with a role in cancer progression could represent optimal biomarkers for cancer diagnosis and therapeutic responses[67] . Thanks to their structure, in fact, circRNAs result highly stable, they commonly are expressed in a cell-type specific manner, they can be detected in all bodily fluids and generally result more expressed in the exosomes derived from cancer cells versus those from non-cancer cells [68,69].

Studying the specific role and mechanism trough which circRNAs can influence cancer expression could also allow to develop new anti-tumoral therapeutic strategies.

Most circRNAs influence cancer progression by regulating the expression of genes with a key role in tumour promotion or suppression. For example, circCTIC1, circRHOT1 and circACTN4 can promote MYC transcription through different mechanisms[70–72], circFOXO3 can promote MDM2-induced p53 degradation[45] and circSMARCA5, by sponging the splicing factor SRSF1, can induce the conversion of pro-angiogenic to anti-angiogenic VEGFA splicing isoforms to inhibit angiogenesis[73].

In other less common cases, circRNAs can also directly be involved in cells transformation and tumour onset. For example, in the context of haematological malignancies, circRNAs can drive oncogenic mutations and chromosome rearrangements. In particular, circRNAs which originate from MLL gene or their recombinase partner genes have been shown to form R-loops with their cognate genomic DNA locus, boosting genomic instability and driving oncogenic mutations and chromosomal rearrangements[74]. CircRNAs may also originate from transcription of fusion genes generated by tumor-specific chromosomal translocation, such as MLL/AF9 in acute myeloid leukemia and PML/RARα in promyelocytic leukemia. These molecules, called fusion-circRNAs (f-circRNAs), commonly drive cancer onset[61].

BRCA1 and DNA-damage repair

Introduction to DNA damage: causes, types and main repair pathways

The human genome is continuously subjected to genotoxic stress. DNA damage can accumulate during physiological and essential cellular processes such as DNA replication, can be caused by endogenous sources such as the formation of free radicals, or can be induced by exogenous agents such as ultraviolet light and ionising radiations[75].
The most common DNA lesions in the human genome consist in the generation of apurinic/apyrimidinic sites (AP), base substitutions, single-strand breaks (SSBs) and double strand breaks (DSBs)[76].

To maintain genome stability, cells have evolved a complex machinery able to sense DNA damage, activate the cell cycle checkpoint and execute DNA repair.
The activation of the DNA damage response is a mechanism that prevents tumorigenesis. Inactivating mutations of genes involved in DNA-repair pathway correlates with genomic instability and tumour progression and can cause cancer-predisposing clinical syndromes[77,78].

Double Strand Breaks (DSBs) are considered the most alarming form of DNA damage, since the integrity of both strands of the genome is compromised simultaneously.
In mammalian cells, DSBs can be repaired by the error-prone Non-Homologous End-Joining (NHEJ) machinery
or by the mostly error-free Homologous Recombination (HR) pathway.
During the G1 phase of cell cycle, before DNA replication, cells can only repair DSBs through NHEJ, which modifies the broken DNA ends and ligates them together generating

deletions or insertions[79]. On the other hand, HR repairs DSBs during the S and G2 phases of the cell cycle, after DNA replication, and utilizes the intact sister chromatid as a template for repair, leading to the reconstitution of the original sequence[80]. The Homologous Recombination response to DBSs involves sensors that detect broken ends, effectors that execute repair and mediators that allow the interactions between sensors and effectors[81].

BRCA1 role in Homologous Recombination repair

Among the key mediators of HR response to DNA damage, there is BRCA1 (BReast Cancer type 1 suscettibility protein), a protein of 1,863 amino acids encoded by a gene located in chromosome 17q21[82]. BRCA1 protein contains the zinc-binding finger domain RING at the N-terminal, two tandem BRCT domains at the C-terminal, a coiled coil domain and two Nuclear Localization Sequences (NLS) in the central portion[83]. After its recruitment to the DNA-damage site, BRCA1 regulates DSBs resection and repair through the interaction with different protein partners through its functional domains. (Figure 5)

Fig. 5

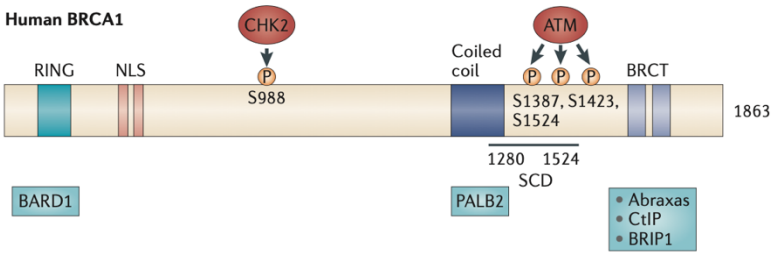

Fig. 5
BRCA1 functional domains and interactors (Roy *et al*., 2012)

The phosphorylation by the PIKK kinases ATM, ATR, and DNA-PK of the histone H2A variant, H2AX, in proximity to the DSB site, is the event that activates both HR and the NHEJ repair pathways[84–86].
During S and G2 phases, after DSBs, ATM-phosphorylated MDC1 recruits on the site of damage RNF8, that catalyses a specific ubiquitination of histones H2A and H2AX[87,88]. This modification is then recognized by the protein RAP80 which forms a macro-complex with ABRAXAS and BRCA1. BRCA1 directly interacts with **ABRAXAS** through the BRCT domain and indirectly with RAP80[89–91]. Once recruited to the DSB site, BRCA1 binds, with its BRCT domain, the CDK-phosphorylated **CtIP** protein[92] which, in turn, interacts with the MRE11-RAD50-NBS1 complex (MRN), responsible of catalysing DSB resection[93–95]. BRCA1 protein is then phosphorylated at Ser988 by CHK2[96] and this modification promotes the indirect interaction of BRCA1 to BRCA2 through the binding of BRCA1 coiled coil domain with **PALB2**[97,98]. BRCA2 is so recruited to the DNA-damage site, where it recruits the final effector of the HR repair pathway: RAD51[99]. The DNA strand-exchange protein RAD51 binds to the ssDNA to form a nucleoprotein filament, which promotes strand invasion into the unbroken homologous DNA duplex of the sister chromatid, to initiate repair synthesis[100]. (Figure 6)

Fig. 6

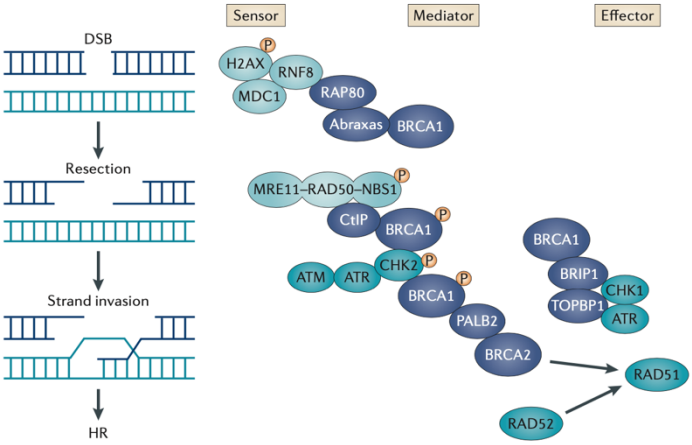

Fig. 6
Molecular mechanisms of Homologous Recombination (HR) Repair of Double Strand Breaks (DSBs) involving BRCA1. (Roy *et al*., 2012)

Simultaneously to its active role in repairing DNA-damage, BRCA1 is also involved in regulating cell cycle checkpoints during the process of HR[101].
The BRCA1-**BARD1** heterodimer, formed through RING domains interaction, has E3 ligase activity and catalyzes the formation of noncanonical lysine6-linked ubiquitin chains (K6-polyUb), which seem to serve as a signal for assembly and protein stabilization (also of BRCA1 itself) rather than degradation[102–104]. The BRCA1–BARD1 complex is involved in the activation of G1/S checkpoint after DNA-damage by promoting the phosphorylation of p53 on Ser15, essential for p21 induction[105].
The interaction of BRCT BRCA1 domain to **BRIP1** allows the formation of the BRCA1–BRIP1–TOPBP1 macrocomplex, able to unwind secondary DNA structures and necessary for

the S-phase checkpoint in response to stalled or collapsed replication forks[106,107].
Eventually, also the BRCA1–**ABRAXAS**–RAP80 macro-complex appears to be involved in the G2/M checkpoint in response to ionizing radiation-induced DNA damage[89].

The role of BRCA1 in NHEJ is controversial, since BRCA1 has been observed to facilitate[108,109], suppress[110,111] or have no effect on NHEJ[112]. These discordant observations may be attributed to the different assays used to measure NHEJ, to the possibility that BRCA1 could have different roles in the various subtypes of NHEJ and to the possibility that BRCA1 could act differently in different cellular contexts[113].

BRCA1 mutations in cancer progression and treatment

Considering it essential role in DNA-damage repair through HR, inactivating mutations of BRCA1 are associated to cancer onset[114].
One mutated copy, transmitted by one parent, of BRCA1 gene in the germ line causes Hereditary Breast and Ovarian Cancer (HBOC) syndrome, which is inherited in an autosomal dominant manner. This syndrome is associated with early breast and ovarian cancer onset but also with an increased risk of develop other forms of cancer such as pancreatic, stomach, laryngeal, fallopian tube and prostate cancer. HBOC syndrome accounts for 5–7% of all cases of breast cancer and individuals with HBOC syndrome have a 50–80% and 30-50% risk of developing breast and ovarian cancer respectively[115–117].
The majority of BRCA1 gene mutations are frameshift insertions/deletions, non-sense mutations, or alteration of splice sites, resulting in the production of a truncated non-functional form, generally destined for degradation[118,119]. The condition of BRCA1 haploinsufficiency, caused by the

presence of a non-functional BRCA1 gene, promotes genome instability and can favour the mutation of the second BRCA1 allele, condition necessary, in most of the cases, for the onset of the tumour[120].

Loss-of function mutations in HR pathway components can be exploited to induce non repairable DNA damage, leading to cancer cell death. In particular, BRCA1 inactivating mutations confer sensitivity to certain DNA-damaging agents, such as platinum compounds, hence these chemotherapeutics result more efficient against BRCA1-mutated tumours[121].
Moreover, the presence of mutations in BRCA1 or other genes involved in DSBs repair through HR opens the intriguing possibility to induce cancer cells death through synthetic lethality. Synthetic lethality occurs when the misfunction of two different genes alone is not able to induce cell death but results lethal only if combined together[122].
PARP1 and PARP2 are enzymes with a crucial role in DNA-repair of single-strand DNA breaks (SSBs)[123]. In case of PARP1/PARP2 misfunction, SSBs are not properly repaired and this could lead to the collapse of the replication fork and to probable formation of DSBs[121]. In case of the presence of a functional and intact HR DNA-repair pathway, the DSBs can be properly repaired, hence PARPs misfunction could have lethal consequences only in cells with at least one of the HR key factors altered[121,124].
PARP inhibitors (PARPi) are small molecules able to inhibit the activity of PARP1, PARP2 or both[125]. It has been shown that PARPi activity increases a lot in BRCA1-mutated cancer cells through a synthetic lethality mechanism[121].
So far, the clinically approved PARP inhibitors (olaparib, niraparib, rucaparib, talazoparib) are only utilized for the treatment of BRCA1/BRCA2 mutated cancers in which the HR repair pathway result altered[126].

Rhabdomyosarcoma

General characteristics of Rhabdomyosarcoma

Rhabdomyosarcoma (RMS) is a paediatric malignant tumour of muscular origin which derive from mesenchymal cells committed to a myogenic lineage which fail to properly differentiate[127]. It represents about 5% of all paediatric tumours and is the most common soft tissue sarcoma in children and adolescents, while it's very rare in adults[128,129]. The majority of RMS cases occurs sporadically; however, this tumour can also be associated with familial diseases such as neurofibromatosis and Li-Fraumeni syndrome[130,131].

Rhabdomyosarcoma subtypes

The World Health Organization (WHO) classifies RMS into four subtypes on the bases of histological characteristics (Figure 7): the alveolar rhabdomyosarcoma (ARMS), the embryonal rhabdomyosarcoma (ERMS), the pleomorphic rhabdomyosarcoma (PRMS), and the sclerosing/spindle cell rhabdomyosarcoma (SRMS). ERMS and ARMS are the most common subtypes and occur mainly in children and adolescents, while PRMS and SRMS are rarer and generally occur in adults. Every subtype is characterized by different molecular mechanisms, different clinical prognoses and pose distinct therapeutic challenges[127].

ARMS accounts the 20% of RMS cases. It is the most aggressive subtype, it often shows metastasis at diagnosis and is characterized by unfavourable prognosis[132]. It mainly concerns tissues of extremities, chest, abdomen and genital area in adolescents and young adults. Its cells resemble muscle cells of a 10-week-old foetus[133].80% of ARMS cases associate with aberrant chromosomal translocations which

fuse the 5' exons of a Paired Box gene (Pax3 on chromosome 2 or Pax7 on chromosome 1), encoding for a DNA-binding-domain, to the 3′ exons of the Forkhead Box O1 gene (Foxo1) on chromosome 13, encoding for a transactivation domain[134]. PAX3 and PAX7 participate in skeletal muscle development[135], while FOXO1 is a transcription factor involved in the regulation of insulin signalling[136]. The translocations lead to the formation of chimeric PAX3–FOXO1 or PAX7–FOXO1 proteins, which act as oncoproteins[129,137]. 20% of ARMS cases, classified as fusion-negative ARMS, does not present those translocations and results less aggressive than fusion-positive ARMS[133].

ERMS is the most common subtype, accounting for almost 60% of RMS cases, and the most precocious one. It mainly affects children within their first 10 years of life and often has a better prognosis than ARMS. It generally arises in sites such as eye, head, neck, urinary tract, uterus and testes. ERMS cells are small, round or elongated, very similar to those of a 6/8-week-old fetal muscle[133] (American Cancer Society).
ERMS is genetically more heterogeneous than ARMS, it is not characterized by chromosomal translocations and is often associated with mutation which activate tumour-promoting pathways, especially the RAS one[133,138].

Fig. 7

Subtype	Embryonal	Pleomorphic	Spindle cell	Alveolar
Histology	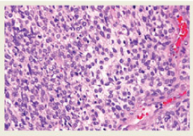 Small, round-to-elongated cells with interspersed loose myxoid stroma	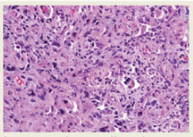 Large anaplastic cells with enlarged, hyperchromatic nuclei, multipolar mitotic figures	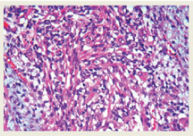 Relatively differentiated spindle cells with features reminiscent of smooth muscle neoplasms	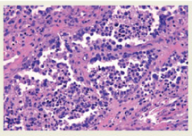 Discohesive primitive round cells within interwoven fibrous septa
Location	Genitourinary tract, head and neck, urinary bladder, prostate, biliary tract, abdomen, pelvis, retroperitoneum	Extremities, chest and abdomen	Paratesticular, and head and neck in children; head and neck in adults	Extremities, head and neck, chest, genital organs, abdomen, and anal area
Age (years)	<10	60–80	<10 >40	10–25
~% of all RMS cases	60%	10%	10%	20%
Prognosis*	Favourable	Unfavourable	Favourable (children) Unfavourable (adults)	Unfavourable

Fig. 7
Rhabdomyosarcoma subtypes and their histological classification (Kashi *et al*., 2015)

Rhabdomyosarcoma survival rate and treatments

RMS patients can be categorized into specific risk groups based on factors such as tumours location and size, the presence of metastasis in lymph nodes and other areas, tumour subtype, and the presence of the PAX-FOXO translocations in ARMS cases. The 5-year survival rate for RMS is strongly related to the individual patient's risk group. In the low-risk group, overall survival rate is approximately 70% to 90%, for the intermediate-risk group, the survival rate range is 50%-70%, while for the high-risk group, the overall survival decreases to 20%-30% (American Cancer Society).

Standard treatments to fight RMS include surgery, radiotherapy and chemotherapy. Surgery is the first-line approach to remove resectable tumours and is often

associated to radiotherapy, especially in case of lymph nodes involvement. The standard recommended chemotherapeutical treatment for RMS patients includes three drugs: Vincristine, Actinomycin D and Cyclophosphamide (VAC)[139]. Though the chemotherapeutic strategy for RMS treatment has remained unchanged over the last few decades, current research is still evaluating the efficacy of other drugs for the treatment of this paediatric sarcoma and other chemotherapeutic agents such as doxorubicin and etoposide have been tested for RMS treatment[140].

Advancements in diagnostic and therapeutic strategies have increased the 5-year overall survival, however the RMS survival rate is still low, especially for patients with high-risk rhabdomyosarcoma. Moreover, the strong treatments-related toxicities can have important side-effects in children and severely decrease their quality of life[141,142].

A strategy to increment the survival of RMS patients and reduce side-effects could be represented by targeted approaches, intended to specifically attack molecular pathways altered in the tumoral context. However, the main limitation of targeted therapies is the high frequency of intrinsic and acquired resistance mechanisms which result very common in rhabdomyosarcoma. Currently, the combination of target therapies and chemotherapy seems to represent the best compromise to avoid tumour resistance and increase patients' survival rates[143].

In order to improve the efficiency of targeted therapies there is the need to expand the knowledge about the molecular pathways involved in the progression of this cancer, that in many cases have not been fully characterized yet[133].

RESULTS

CircHIPK3 is upregulated in rhabdomyosarcoma cells and interacts with several mRNAs *in vivo*

CircHIPK3 is a covalently closed RNA molecule, composed by 1099-nucleotides, originated from the back-splicing of the second exon of the HIPK3 locus (Figure 8A). According to literature[144–146], circHIPK3 results de-regulated in different tumoral contexts, thus we decided to prioritize its selection for functional studied of its role in cancer progression.

As results from RNA-sequencing[147] and qRT-PCR (Figure 8B), circHIPK3 is up-regulated in both embryonal (RD) and alveolar (RH4) Rhabdomyosarcoma cell lines compared to myoblasts, which represent the healthy condition. Interestingly, in RD cells we observed a specific increase of circHIPK3 and not of the linear *HIPK3* mRNA in respect to the healthy control, suggesting a possible specific regulatory role of the circRNA in this context. Analysis of the expression levels by qRT-PCR of circHIPK3 in tumour biopsies and healthy donor samples also indicated increased levels of circHIPK3 in both embryonal and alveolar tumours compared to healthy muscle tissue (Figure 8C)

Fig. 8

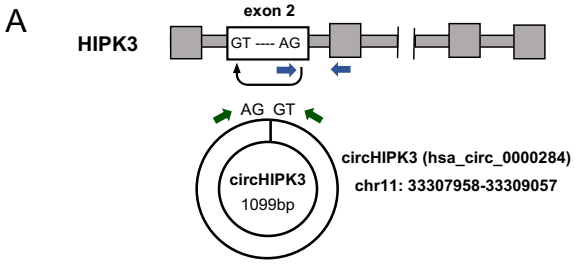

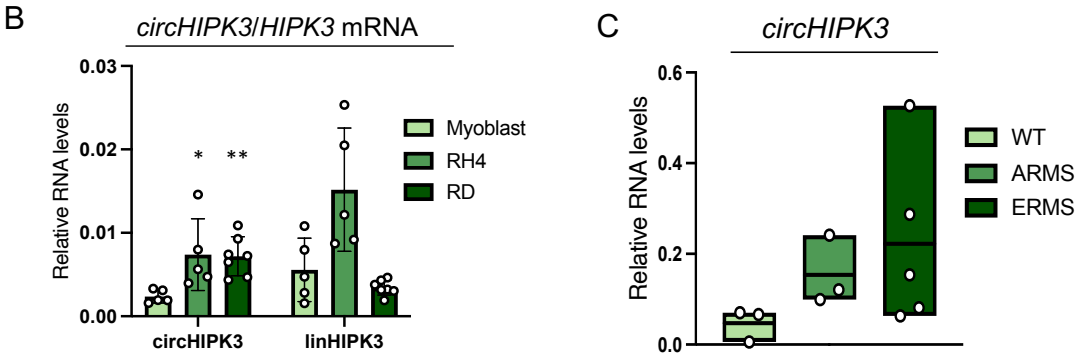

Fig. 8
(A) Schematic representation of circHIPK3 formation through HIPK3 exon-2 back-splicing. Green and blue arrows represent the oligonucleotides used to amplify circHIPK3 and *HIPK3,* respectively. (B) RNA levels (rel.to *GAPDH*) measured by qRT-PCR of circHIPK3 and *HIPK3* mRNA in wild-type human primary myoblasts, RH4 cell line (ARMS) (circHIPK3 p=0,033) and RD cell line (ERMS) (circHIPK3 p=0,0014). n>3. Data are represented as mean ±SD. (C) RNA levels (rel.to *GAPDH*) measured by qRT-PCR of circHIPK3 in healthy skeletal muscle (WT, n=3), alveolar RMS (ARMS, n=3) and embryonal RMS (ERMS, n=5) samples from paediatric age-matched patients.

In Rhabdomyosarcoma cells, circHIPK3 has cytoplasmatic localization (Figure 9A). Its resistance to RNAse R (Figure 9B), and the presence of the back-splicing junction in its amplicon (Figure 9C) strongly suggest that circHIPK3 is indeed a circular RNA in this system.

Fig. 9

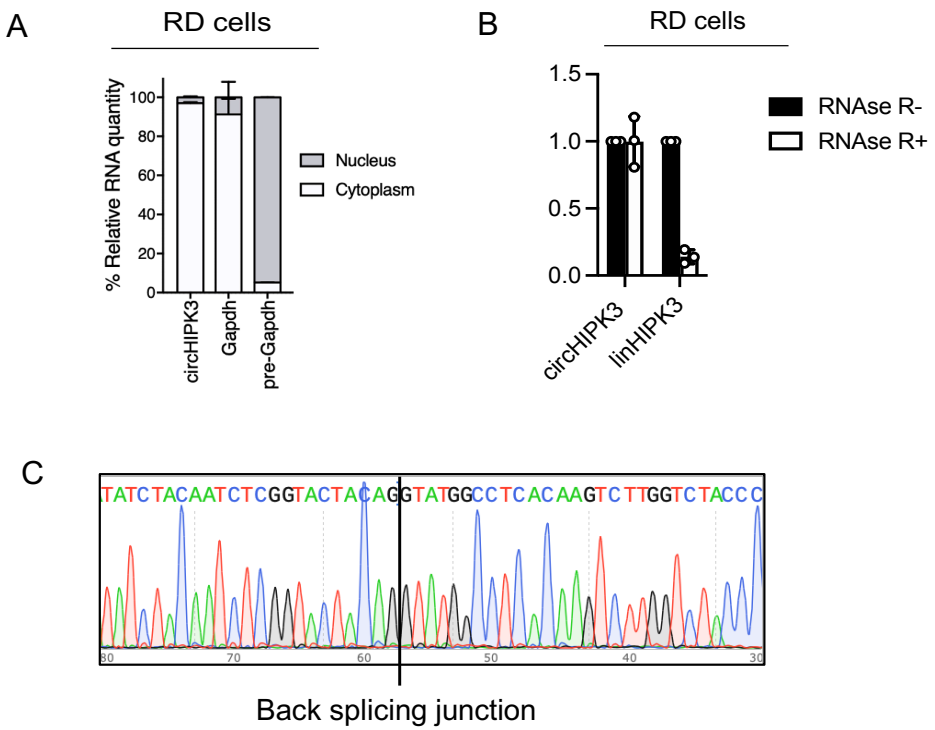

Fig. 9
(A) qRT-PCR data representing the subcellular localisation of circHIPK3 in RD cells; *GAPDH* mRNA and *pre-GAPDH* were used as positive controls for cytoplasmic and nuclear RNAs, respectively. n=2. (B) qRT-PCR experiment showing circHIPK3 and HIPK3 mRNA levels in RD cells in control conditions (RNase R (-)) and upon RNase R treatment (RNase R (+)). n=3. Data are represented as mean of Fold Changes ± standard deviation. (C) Sanger sequencing which confirms the presence of the back-splicing junction in the sequence amplified with the oligonucleotides for circHIPK3 designed in this work.

To look for possible direct mRNA interactors of circHIPK3, we performed a pull-down of the endogenous circRNA in RH4 cells after RNA-RNA crosslinking through 4'aminomethyl 4,5'-8 trimethylpsoralen (AMT). AMT intercalates into RNA duplexes and upon 365 nm UV irradiation generates inter-strand adducts between juxtaposed pyrimidine bases, crosslinking RNAs which are in very close proximity[148]. The pull-down was performed by utilizing streptavidin beads and two sets of 20-nt-long biotinylated probes, randomly named ODD and EVEN, both targeting *HIPK3* exon2, including one specific for the Back-Splicing Junction (BSJ). (Figure 10A). A set of probes, targeting *E. coli* LacZ sequence, was used as a negative control.

Two replicates of AMT-crosslinked circHIPK3 pulldown, in which qRT-PCR indicated a much higher enrichment of the circRNA in respect to the linear counterpart and to a non-specific mRNA (*GAPDH*) (Figure 10B), were subjected to high-throughput RNA sequencing for target identification. Reads were aligned to reference genome, and genes were considered enriched when both ODD and EVEN coverages were at least 4-fold greater than input and LacZ coverages. The specific enrichment of the circular isoform was confirmed by the observation of almost all HIPK3 reads aligned to the exon2, the only one present in circHIPK3 (Figure 10C). The RNA-sequencing detected several mRNAs enriched in AMT-crosslinked circHIPK3 pulldown. Native RNA pulldown and qRT-PCR allowed to validate 10-15 mRNAs as circHIPK3 interactors in both RH4 and RD cells. (Figures 11A-B). Considering the specific upregulation of circHIPK3, and not of *HIPK3* mRNA, in RD cells, which suggests a cancer-related regulatory role of the circRNA, we decided to continue our investigation in these cells.

Fig. 10

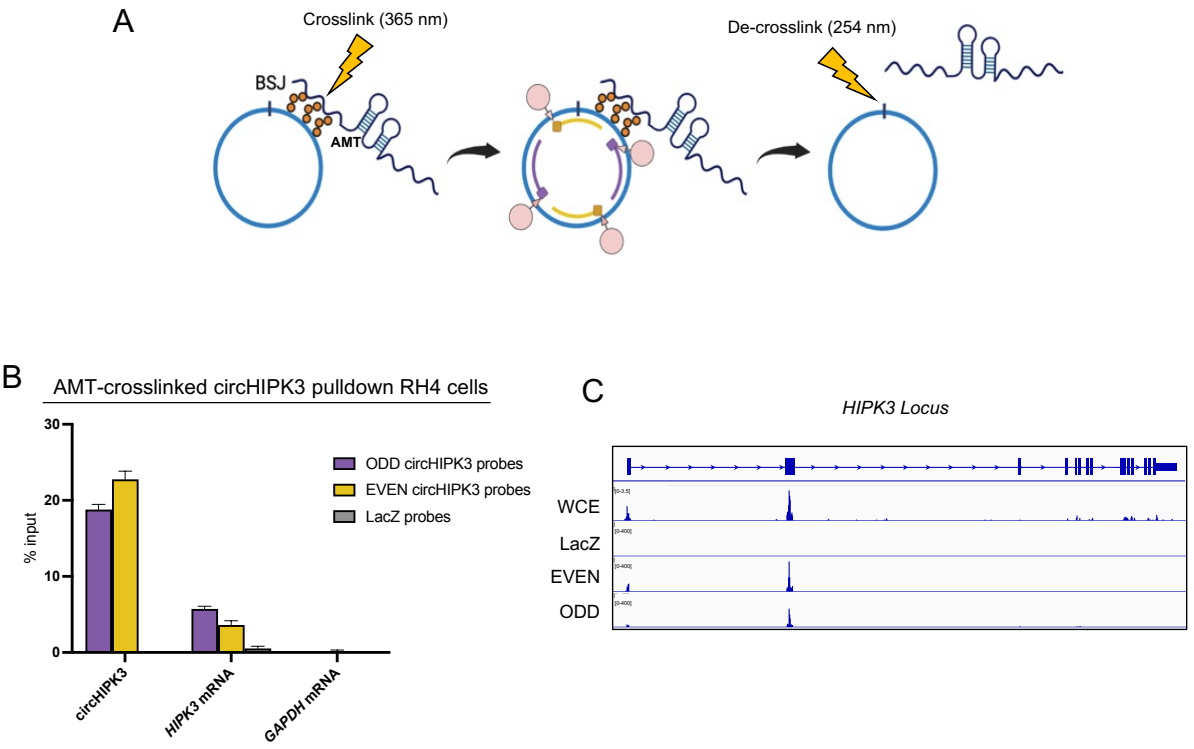

Fig.10
(A) Cartoon representing circHIPK3 pulldown approach with AMT (4'aminomethyl 4,5'-8 trimethylpsoralen). ODD and EVEN biotinylated probes are represented in violet and yellow, respectively, while streptavidin beads are represented in pink. (B) qRT-PCR showing the enrichment of circHIPK3, *HIPK3* mRNA, and *GAPDH* mRNA in one replicate of AMT-crosslinked circHIPK3 pulldown and control LacZ pulldown performed in RH4 cells. Data are shown as mean of enrichment versus input ±SE of technical triplicates. (C) Normalized Integrative Genomics Viewer (IGV) RNA-sequencing reads densities in HIPK3 locus for WCE, ODD, EVEN, and LacZ pulldown.

Fig. 11

A

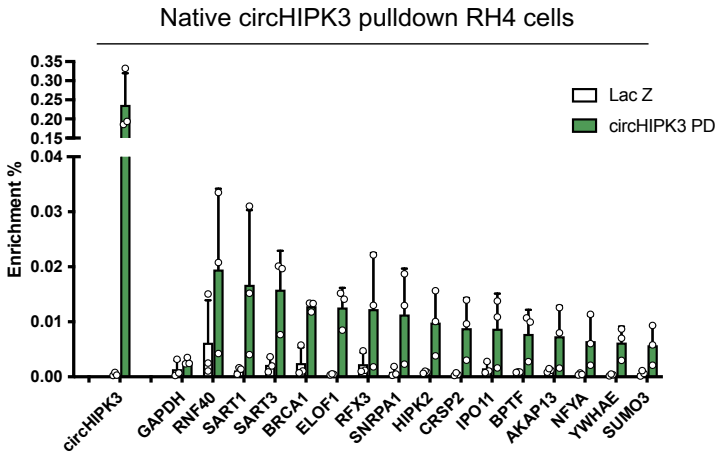

B

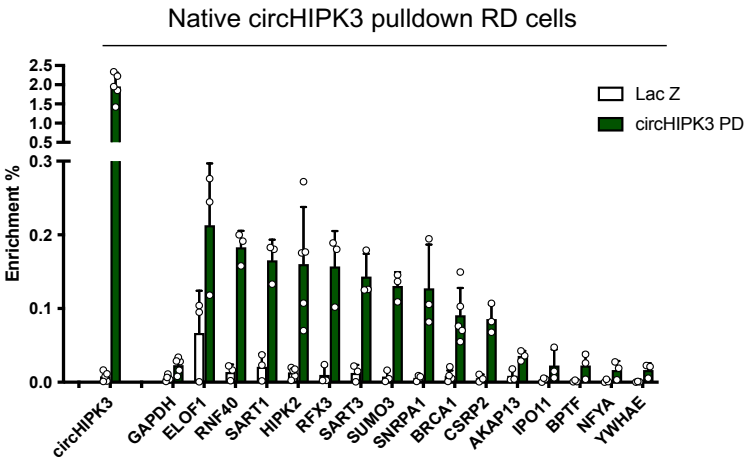

Fig.11
(A-B) qRT-PCR showing the enrichment of circHIPK3, GAPDH mRNA (negative control) and some circHIPK3 candidate interactors in circHIPK3 native pulldown and control LacZ pulldown performed in RH4 and RD cells. n=3. Data are shown as mean of enrichment versus input ±SD.

CircHIPK3 regulates BRCA1 expression through a direct circRNA-mRNA interaction

To investigate whether circHIPK3 could be involved in the post-transcriptional regulation of its mRNA interactors, we transfected RD cells with a siRNA against circHIPK3 BSJ to specifically knock-down the circular RNA (si-circHIPK3). To exclude the involvement of *HIPK3* mRNA we also transfected cells with a siRNA which only targets the linear isoform (si-linHIPK3) (Figure 12A). Among the mRNA interactors which resulted specifically downregulated after circHIPK3 depletion, we found *BRCA1* mRNA (Figure 12B) and we decided to focus on the possible regulation of this interactor due to its crucial role in cancer onset and progression. We then tested BRCA1 protein levels in circHIPK3 knockdown condition and in this case, we observed an even stronger reduction induced by the circRNA depletion (Figure 12C).
To avoid possible off-targets of the RNA interference approach, we transfected cells with another siRNA which targets another region of circHIPK3 BSJ (si-circHIPK3-II). The second siRNA induces the same reduction of BRCA1 both at RNA and protein levels, excluding possible off-targets effect (Figure 12D).

Fig. 12

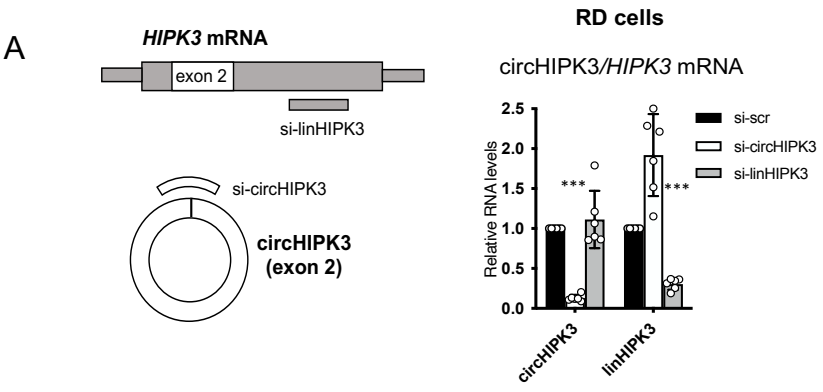

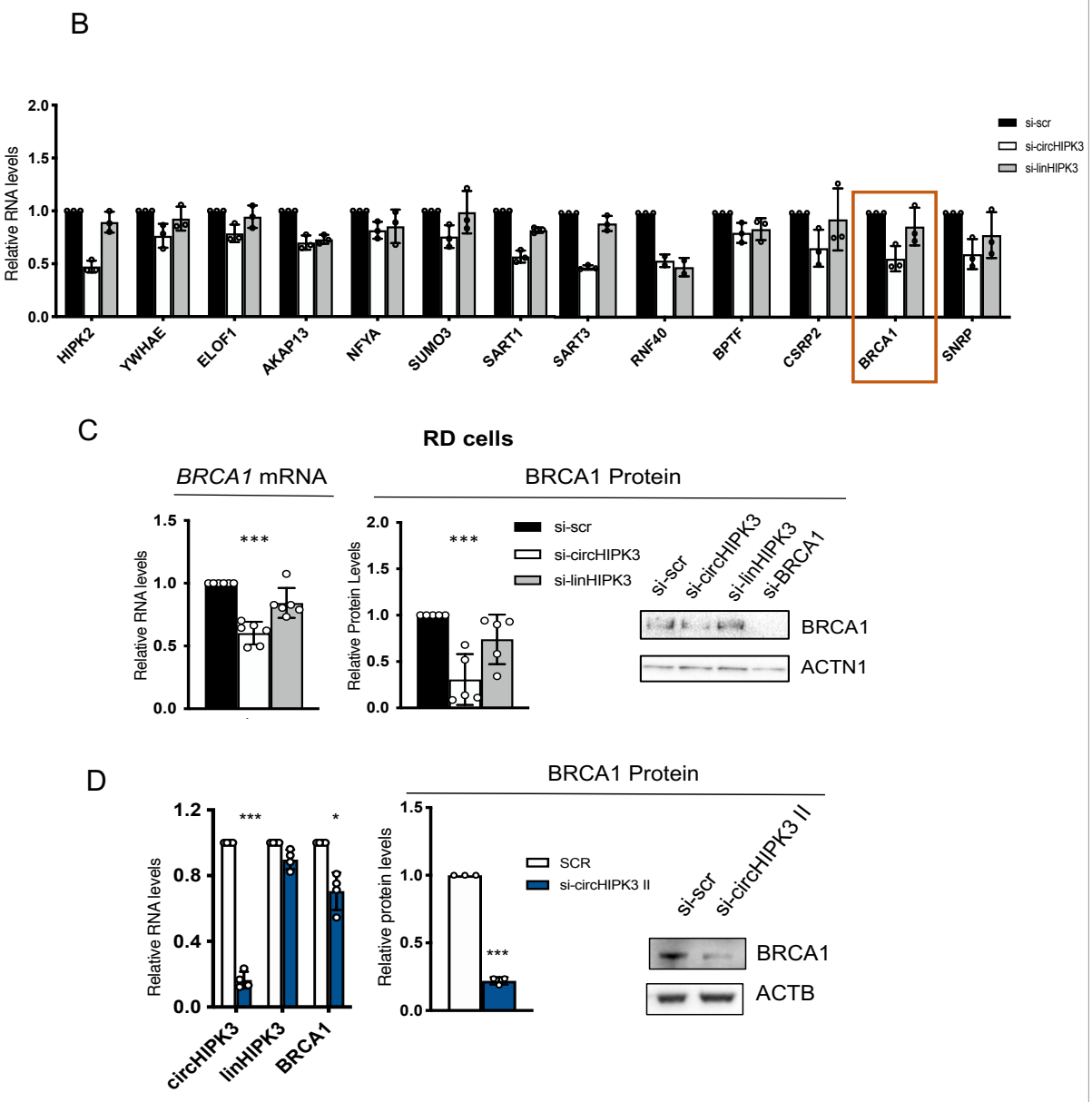

Fig. 12
(A) Schematic representation of siRNAs targeting circHIPK3 (si-circHIPK3) and HIPK3 mRNA (si-linHIPK3). (B) RNA levels (rel.to GAPDH) measured by qRT-PCR of circHIPK3 and HIPK3 in RD

cells in si-scr, si-circHIPK3 (circHIPK3 p<0,0001) and si-linHIPK3 (HIPK3 p=<0,0001) conditions. n>3. (C) RNA levels (relative to GAPDH mRNA) measured by qRT-PCR of some of circHIPK3 candidate interactors in RD cells in si-scr, circHIPK3 and si-linHIPK3 conditions. n=3. (D) Left, RNA levels (rel.to GAPDH) measured by qRT-PCR of BRCA1 mRNA in RD cells in si-scr, si-circHIPK3 (p<0,0001). n>3. Right, protein quantification (rel. to actinin) and representative western blot of BRCA1 in RD cells in si-scr, si-circHIPK3 (p=0,0005) and si-linHIPK3 conditions. n>3.
Data are represented as mean of fold changes or of protein levels ± SD.

Upon circHIPK3 knockdown we did not observe changes in the levels of the nascent *BRCA1* pre-mRNA (Figure 13A), while transcription blockage with alpha-amanitin reduced *BRCA1* mRNA stability (Figure 13B), indicating that circHIPK3 regulates BRCA1 expression at a post-transcriptional level.

Fig. 13

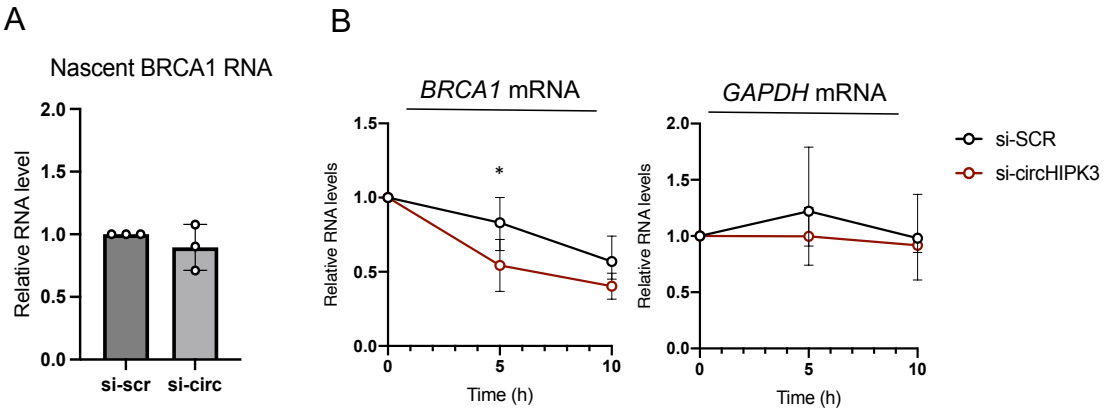

Fig. 13
(A) RNA levels (relative to pre-ATP5O) measured by qRT-PCR of pre-BRCA1 mRNA si-scr and si-circHIPK3 conditions. n=3. Data are represented as mean of fold changes ± standard deviation.

(D) qRT-PCRs showing BRCA1 and GAPDH (negative control) RNA levels upon α-Amanitin treatment in RD cells in si-scr (black) or si-circHIPK3 (red) conditions. n = 3. Referred to BRCA1 mRNA stability, p = 0,0457 (5 h). n>3. Graphs represented fold changes calculated as 2-DCt, normalized to the reference sample (0h) which was set as 1.

Since the probes used for circHIPK3 pulldown also target the exon 2 of *HIPK3* mRNA, we performed a series of experiments in order to definitively exclude the possible regulatory interaction between *HIPK3* and *BRCA1* mRNA. First of all, we performed a native pulldown of circHIPK3 in control condition (si-scr) and after circHIPK3 knock-down (si-circHIPK3). The abrogation of *BRCA1* mRNA enrichment in absence of circHIPK3 indicated that the presence of *BRCA1* in circHIPK3 pulldown indeed depends on the presence of the circRNA (Figure 14A). Along this line, we also performed a specific pull-down of the linear *HIPK3* mRNA, and we did not detect any *BRCA1* enrichment (Figure 14B). These data confirm that only circHIPK3 and not its linear counterpart, *HIPK3* mRNA, interacts with the *BRCA1* mRNA.

Fig. 14

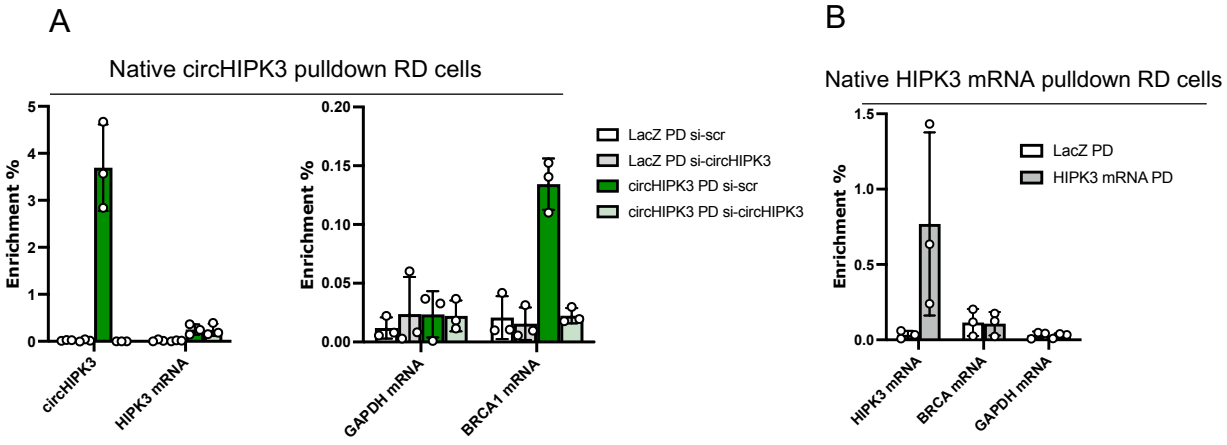

Fig. 14
(A) qRT-PCR showing the enrichment of circHIPK3, HIPK3, GAPDH (negative control) and BRCA1 in circHIPK3 native pull-down and control LacZ pull-down performed in RD cells in si-scr or si-circHIPK3 conditions. n=3. (B) qRT-PCR showing the enrichment of HIPK3, BRCA1 and GAPDH (negative control) in HIPK3 mRNA native pull-down and control LacZ pull-down performed in RD cells. n=3.
Data are represented as mean of enrichment versus input ±SD.

Since it has been largely reported that circHIPK3 could have a competing endogenous role, we then tested whether circHIPK3 could regulate BRCA1 levels in RD cells by acting as a sponge of miRNAs.
Transfected luciferase constructs containing circHIPK3 sequence or the 3'UTR of *BRCA1* downstream of the reporter did not induce any alteration in the luciferase signal upon circHIPK3 depletion, indicating that in our system miRNAs seem not to bind circHIPK3 or to regulate BRCA1 expression in a circHIPK3-dependent way (Figure 15A).
To definitely rule out the possible involvement of miRNAs in circHIPK3-mediated regulation of BRCA1, we performed a native pulldown of circHIPK3 followed by high-throughput small RNA sequencing. Using the same stringent enrichment analysis previously applied to the AMT-crosslinked pulldown, only three micro RNAs resulted enriched: hsa-let7b-5p, hsa-miR21-5p and hsa-miR877-5p (Figure 15B). However, validation of those targets was far from optimal; after circHIPK3 native pulldown we were only able to observe a small and variable enrichment of let7b-5p and miR21-5p (Figure 15C). In any case, we tried to block those microRNAs using Locked Nucleic Acid (LNA) technology. Transfection of LNA blockers induced an upregulation of known specific miRNAs targets (CDC25A, TIMP3 and BCL217–19 for miR21-5p, CDC34, COIL and CCND120 for Let7b-5p), but not of *BRCA1* mRNA (Figure 15D). Moreover, circHIPK3 depletion did not change the levels of known Let7-5p nor miR21-5p

targets (Figure 15E). These data exclude the possibility that circHIPK3-mediated BRCA1 regulation depends on a competing endogenous role of the circRNA.

Fig.15

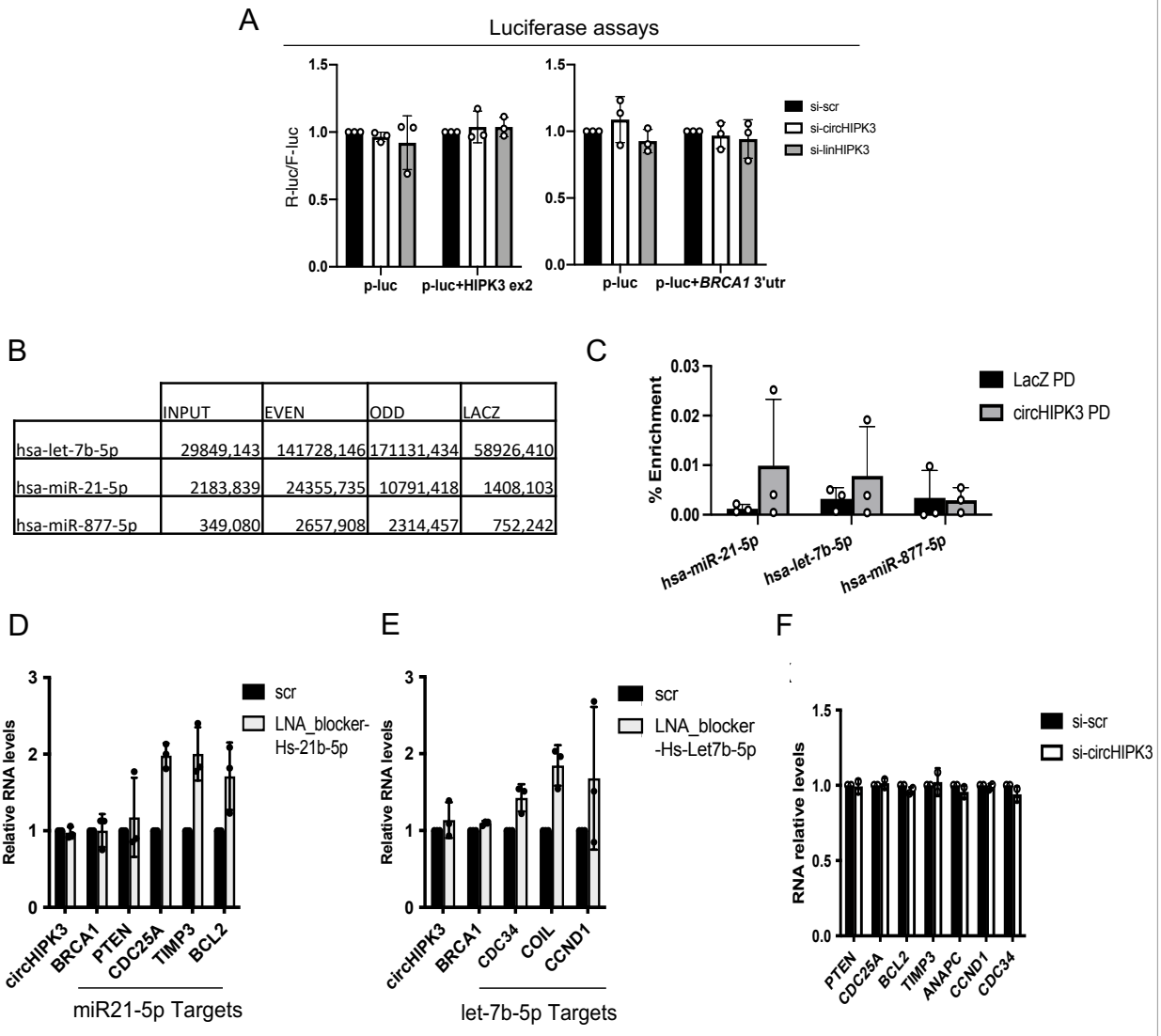

	INPUT	EVEN	ODD	LACZ
hsa-let-7b-5p	29849,143	141728,146	171131,434	58926,410
hsa-miR-21-5p	2183,839	24355,735	10791,418	1408,103
hsa-miR-877-5p	349,080	2657,908	2314,457	752,242

Fig. 15
(A) Left, relative luciferase signal (R-luc/F-luc) produced by psicheck2 empty vector (p-luc) or psicheck2 + HIPK3 exon 2 (p-luc + HIPK3 ex2) in si-scr, si-circHIPK3 (p-luc + HIPK3 ex2 p=n.s.) and si-linHIPK3 (p-luc + HIPK3 ex2 p=n.s.) RD cells; right, relative luciferase signal (R-luc/F-luc) produced by psicheck2 empty vector (p-luc) or psicheck2 + BRCA1 3'utr (p-luc + BRCA1 3'utr) in si-scr, si-circHIPK3 (p-luc + BRCA1 3'utr p=n.s.) and si-linHIPK3 (p-luc + BRCA1 3'utr p=n.s.) RD cells. n=3. Data are represented as mean of fold changes ± standard deviation. (B) High-throughput small RNA sequencing Counts Per Million of hsa-let-7b-5p, hsa-miR-21-5p and hsa-miR-877-5p in RD cells from input, circHIPK3 native pulldown performed with EVEN and ODD probes and LacZ pulldown. (C) qRT-PCR showing the enrichment of hsa-miR-21-5p, hsa-let-7b-5p and hsa-miR-877-5p in circHIPK3 native pull-down and control LacZ pull-down performed in RD cells. n=3. Data are shown as mean of enrichment versus input ± SD.(D) RNA levels (relative to *GAPDH* mRNA) measured by qRT-PCR of circHIPK3, *BRCA1*, *PTEN*, *CDC25A*, *TIMP3* and *BCL2* mRNAs (transcripts demonstrated or predicted to be regulated by hsa-miR-21-5p) in RD cells after the transfection of a control LNA (scr) or of a LNA which binds and blocks hsa-miR-21-5p. n=3. Data are represented as mean of fold changes ± SD. (E) RNA levels (relative to *GAPDH* mRNA) measured by qRT-PCR of circHIPK3, *BRCA1*, *CD343*, *COI*L and *CCND1* mRNAs (transcripts demonstrated or predicted to be regulated by hsa-let-7b-5p) in RD cells after the transfection of a control LNA (scr) or of a LNA which binds and blocks hsa-let-7b-5p. n=3. Data are represented as mean of fold changes ± SD. (F) RNA levels (relative to *GAPDH* mRNA) measured by qRT-PCR of *PTEN*, *CDC25A*, *TIMP3* and *BCL2* mRNAs (transcripts demonstrated or predicted to be regulated by hsa-miR-21-5p), *ANAPC*, *CCND1* and *CD343* mRNAs (transcripts demonstrated or predicted to be regulated by hsa-let-7b-5p) in RD cells in si-scr and si-circHIPK3 conditions. n=2. Data are represented as mean of fold changes ± SD.

An RNA-RNA interaction occurs between the back-splicing junction of circHIPK3 and the last coding exon of *BRCA1* mRNA

To deepen the molecular interaction occurring between circHIPK3 and *BRCA1* mRNA, we consulted the IntaRNA program[149], which calculates the optimal free energy between interacting regions of two RNAs. The software indicated an interaction between nucleotides 5595 and 5634 of *BRCA1* mRNA, in the last coding exon of the transcript (ENST00000357654.9), and nucleotides 1068-13 of circHIPK3, across the BSJ, as the putative pairing with the highest energy (Figure 16A).
We decided to validate the predicted interaction, first of all *in vitro*. We performed Electrophoretic Mobility gel Shift Assay (EMSA) incubating an *in vitro* transcribed biotinylated RNA covering nucleotides 5581-5880 of BRCA1 (BRCA1 Ex23+3'UTR) together with an unlabelled *in vitro* transcribed RNA spanning nucleotides 1000-99 of circHIPK3-BSJ (circHIPK3 BSJ) or together with an unlabelled *in vitro* transcribed RNA containing a random region (nucleotides 357-562) of circHIPK3 (circHIPK3 CTL) in increasing concentrations. The shift of the biotinylated construct signal was observed only in presence of circHIPK3 BSJ construct and not of circHIPK3 CTL, indicating that the BSJ region of circHIPK3 is able to interact with the BRCA1 Ex23+3'UTR construct (Figure 16B).
We then compared the migration of biotinylated BRCA1 Ex23+3'UTR RNA or of a mutated version lacking the predicted interaction site (BRCA1 Ex23+3'UTR-Δ, nucleotides 5581-5595/5634-5880), in the presence of unlabelled circHIPK3-BSJ RNA. The deletion of the predicted interaction site on the BRCA1 construct produced an almost complete abrogation of the gel shift, confirming the importance of

BRCA1 mRNA region 5595-5634 in the interaction with circHIPK3 (Figure 16C).
As a control, we also substituted the interaction region on BRCA1 construct with a random sequence (biotinylated BRCA1 Ex23+3'UTR-mut) and, also in this case, we observed an abrogation of the gel shift that could only be recovered in presence of circHIPK3-BSJ RNA mutated with the complementary sequence (Figure 16D). Altogether, these data confirm the involvement of the BSJ region of circHIPK3 and of the last coding exon region of *BRCA1* mRNA in the binding.

Fig.16

A

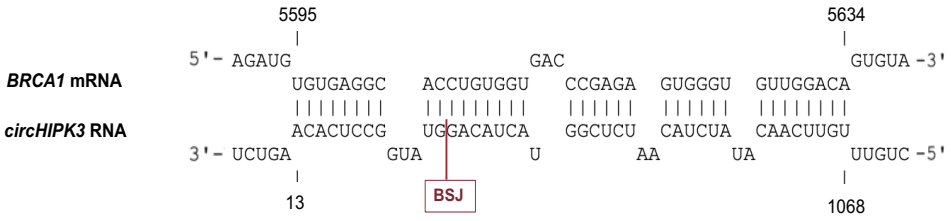

B

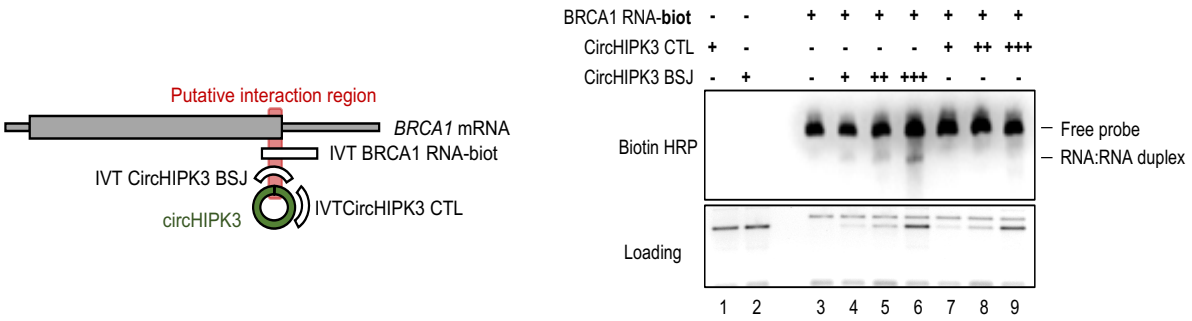

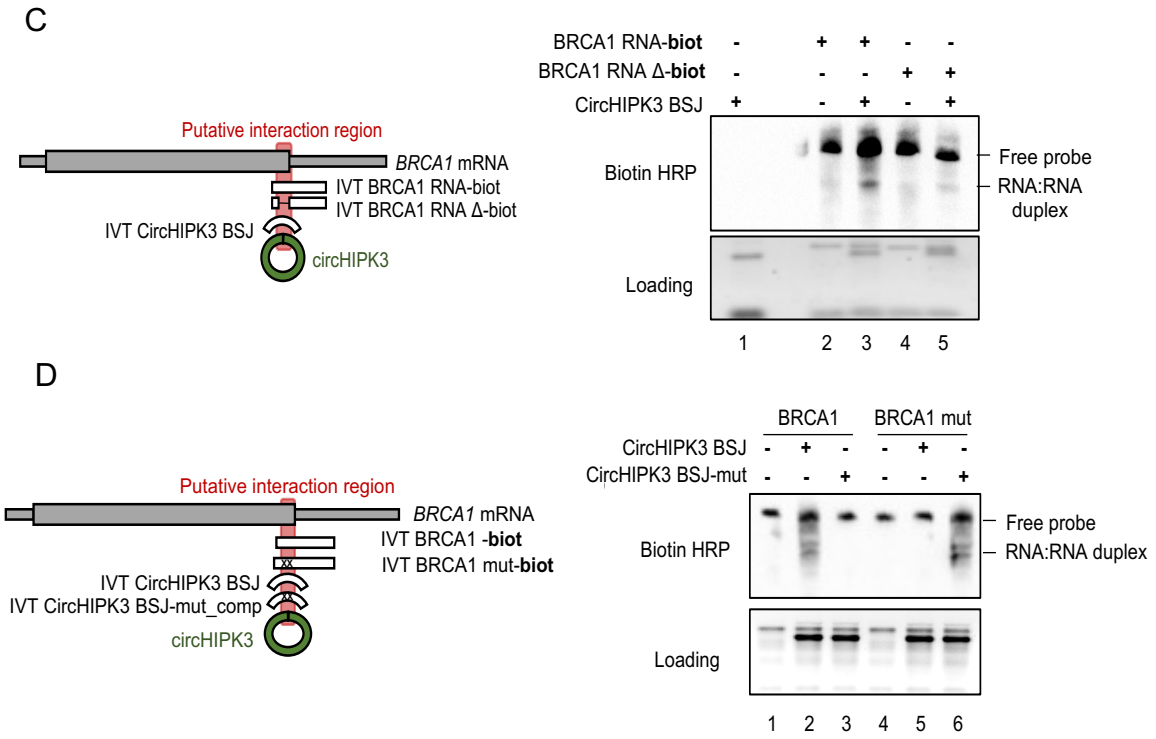

Fig. 16

(A) circHIPK3/*BRCA1* mRNA interaction with the highest binding energy predicted by IntaRNA. (B-C-D) Left, cartoon depicting IVT constructs. (B) Right, EMSA of biotinylated IVT BRCA1 exon-23 + 3'UTR construct alone (lane 3), in increasing concentration of IVT circHIPK3-BSJ (lanes 4-6) or in increasing concentration of another IVT region of circHIPK3, circHIPK3-CTL (lanes 7-9). (C) Right, EMSA of biotinylated IVT BRCA1 exon-23 + 3'UTR construct alone (lane 2) or in presence of IVT circHIPK3-BSJ (lane 3) and of biotinylated IVT BRCA1 exon-23+3'UTR, with the predicted circHIPK3 interaction site deleted, construct alone (lane 4), or in presence of IVT circHIPK3-BSJ (lane 5). (D) Right, EMSA of biotinylated IVT BRCA1 exon-23+3'UTR construct alone (lane 1), in presence of IVT circHIPK3-BSJ (lane 2) or in presence of IVT circHIPK3-BSJ with the predicted BRCA1 interaction site mutated (lane 3); EMSA of biotinylated IVT BRCA1 exon-23+3'UTR with the predicted circHIPK3 interaction site mutated (complementary with

the circHIPK3-BSJ-mut construct) alone (lane 4), in presence of IVT circHIPK3-BSJ (lane 5) or in presence of IVT circHIPK3-BSJ-mut (lane 6).

We then decided to test whether circHIPK3 BSJ region is involved in BRCA1 regulation in the cell. We transfected RD cells with LNA antisense oligonucleotides, able to prevent interactions between RNAs without altering their expression, one targeting 30 nucleotides across circHIPK3 BSJ (LNA BSJ) and another one targeting another control region on the circRNA (LNA ex2 circ) (Figure 17A). In respect to a random control LNA (LNA scr), we observed a significant downregulation of BRCA1 both at RNA and protein levels only in presence of LNA BSJ and not of LNA ex2 circ, indicating that circHIPK3 BSJ region regulates BRCA1 levels *in vivo* (Figure 17B).

Fig.17

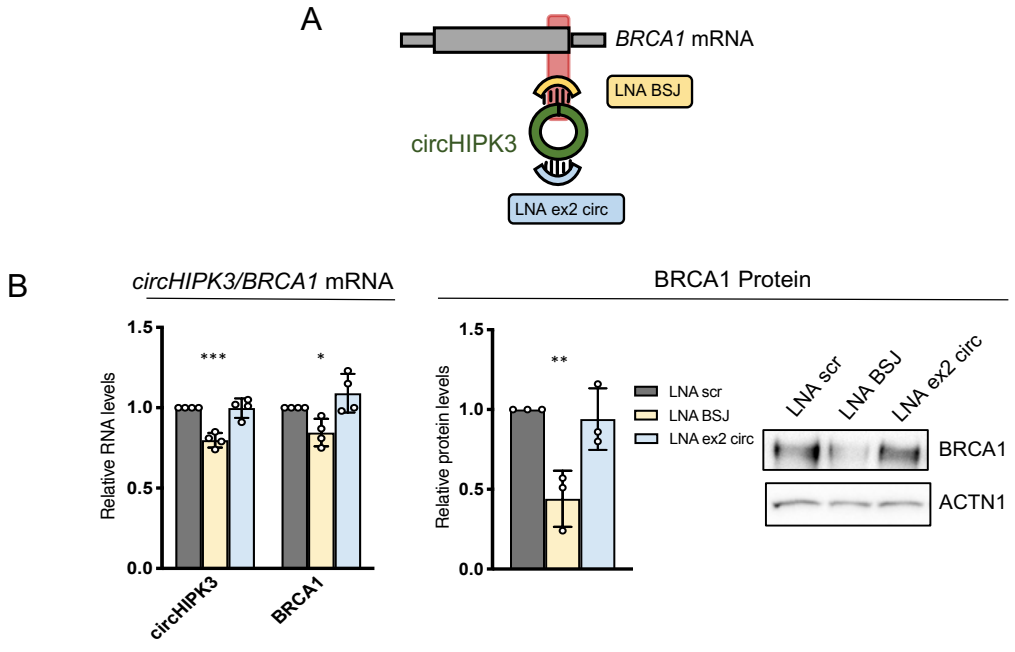

Fig. 17
(A) Representation of LNAs targeting circHIPK3 on *BRCA1* binding site (LNA BSJ) or on another random sequence (LNA ex2 circ). (B) Left, RNA levels (rel.to *GAPDH*) measured by qRT-PCR of circHIPK3 and *BRCA1* mRNA in RD cells transfected with LNA scr, LNA-BSJ (circHIPK3 p=0,0001; BRCA1 p=0,0110) or LNA ex2 circ. n>3. Data are represented as mean of fold change ±SD. Right, protein quantification (rel.to *ACTININ*) and representative western blot of BRCA1 in RD cells transfected with LNA scr, LNA BSJ (p=0,0053), or LNA ex2 circ. n=3. Data are represented as mean of relative protein levels ±SD.

CircHIPK3 prevents FMRP binding to *BRCA1* on exon 23

Considering the central role of RNA-binding proteins in regulating mRNAs fate in the cytoplasm, we asked whether an RBP could be involved in circHIPK3-mediated regulation of BRCA1 expression. To find proteins that could bind *BRCA1* mRNA, we consulted catRAPID v2.122[150], an algorithm which computes RNA-protein interaction propensities. The program predicted FMRP and its paralog FXR2 as BRCA1-binding RBPs with the highest interaction ranking (Figure 18A). FMRP (Fragile-X Mental Retardation 1 protein) is a protein involved in different aspects of RNA metabolism, including splicing, stability, editing, transport and translation and in many cases a translational inhibitor role has been attributed to this RBP[151–153]. By consulting CrossLinked ImmunoPrecipitation sequencing (CLIP-seq) data[152,154], we found several FMRP CLIP-signals on *BRCA1* mRNA and, interestingly, different CLIP experiments show that FMRP binds a sequence on exon 23 of *BRCA1* overlapping the circHIPK3 interacting site (Figure 18B). Considering that, we hypothesized that circHIPK3 and FMRP could compete to bind *BRCA1* mRNA on the exon 23 region.

Fig.18

A

Protein	Interaction Ranking
P51116_FXR2	0,812542
Q06787_FMR1	0,802833
Q12906_ILF3	0,800625
P52597_HNRNPF	0,796583
P26599_PTBP1	0,794042
Q9NR56_MBNL1	0,792708
P35637_FUS	0,790917
P84103_SRSF3	0,789458

B

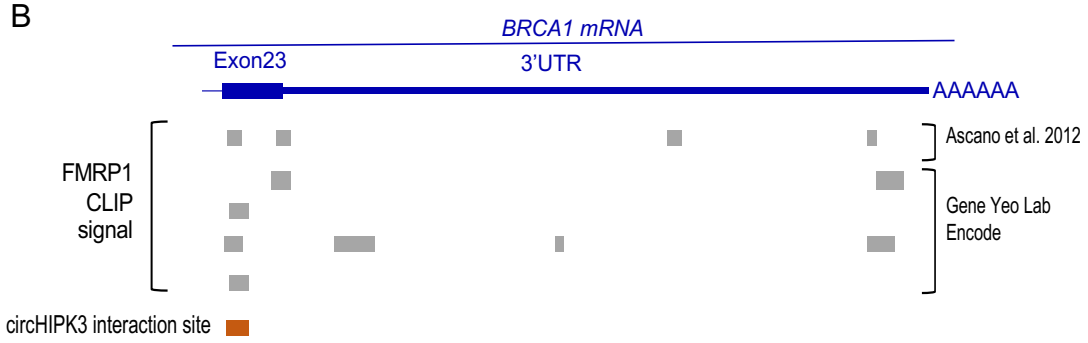

Fig. 18
(A) Table showing RBPs with the highest interaction energy with BRCA1 mRNA according to CatRapid predictions. (B) Integrative Genomics Viewer (IGV) reads from FMRP-CLIP (grey) from Ascano *et al*. and Gene Yeo Lab Encode on BRCA1 mRNA exon-23 and 3'UTR. In orange, circHIPK3 binding site on BRCA1 mRNA.

To test this competition hypothesis, we performed an EMSA and observed the migration of biotinylated BRCA1 Ex23+3'UTR RNA in presence of the circHIPK3 BSJ RNA alone, of the recombinant FMRP alone or in presence of both the molecules. The incubation of biotinylated BRCA1 Ex23+3'UTR RNA with circHIPK3 BSJ RNA generated a faster migrating band, while the combination with FMRP produced a slower migrating band. In presence of both circHIPK3 BSJ RNA and FMRP, only the circHIPK3 BSJ-mediated migration was observed, indicating that the pairing with circHIPK3 BSJ is able to inhibit *BRCA1* mRNA interaction with FMRP *in vitro* (Figure 19A).

To assess whether the competition between circHIPK3 and FMRP for the binding of *BRCA1* mRNA could be possible at a stoichiometry level, we performed absolute quantification of circHIPK3 and *BRCA1* mRNA copies per cell. We established

a correlation between RNA copy number and qRT-PCR efficiency using a known amount of both RNAs transcribed *in vitro*. Quantifications indicated that the RD cells contain 334 copies of circHIPK3 and 14 copies of *BRCA1* mRNA per cell (Figure 19B) An extrapolation from RNAseq data indicates that the total number of copies per cell of all other circHIPK3 mRNA interactors, is 407 (Figure 19C). These quantifications are compatible with a direct competition model.

Fig.19

A

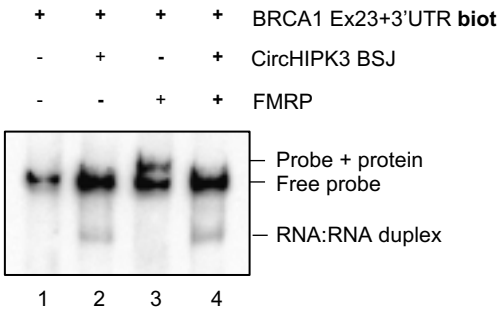

B

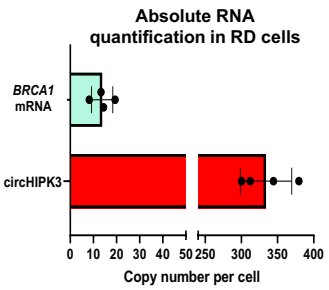

C

	Av. TPM RD	Absolute Quantification	Relative quantification based on RNA seq	
HIPK2	20,00	-	19,73	
ELOF1	58,23	-	57,44	
AKAP13	19,89	-	19,62	
SUMO3	97,27	-	95,95	
SART1	19,83	-	19,56	
SART3	45,77	-	45,15	
RNF40	39,28	-	38,75	
CSRP2	64,61	-	63,73	
SNRP	33,72	-	33,26	
BRCA1	14,00	13,81	13,81	
			407,00	Summatory of total interactors

Fig. 19
(A) EMSA of biotinylated IVT BRCA1 exon-23+3'UTR construct alone (lane 1), in the presence of IVT circHIPK3-BSJ (lane 2), in the presence of human recombinant FMRP protein (lane 3) or in the

presence of both circHIPK3-BSJ and FMRP (lane 4). (B) Copy number per cell, detected by qRT-PCR, of BRCA1 mRNA (cyan) and circHIPK3 (red) in RD cells. (C) Relative quantification, based on RNA-seq, of the number of molecules per cell of circHIPK3 interactors.

To test if circHIPK3 could indeed prevent the binding of FMRP to *BRCA1* mRNA, we performed an RNA-immunoprecipitation (RIP) of FMRP in RD cells in control conditions (si-scr) or after circHIPK3 KD (si-circHIPK3). In control condition we observed an enrichment of *BRCA1* mRNA after FMRP immunoprecipitation, and not of circHIPK3 or of negative control *GAPDH*, indicating that in our system FMRP binds *BRCA1* but not circHIPK3. Notably, in circHIPK3 KD condition, we observed an increase of *BRCA1* mRNA associated to FMRP but not of the known FMRP interactor *HUWE1*, compared to si-scr, indicating that the circRNA specifically regulates *BRCA1* association with FMRP (Figure 20A).

To discern the sites of *BRCA1* transcript to which FMRP can bind in RD cells, and to understand which binding site is specifically affected by the presence of circHIPK3, we performed UV-CrossLinked ImmunoPrecipitation (CLIP) of FMRP in control condition (si-scr) and after circHIPK3 depletion (si-circHIPK3). After UV-crosslinking, cells were lysed, RNA was fragmented and FMRP was immunoprecipitated. We then tested, through qRT-PCR, the association of FMRP to different *BRCA1* mRNA regions, in which CLIP signals were observed in published CLIP experiments performed in other models. We confirmed the association of FMRP to three sites inside *BRCA1* CDS, across exons 1-2, 10-11 and 22-23 respectively, but not to the 3'UTR region (discrimination of FMRP binding in the 5'UTR was impossible due to the resolution of the fragmentation). Notably, in circHIPK3-depleted cells, we observed an

increase of *BRCA1* mRNA associated with FMRP only in the region around the circHIPK3 interaction site (Exon 22-23), but not in other binding sites along the CDS, indicating that circHIPK3 specifically inhibits the binding of FMRP on exon 23. Even in this case, we did not observe an association of circHIPK3 to FMRP (Figure 20B).

Fig. 20

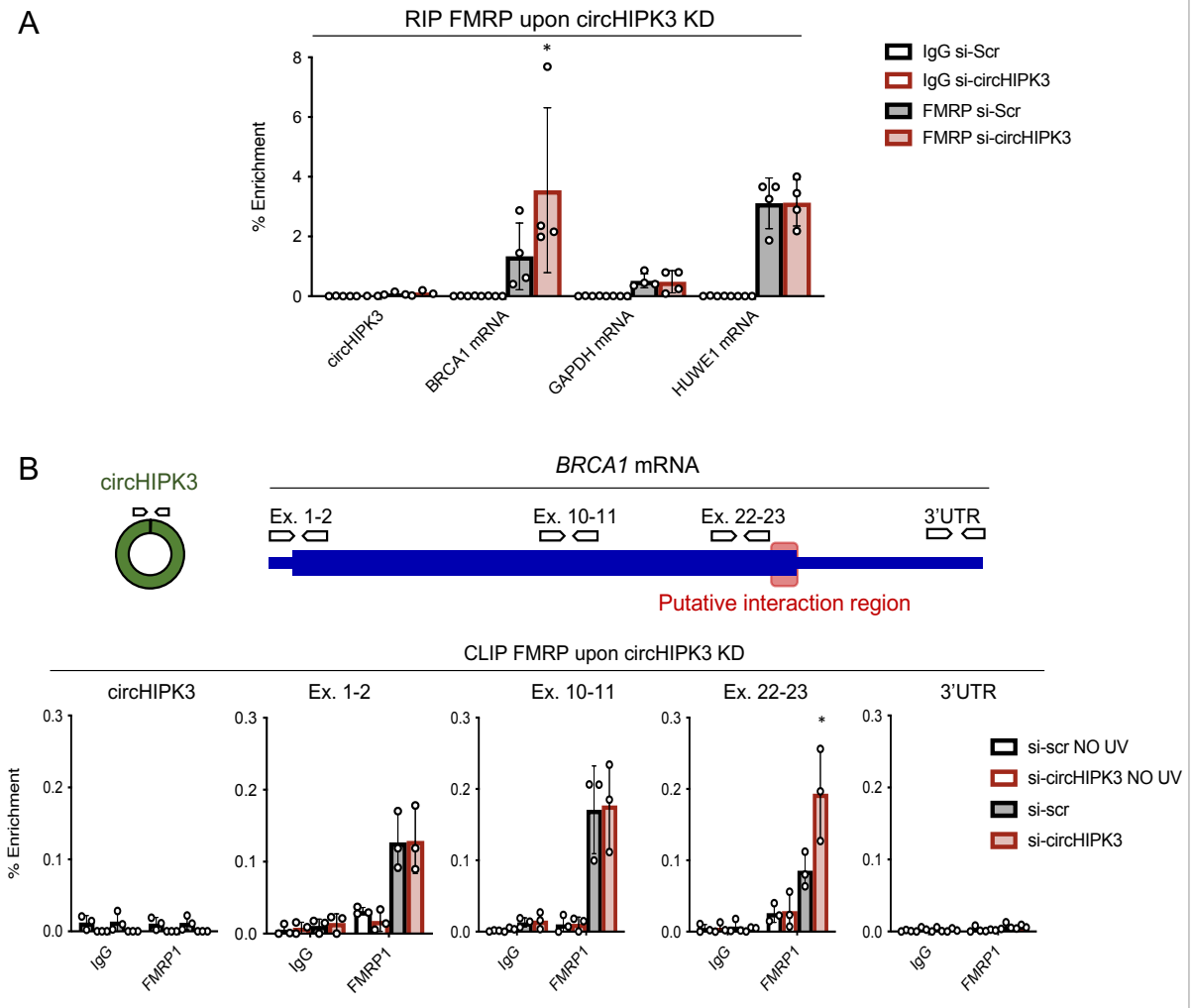

Fig. 20
(A) RNA enrichment measured by qRT-PCR of circHIPK3, *BRCA1* mRNA, *GAPDH* mRNA and *HUWE1* mRNA in FMRP and IgG RIP assay performed in RD cells in si-scr or si-circHIPK3 (BRCA1 p=0,0236) conditions. n=4. (C) RNA enrichment measured by qRT-PCR of circHIPK3 and four different regions of *BRCA1* mRNA (Ex.1-2, Ex.10-11, Ex. 22-23, 3'UTR), in FMRP and IgG immunoprecipitation assay performed, after RNA fragmentation, in si-scr or si-circHIPK3 (p=0,044 for ex.22-23) RD cells, in NO UV and UV (CLIP) conditions. n=3. The cartoon shows the oligonucleotides used to amplify circHIPK3 and BRCA1 regions. For C-D, data are shown as mean of enrichment versus input ±SD.

CircHIPK3 and FMRP have opposite role in regulating *BRCA1* translation

To study the role of FMRP binding on BRCA1 regulation, we set up a loss-of function approach. Since after the transfection of a single siRNA against FMRP mRNA, we only observed a moderate FMRP protein down-regulation (around 50%), we tested the combination of si-FMRP together with a siRNA against FXR2 (FMRP paralogue). The transfection of the two siRNAs together induced a robust downregulation of the FMRP protein (around 73%), condition in which we decided to analyse BRCA1 expression (Figure 21A).
In FMRP-downregulated (si-FXR2+si-FMRP) cells, we detected a significant increase of BRCA1 both at RNA and protein levels (Figure 21B-C), indicating that FMRP represses BRCA1 expression at the post-transcriptional level. We also reinforced the competition model by observing a rescue of BRCA1 RNA and protein levels, downregulated in si-circHIPK3 condition, with the simultaneous downregulation of FMRP (si-circHIPK3+si-FXR2+si-FMRP) (Figure 21D).

Fig. 21

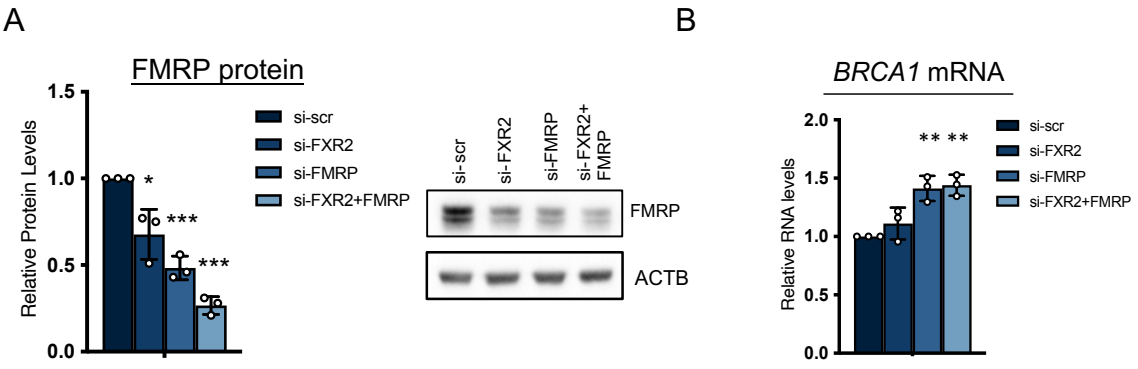

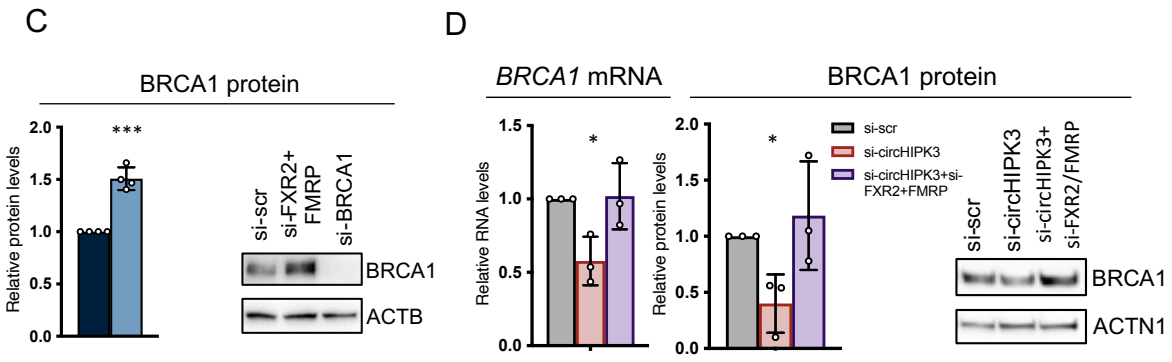

Fig. 21
(A) Protein quantification (relative to β-actin) and representative western blot of FMRP protein in RD cells in si-scr, si-FXR2 (p=0,0180), si-FMRP (p=0,0002) and si-FXR2+FMRP (p<0,0001) conditions. n=3. (B) RNA levels (rel.to *GAPDH*) measured by qRT-PCR of *BRCA1* mRNA in RD cells in si-scr, si-FXR2, si-FMRP (p=0,0027) and si-FXR2+FMRP (p=0,0011) conditions. n=3. (C) Protein quantification (rel.to ACTB) and representative western blot of BRCA1 in RD cells in si-scr and si-FXR2+FMRP (p=0,0027) conditions. n=4. (D) Left, RNA levels (rel.to *GAPDH*) measured by qRT-PCR of *BRCA1* mRNA in RD cells in si-scr, si-circHIPK3 (p=0,0114) and si-circHIPK3+si-FXR2+FMRP conditions. Right, protein quantification (rel.to ACTININ) and representative western blot of BRCA1 protein in RD cells in si-scr, si-circHIPK3 (p=0,0162) and si-circHIPK3+si-FXR2+FMRP conditions. n=3. Data are represented as mean of fold changes or of protein levels ±SD.

Considering the known role of FMRP in inhibiting transcripts translation, together with the observed alteration of BRCA1 protein after circHIPK3 and FMRP knockdown, we asked whether the circRNA and the RBP could regulate BRCA1 translation with opposite effects.
To investigate the role of circHIPK3 and FMRP in regulating BRCA1 translation, at first, we took advantage of a Ribo-TAG approach. We transfected RD cells with a construct encoding

for a flagged-ribosomal protein (60S ribosomal protein L22; RPL22) that we then immunoprecipitated with the aim to test *BRCA1* mRNA association to ribosomes. In RD cells transfected with si-circHIPK3, we observed a decrease of *BRCA1* mRNA association to RPL22, while after FMRP knockdown we detected more *BRCA1* transcript bound to ribosomes. The association of *GAPDH* (positive control for ribosome association) to flagged-RPL22 did not significantly change in the two conditions. Data are represented as percentage of input RNA so that differences in the total *BRCA1* RNA among the different conditions does not affect the results (Figure 22A-B).
To confirm the role of circHIPK3 and FMRP in the regulation of BRCA1 translation, we also performed polysomes fractionations trough sucrose gradients. As controls of proper fractionation, we observed that the majority of a house-keeping mRNA (*ACTININ*) is associated to polysomes, while circHIPK3, which lacks coding potential, is not found in the polysomes fraction (Figure 22C). Interestingly, most of circHIPK3 results associated to single 40S and 60S subunits of ribosomes, indicating that the circRNA, even if not actively translated, is associated to ribosomes, probably playing a regulatory role. The polysome fractionation confirmed what observed through the Ribo-TAG approach. In circHIPK3 KD RD cells we observed a decreased association of *BRCA1* mRNA to polysomes and a higher bond to single subunits (40S, 60S) and monosomes (80S); on the contrary, FMRP depletion induced a higher association of *BRCA1* mRNA to polysomes and a decreased association to 40S, 60S and 80S fractions. The association of *ACTININ* mRNA (positive control) to the different fractions did not significantly change in the different conditions (Figure 22D-E).
Altogether, these data suggest that circHIPK3 and FMRP respectively promotes and inhibits BRCA1 translation.

Fig.22

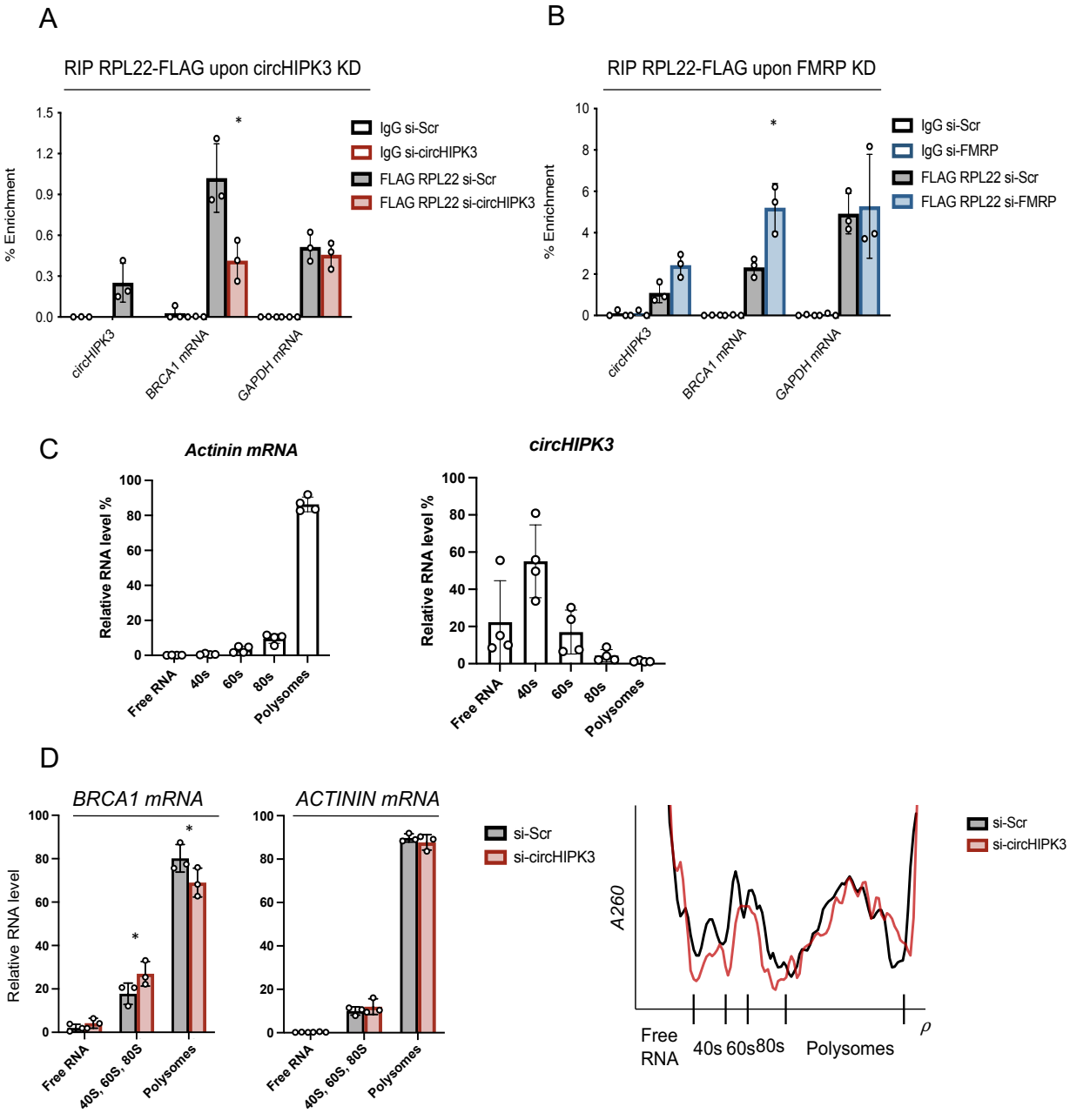
A
RIP RPL22-FLAG upon circHIPK3 KD
% Enrichment
IgG si-Scr
IgG si-circHIPK3
FLAG RPL22 si-Scr
FLAG RPL22 si-circHIPK3
circHIPK3
BRCA1 mRNA
GAPDH mRNA
B
RIP RPL22-FLAG upon FMRP KD
% Enrichment
IgG si-Scr
IgG si-FMRP
FLAG RPL22 si-Scr
FLAG RPL22 si-FMRP
circHIPK3
BRCA1 mRNA
GAPDH mRNA
C
Actinin mRNA
circHIPK3
Relative RNA level %
Free RNA
40s
60s
80s
Polysomes
D
BRCA1 mRNA
ACTININ mRNA
Relative RNA level
Free RNA
40S, 60S, 80S
Polysomes
si-Scr
si-circHIPK3
A260
Free RNA
40s 60s
80s
Polysomes
ρ

E

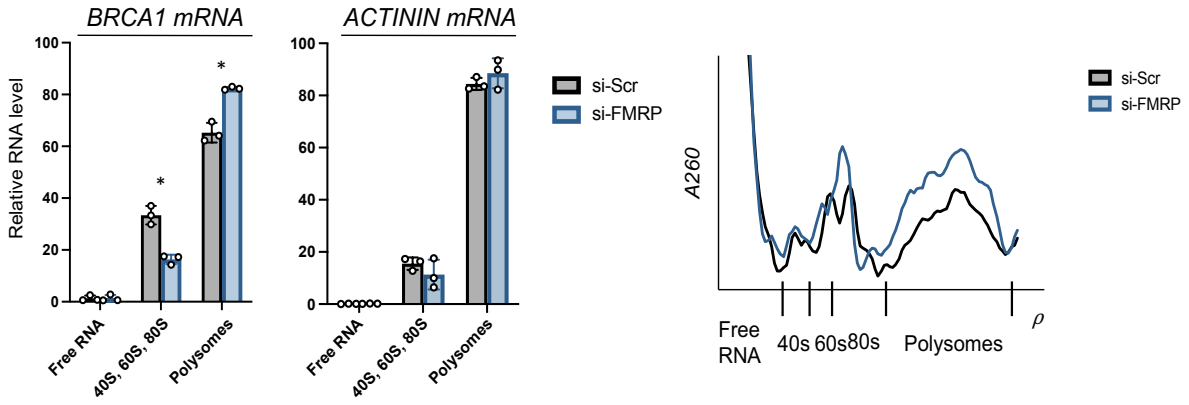

Fig. 22

(A-B) RNA enrichment measured by qRT-PCR of circHIPK3, *BRCA1* mRNA and *GAPDH* mRNA in RPL22-FLAG and IgG RIP assay performed in RD cells in si-scr/si-circHIPK3 (*BRCA1* p=0,020) condition (A) or si-scr/si-FXR2+FMRP (*BRCA1* p=0,0449) condition (B). n=3. (C) qRT-PCR experiment showing the distribution of circHIPK3 and *ACTININ* mRNA free, associated to 40S and 60S subunits, 80S monosomes or polysomes in sucrose gradient. n>3. (D-E) Left, RNA enrichment measured by qRT-PCR of *BRCA1* mRNA and *ACTININ* mRNA free, associated to ribosome subunits and monosomes or to polysomes in si-scr/si-circHIPK3 (*BRCA1* polysomes p=0,028, monosomes=0,034) conditions (D) or si-scr/si-FXR2+FMRP (BRCA1 polysomes p=0,016, monosomes=0,016) conditions (E). Right, polysome profile of RNA in si-scr/si-circHIPK3 (D) or si-scr/si-FXR2+FMRP (E) RD cells obtained by sucrose gradient.

Data are represented as mean of enrichment versus input (A-B) ±SD or as percentage of RNA related to total RNA (C-D-E).

The inhibition of circHIPK3/*BRCA1* mRNA interaction promotes DNA damage and sensitizes RD cells to DNA damage-inducing agents.

Once identified the mechanism through which circHIPK3 regulates BRCA1 expression, we decided to investigate the phenotypic effects determined by the inhibition of circHIPK3/*BRCA1* interaction.
BRCA1 is involved in different crucial cellular pathways that preserve genome stability, such as DNA damage repair, DNA damage-induced cell cycle checkpoint activation, chromatin remodelling, transcriptional regulation and apoptosis. In particular, BRCA1 is an essential mediator for DNA-repair of Double Strand Breaks (DBSs) through the error-free Homologous Recombination (HR) pathway and its down-regulation is associated to different kind of cancer, especially the breast and ovarian ones. However, according to the AACR Project GENIE, only 1.59% of rhabdomyosarcoma tumours present mutations in the BRCA1 gene. Moreover, contrary of what could be expected, St. Jude Children's Research Hospital database shows a higher expression of BRCA1 protein levels in RMS samples in comparison with myoblasts or myotubes (Figure 23A). In line with that, we also observed an increase of both BRCA1 RNA and protein levels in RH4 and RD cell lines compared to myoblasts (Figure 23B). All these data together indicate that, as well as circHIPK3, also BRCA1 is upregulated in Rhabdomyosarcoma.

Considering the essential role of BRCA1 in regulating DNA-damage repair, we decided to test whether circHIPK3 knockdown can alter the DNA-damage repair in RD cells. Upon circHIPK3 knockdown, we detected an accumulation of DNA damage in RD cells by Comet assay which was partially rescued by the ectopic overexpression of BRCA1 protein (Figure 23C). Moreover, the increased levels of the DNA-

damage associated phosphorylated histone variant γ-H2AX, detected by immunofluorescence, also indicate an increase of DNA-damage in absence of circHIPK3 (Figure 23D). Notably, no alterations in DNA damage were observed upon depletion of the linear *HIPK3* mRNA (Figure 23E).

BRCA1 is mainly involved in DSBs repair through HR, but some works also reported its role in other DNA-damage repair pathways[108,109], in particular the Non-Homologous End Joining (NHEJ), an error-prone pathway which can repair DSBs before DNA replication.
To dissect the specific DNA damage repair pathway affected upon circHIPK3 knockdown, we took advantage of two reporter cellular systems: U2OS DR-GFP and U2OS EJ5-GFP. In U2OS DR-GFP cells, the restoration of a functional GFP gene depends on the repair of a SceI nuclease-mediated DSBs by the HR repair pathway, while in U2OS EJ5-GFP cells it depends on the activation on NHEJ repair pathway. At first, we confirmed that, as in RD, also in U2OS cells (osteosarcoma), circHIPK3 knockdown induces a downregulation of BRCA1 protein (Figure 23F). We then measured by FACS the percentage of GFP positive cells in U2OS DR-GFP and U2OS EJ5-GFP cells after SceI expression. FACS analysis indicated that HR pathway activation, which resulted, as expected, almost totally abrogated after BRCA1 knockdown, is also impaired after circHIPK3 depletion (GFP reduction of 40%) (Figure 23G) consistently to the observed BRCA1 protein reduction. Testing the NHEJ we also found a significant, though lower (28%), reduction of GFP production after circHIPK3 knockdown, while the depletion of BRCA1 did not show any effect on NHEJ activation (Figure 23H). These data indicate that circHIPK3 also affects at a minor extent the NHEJ pathway through a mechanism independent from BRCA1,

consistently with the fact that BRCA1 ectopic expression does not totally restore circHIPK3 KD-induced DNA damage.

Fig. 23

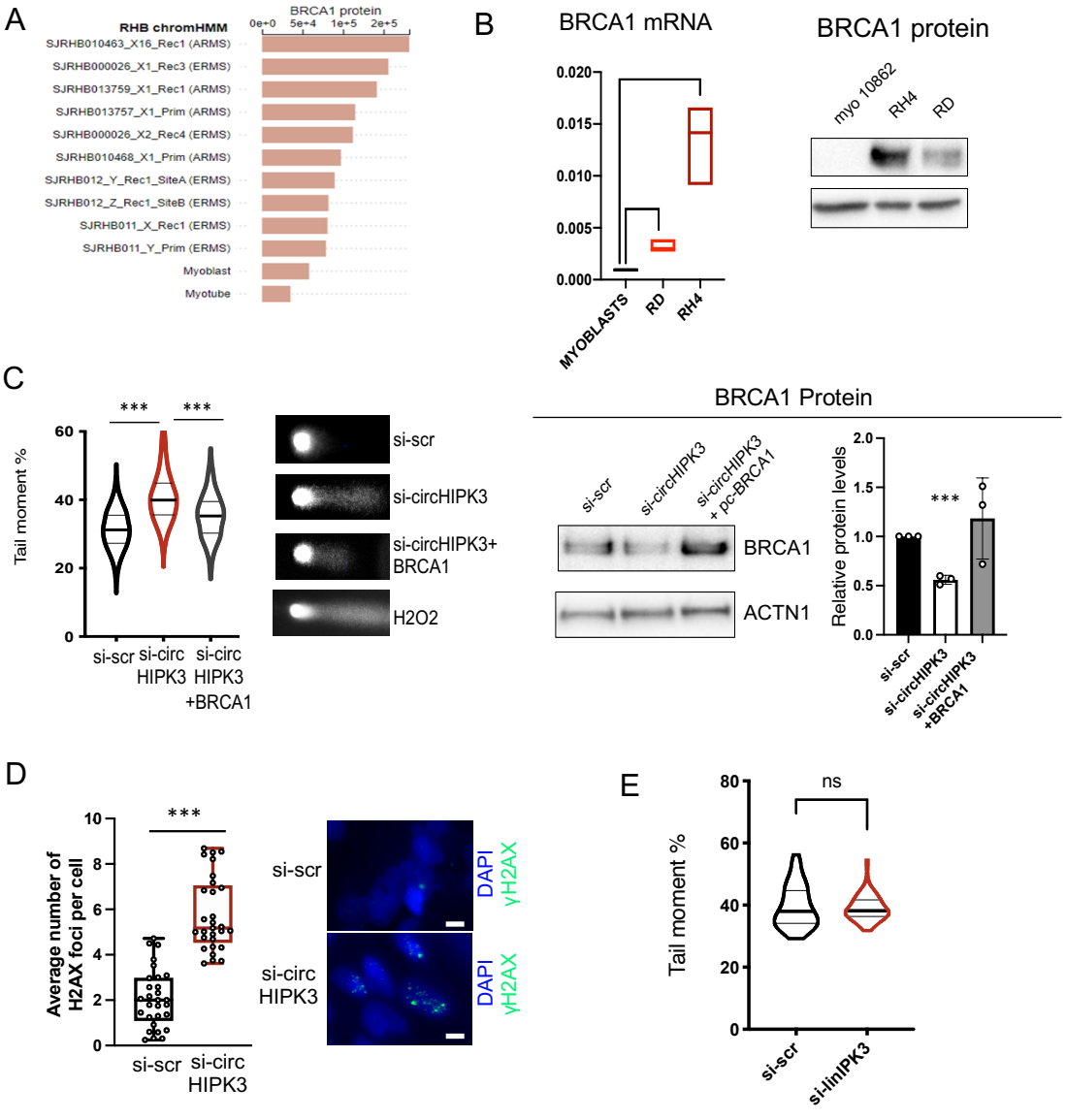

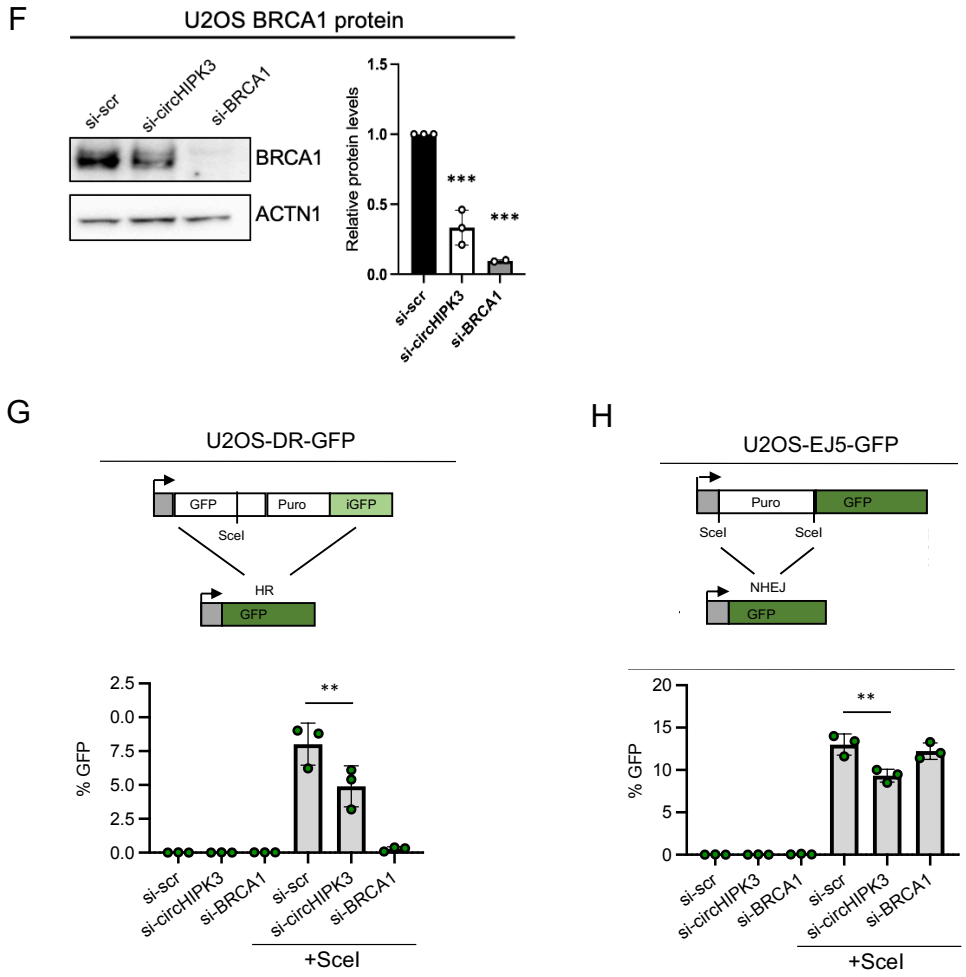

Fig. 23
(A) BRCA1 protein levels in orthotopic RMS patient-derived xenografts, compared to healthy myoblasts and myotubes. Data from https://pecan. stjude.cloud/proteinpaint/study/RHB2018.
(B) Left, data derived from RNA-sequencing (GSE207453; Dattilo *et al.*, 2023) showing BRCA1 RNA levels (relative to *GAPDH* mRNA), expressed in TPM, in myoblasts, RD (p=0,0036) and RH4 (p=0,0180) cells. n=3. Right, protein quantification (relative to

GAPDH) and representative western blot of BRCA1 in 10862 human myoblasts, RH4 and RD cells. n=3. (C) Left, representative COMET images of the different experiments and quantification of the tail moment in the Comet assay in si-scr and si-circHIPK3 ($p<0,0001$) and si-circHIPK3+pc-BRCA1 ($p<0,0001$) conditions. n=3. Right, protein quantification (relative to ACTININ) and representative western blot of BRCA1 protein in RD cells treated with si-scr, si-circHIPK3 ($p <0,0001$) and si-circHIPK3+pc-BRCA1 (ectopic expression of BRCA1). n=3. (D) Representative immunofluorescence images of γH2AX (green) merged with DAPI DNA-staining (blue) in si-scr and si-circHIPK3 ($p<0,0001$) conditions and quantification of γH2AX foci per cell. n=3. (E) Right, quantification of the tail moment in the Comet assay in si-scr and si-linHIPK3 conditions. n=3 (F) Protein quantification (relative to ACTININ) and representative western blot of BRCA1 protein in U2OS cells treated with si-scr, si-circHIPK3 ($p =0,0008$) and si-BRCA1($p<0,0001$). n=3. Data are represented as mean of BRCA1 protein levels ± standard deviation. (G-H) Left, cartoon depicting the reporter construct to detect HR in U2OS-DR GFP (G) and NHEJ in U2OS- EJ5 GFP (H). Right, percentage of GFP positive cells in si-scr, si-circHIPK3 ($p=0.005$ and $p=0.007$) and si-BRCA1 conditions in non-transfected and SceI transfected cells. n=3.

Induction of DNA damage, with chemotherapeutics agents such as cisplatin (CDDP) and Doxorubicin (Dox), represents one of most common strategies used in therapy to promote DNA damage and cancer cells death.
We, then, wondered whether the accumulation of DNA-damage due to circHIPK3-mediated BRCA1 downregulation could strengthen the effects of DNA-damage inducing agents against RD cells. In circHIPK3-depleted RD cells, we observed a reduced viability and an increase apoptosis rate (observed as an increase of PARP1 levels) after treatment for 24h with 25 μg/ml CDDP or 5 μM DOX compared to si-scr treated cells (Figure 24A-B). These data indicate that circHIPK3 knockdown makes RD cells more sensitive to those DNA-damage inducing agents.

A more recent approach to target cancer cells is the induction of synthetic lethality in BRCA1/2 deficient cells with PARP inhibitors. Synthetic lethality occurs when two conditions separately are not able to induce cell death, but they result lethal if they exist together. PARP1 is mainly involved in the repair pathway of Single Strand Breaks (SSB). In case of PARP1 inhibition, the replication fork tends to collapse with consequent formation of DSBs, that can be repaired by HR. In BRCA1/BRCA2 deficient cells, the misfunction of the HR pathway does not allow the repair of the DSBs induced by PARP1 inhibition, leading to DNA damage accumulation and cell death by synthetic lethality. Therefore, the inhibition of PARP1 results only lethal in cancer cells with mutated non-functional BRCA1/2, which cannot repair DSBs through HR, and not in healthy cells.
We asked whether circHIPK3 knockdown, by inducing a down-regulation of BRCA1, could induce synthetic lethality also in BRCA1 wild-type cells such as RD. We treated RD si-scr and si-circHIPK3 cells 24h with Talazoparib 25μM, a PARP inhibitor in clinical use, and we calculated the percentage of surviving cells in respect to the corresponding cells not treated with the inhibitor. The depletion of circHIPK3 reduces the mean survival rate, after Talazoparib treatment, from 74,9% (si-scr) to 41,5% (si-circHIPK3), compared to non-treated cells (Figure 24C). Moreover, we demonstrated that also the specific inhibition of circHIPK3/*BRCA1* interaction through LNA BSJ, can sensitize RD cells to Talazoparib (decrease of mean survival rate from 73% to 47,7%) (Figure 24C). These data indicate that the blockage of circHIPK3-mediated BRCA1 regulation can sensitize BRCA1 wild-type cancer cells to PARP inhibitors, expanding the types of tumours that could be treated with these chemotherapeutic agents.

Fig. 24

A

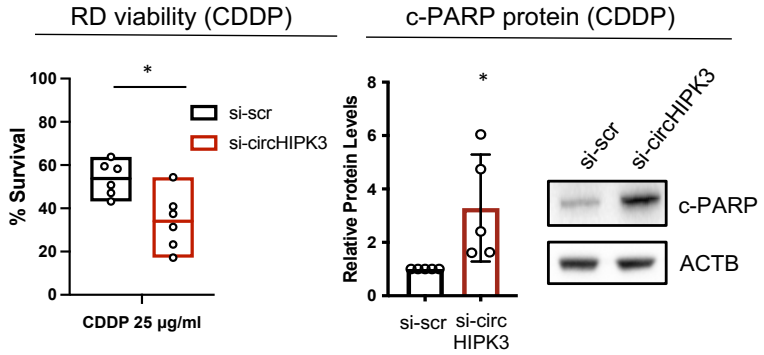
RD viability (CDDP)
c-PARP protein (CDDP)
% Survival
si-scr
si-circHIPK3
CDDP 25 µg/ml
Relative Protein Levels
si-scr
si-circ HIPK3
c-PARP
ACTB

B

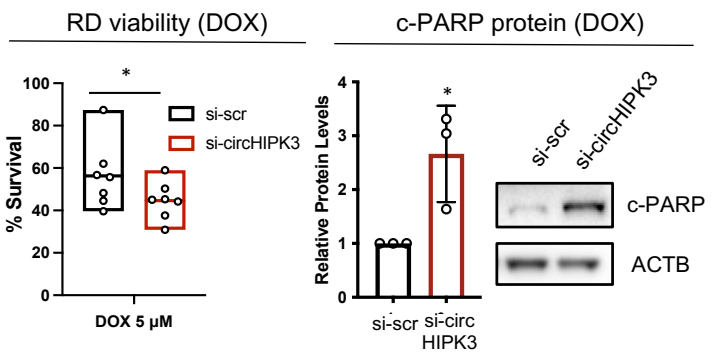
RD viability (DOX)
c-PARP protein (DOX)
% Survival
si-scr
si-circHIPK3
DOX 5 µM
Relative Protein Levels
si-scr
si-circ HIPK3
c-PARP
ACTB

C

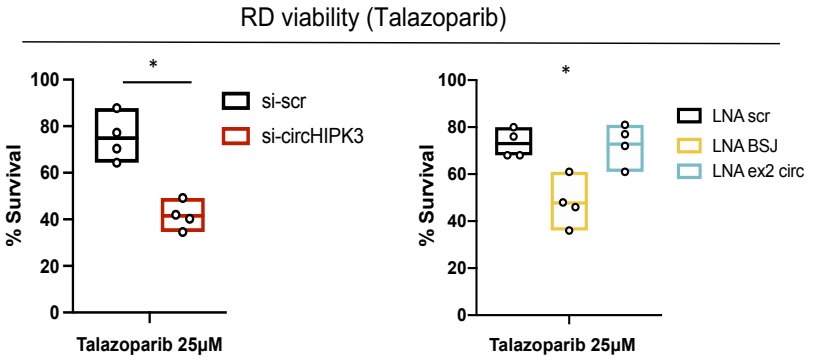
RD viability (Talazoparib)
% Survival
si-scr
si-circHIPK3
Talazoparib 25µM
LNA scr
LNA BSJ
LNA ex2 circ
Talazoparib 25µM

Fig. 24
(A) Left, boxplots representing the percentage of survival of si-scr (black) or si-circHIPK3 (red) (p=0,0231) RD cells treated for 24h with Doxorubicin (DOX) 5 μM. n>3. Right, representative western blot and protein quantification (rel.to ACTB) of cleaved-PARP in si-scr and si-circHIPK3 (p=0,0325) RD cells treated for 24h with Doxorubicin (DOX) 5 μM. n=3. (B) Left, boxplots representing the percentage of survival of si-scr (black) or si-circHIPK3 (red) (p=0,0211) RD cells treated for 24h with Talazoparib 25 μM. n=4. Right, boxplots representing the percentage of survival of LNA-scr (black), LNA-BSJ (yellow) (p=0,0256), LNA-ex2-circ (cyan) transfected RD cells treated for 24h with Talazoparib 25 μM. n>3.
Data are represented as mean of relative protein levels in figures 6B, F right, G right, ±SD.

CircHIPK3-mediated BRCA1 regulation is conserved in several cancer cell lines

Considering that circHIPK3 results upregulated in different cancer types, we asked whether circHIPK3-mediated BRCA1 regulation could exist also in other tumoral contexts.
As in the case of Rhabdomyosarcoma, BRCA1 is only spuriously mutated in other cancer cell types (only 3% of cases according to AACR Project GENIE).
We consulted GENT database, which contain data from patients, and we observed an upregulation of *BRCA1* mRNA in various cancer types compared to healthy tissues (Figure 25A). Notably, circHIPK3 is also upregulated in most of these tumours. Our hypothesis is that, during tumour progression, occurs a selection of cancer cells with high circHIPK3, and consequently BRCA1, levels, which can prevent lethal DNA damage accumulation and can continue to proliferate. FMRP is ubiquitously expressed, so our regulation model would be easily exportable to other cancer types.

We then decided to test whether the circHIPK3/*BRCA1* model is conserved in other cell lines which represent tumoral contexts in which both circHIPK3 and BRCA1 result upregulated. In A172 cells, model of glioblastoma, SKOV-3, model of ovarian adenocarcinoma and MCF7, model of breast ductal carcinoma, we observed *BRCA1* enrichment in circHIPK3 pulldown, a decrease of BRCA1 protein upon circHIPK3 depletion, increased sensitivity to cisplatin or doxorubicin and induction to synthetic lethality with Talazoparib (Figures 25B-C-D). In A172 and MCF7 we also observed an increase of BRCA1 protein after the knockdown of FMRP (Figure 25E). These data indicate that circHIPK3-mediated BRCA1 regulation could represent a widespread mechanism conserved and targetable in different tumoral contexts.

Fig. 25

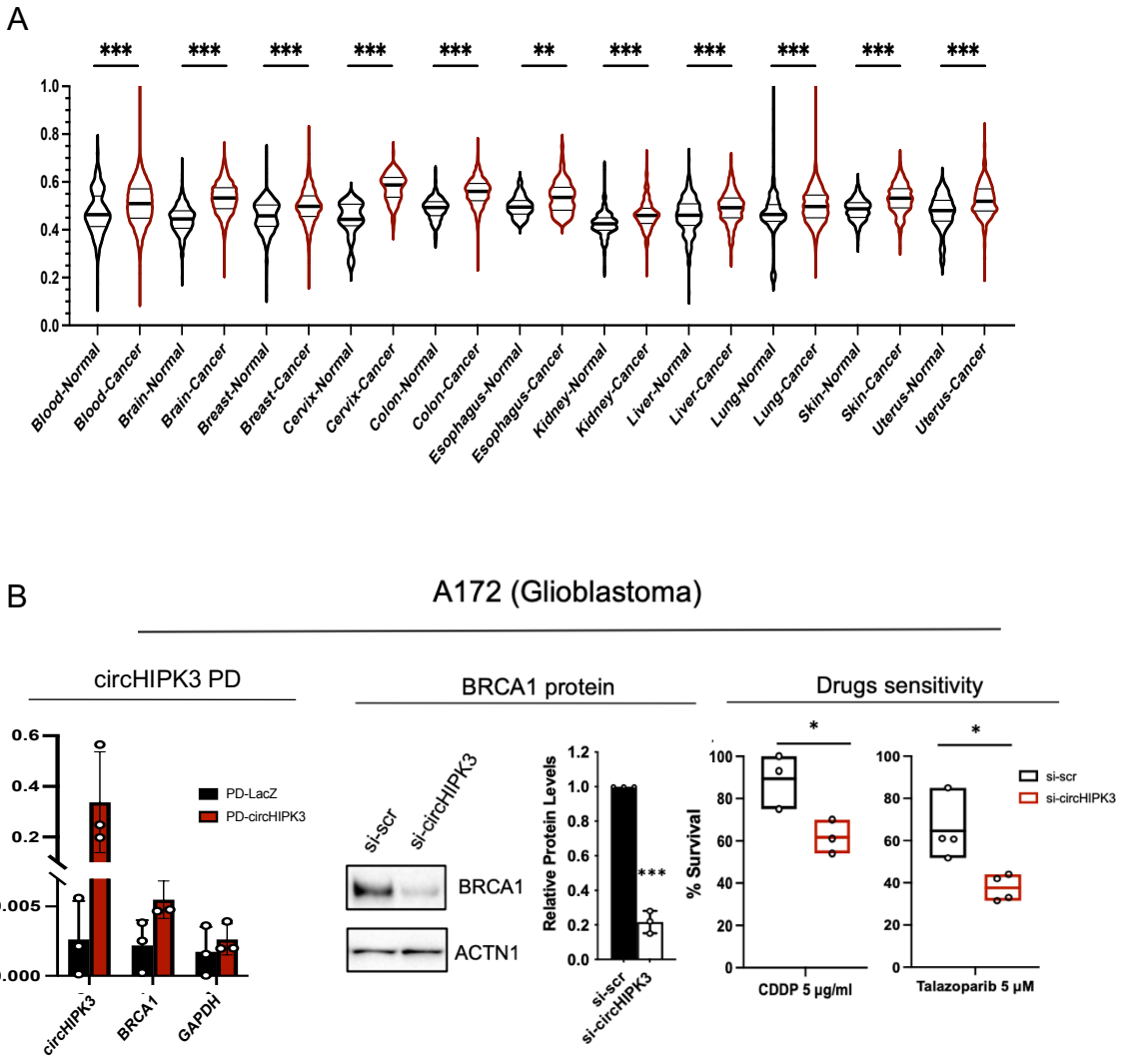
A
***
**
1.0
0.8
0.6
0.4
0.2
0.0
Blood-Normal
Blood-Cancer
Brain-Normal
Brain-Cancer
Breast-Normal
Breast-Cancer
Cervix-Normal
Cervix-Cancer
Colon-Normal
Colon-Cancer
Esophagus-Normal
Esophagus-Cancer
Kidney-Normal
Kidney-Cancer
Liver-Normal
Liver-Cancer
Lung-Normal
Lung-Cancer
Skin-Normal
Skin-Cancer
Uterus-Normal
Uterus-Cancer
B
A172 (Glioblastoma)
circHIPK3 PD
PD-LacZ
PD-circHIPK3
0.6
0.4
0.2
0.005
0.000
circHIPK3
BRCA1
GAPDH
BRCA1 protein
si-scr
si-circHIPK3
BRCA1
ACTN1
Relative Protein Levels
1.2
1.0
0.8
0.6
0.4
0.2
0.0
***
si-scr
si-circHIPK3
Drugs sensitivity
% Survival
100
80
60
40
20
0
*
CDDP 5 µg/ml
Talazoparib 5 µM
si-scr
si-circHIPK3

C

SKOV-3 (Ovarian adenocarcinoma)

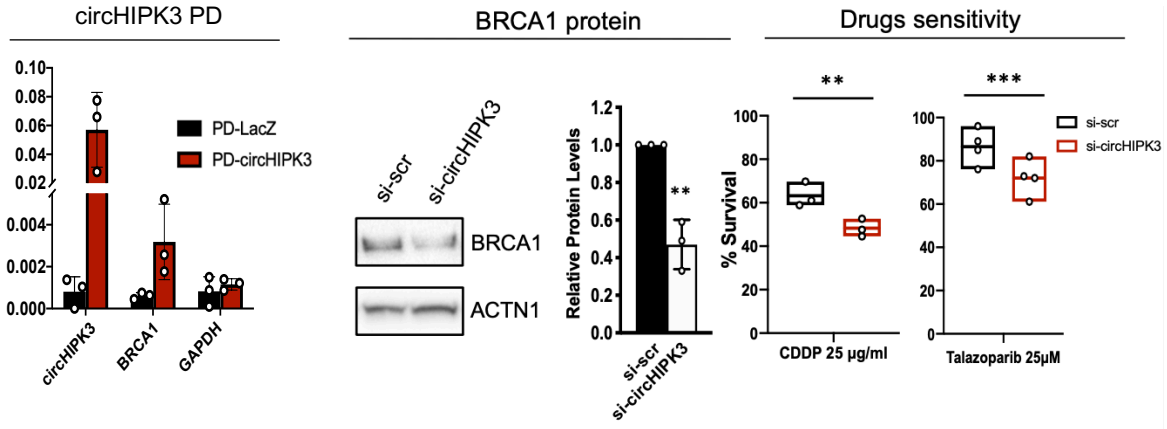

D

MCF7 (breast ductal carcinoma)

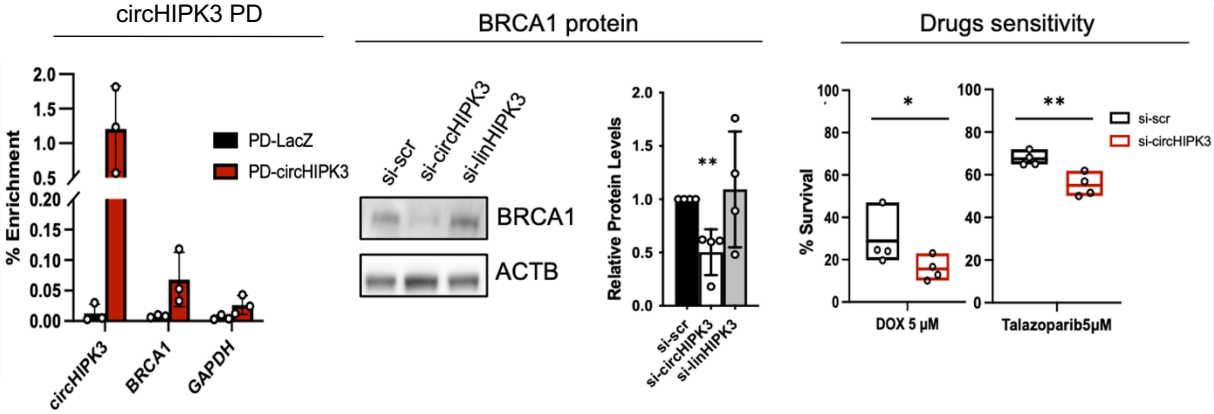

E

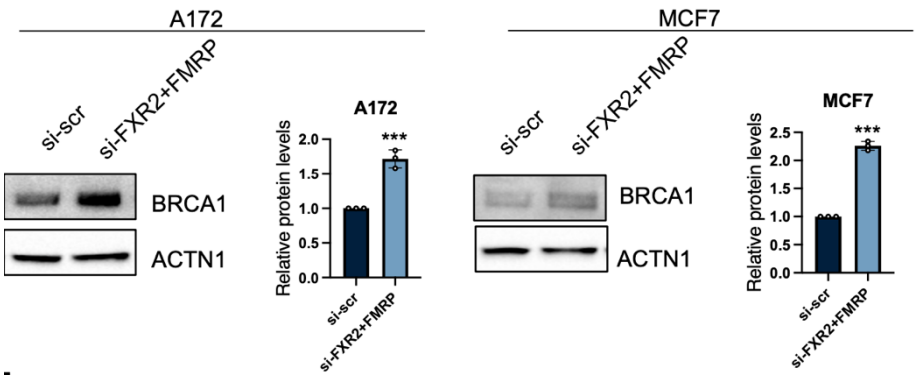

Fig. 25

(A) RNA levels (relative to *β-actin* mRNA) of *BRCA1* mRNA measured by RNA-seq in various cancer types and relative healthy counterparts, from GENT2 database. (B) Left, RT-qPCR showing the enrichment of circHIPK3, *BRCA1*, and *GAPDH* mRNA in circHIPK3 native pull-down and control LacZ pull-down in A172 cells. n = 3. Middle, protein quantification (rel. to ACTININ) and representative western blot of BRCA1 in si-scr and si-circHIPK3 ($p < 0.0001$) A172 cells. n = 3. Right, boxplots representing the survival percentage of si-scr (black) or si-circHIPK3 (red) (CDDP $p = 0.0146$; Tal $p = 0.0144$) A172 cells treated for 48 h with cisplatin (CDDP) or Talazoparib. n=3. (C) Left, RT-qPCR showing the enrichment of circHIPK3, *BRCA1*, and *GAPDH* mRNA in circHIPK3 native pull-down and control LacZ pull-down in SKOV3 cells. n = 3. Middle, protein quantification (rel. to ACTININ) and representative western blot of BRCA1 in si-scr and si-circHIPK3 ($p = 0.0022$) SKOV-3 cells. n = 3. Right, boxplots representing the survival percentage of si-scr (black) or si-circHIPK3 (red) (CDDP $p = 0.0053$; Tal $p = 0.0008$) SKOV-3 cells treated for 24 h with cisplatin (CDDP) or 30 h with talazoparib. n=3. (D) Left, RT-qPCR showing the enrichment of circHIPK3, BRCA1, and GAPDH mRNA in circHIPK3 native pull-down and control LacZ pull-down in MCF7 cells. n = 3. Middle, RNA levels (rel. to *GAPDH*) of circHIPK3, *HIPK3*, and *BRCA1* mRNA in si-scr, si-circHIPK3 (circHIPK3 $p < 0001$), and si-linHIPK3 MCF7 cells (HIPK3 $p < 0001$); protein quantification (rel. to ACTB) and representative western blot of BRCA1 in si-scr, si-

circHIPK3 ($p = 0.035$), and si-linHIPK3 MCF7 cells. $n > 3$. Right, boxplots representing the survival percentage of si-scr (black) or si-circHIPK3 (red) (DOX $p = 0.0382$; Tal $p = 0.0015$) MCF7 cells treated for 24 h with doxorubicin (DOX) or 48 h with talazoparib. $n > 3$. (E) Protein quantification (relative to ACTININ) and representative western blot of BRCA1 protein in A172 and MCF7 cells in si-scr and and si-FXR2+FMRP (A172 p=0,0007; MCF7 p<0,0001) conditions. n=3.

The inhibition of FMRP/*BRCA1* mRNA interaction reverts BRCA1 haploinsufficiency in breast HBOC cell models

Due to its crucial role in HR repair after DNA damage, BRCA1 partial or total abrogation is associated with the onset of different kind of tumours. In the Hereditary Breast and Ovarian Cancer (HBOC) syndrome, the heritage of one mutated allele, which usually produces a truncated protein destined to degradation, causes BRCA1 haploinsufficiency, consequent accumulation of DNA damage and genome instability in healthy cells, making them more prone to become tumoral. Individuals with this condition have high possibility to develop tumours, particularly breast (45-87%) and ovarian cancer (35-63%)[115–117].

We, then, decided to test whether the inhibition of *BRCA1* mRNA interaction with FMRP, which we identified to act as a translational repressor of BRCA1, could restore physiological protein levels in mutated cells characterized by reduced BRCA1 expression. To mimic the BRCA1 haploinsufficiency condition which occurs in HBOC syndrome, we used an MCF7 BRCA1 hemizygous cell line (wt/del), obtained by CRISPR/Cas9-induced deletion of the entire coding region of the BRCA1 gene, leaving only one intact allele (Figure 26A). In both wt/wt and wt/del MCF7 cells, characterized by halved BRCA1 levels, the transfection of an LNA which blocks FMRP/*BRCA1* interaction (LNA ex23) (Figure 26B), corresponding to circHIPK3 BSJ sequence, induces an increase of BRCA1 protein levels. Notably, in wt/del MCF7 cells, the LNA ex23 restores the BRCA1 levels observed in non-transfected wt/wt cells (Figure 26C).
Coherently with the observed changes in BRCA1 levels induced by LNA ex23 transfection, we also noticed variations in DNA damage accumulation by COMET. In both wt/wt and wt/del cells the transfection of LNA ex23 induces a reduction

of DNA damage levels. In particular, in wt/del cells, characterised by higher DNA damage due to BRCA1 haploinsufficiency, the LNA restores the low DNA damage levels observed in the wt/wt cells (Figure 26D).

These data indicate that the blockage of FMRP/*BRCA1* interaction could rescue BRCA1 haploinsufficiency and opens the intriguing therapeutic possibility to prevent cancer onset in the HBOC syndrome.

Fig. 26

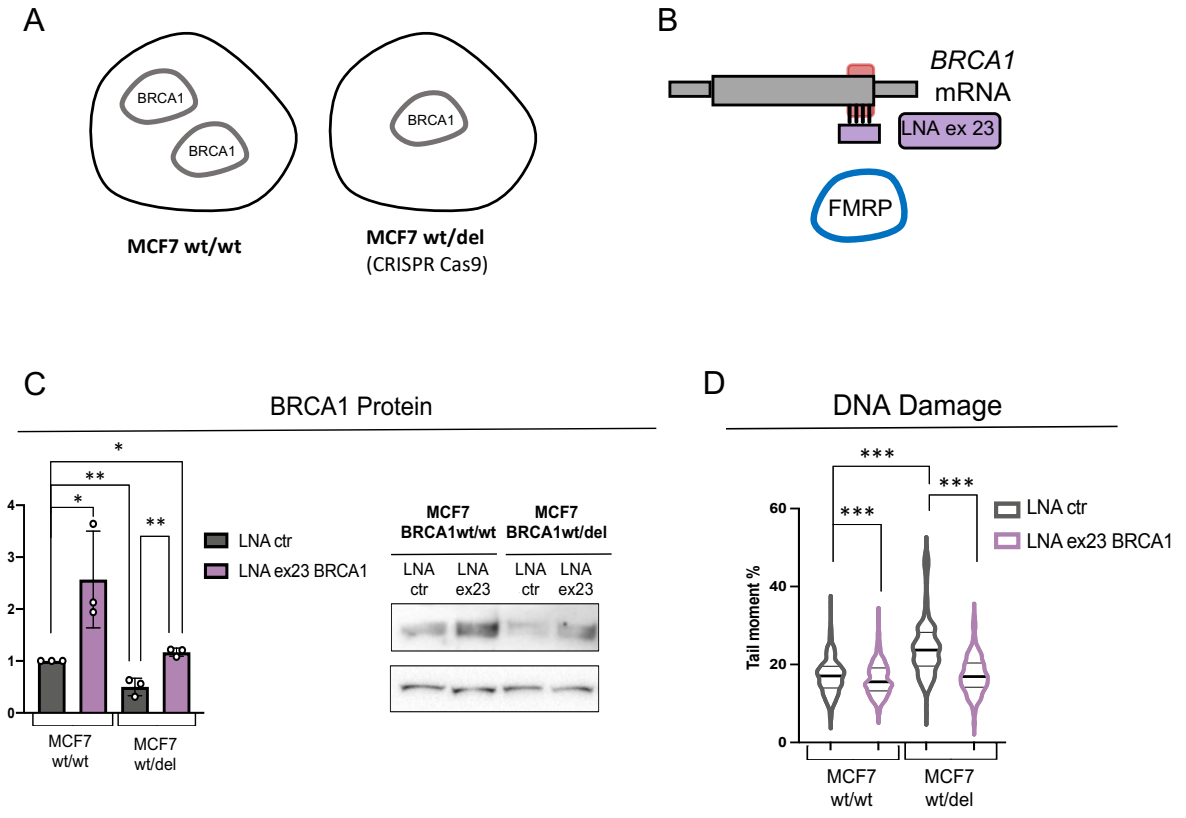

Fig. 26
(A) Cartoon representing MCF7 wt/wt and wt/del cells used to compare a physiological condition to a BRCA1 haploinsufficiency. (B) Representation of the LNA targeting FMRP binding site (LNA ex23) on BRCA1 mRNA (C) Protein quantification (rel.to ACTININ) and representative WB of BRCA1 in wt/wt and wt/del MCF7 cells transfected with LNA ctr or LNA ex23. Data are represented as mean of protein levels ±SD (D) Quantification of the tail moment in the Comet assay in wt/wt and wt/del MCF7 cells transfected with LNA ctr or LNA ex23.

CONCLUSIONS AND DISCUSSION

Circular RNAs are molecules with peculiar and interesting features such as high stability, tissue- and developmental stage-specific expression. Due to these characteristics and because of their deregulated expression in many pathological contexts, the interest in understanding their role in the cells have recently increased. In particular, in pathological contexts, circRNAs could be proposed both as therapeutic vectors[155], especially due to their high stability, and as therapeutic targets.

For most of the circRNAs studied, a miRNAs sponging role has been proposed, but this competing endogenous activity strictly depends on the specific miRNA signature of the cell and on stoichiometry issues such as the expression levels of all the RNAs involved in the regulation. We believe that direct circRNAs/mRNAs interactions could represent more general and widespread mechanisms and that their finding could allow to develop therapeutic strategies more direct and applicable to different tumoral contexts.
In particular, different works suggest that circHIPK3, a circRNA expressed at high levels in many tissues and deregulated in different kind of cancers, act by interacting with miRNAs, preventing their binding to target mRNAs[144–146].To investigate whether circHIPK3 could, instead, influence cancer progression with a more general and widespread mechanism, we looked for possible widely expressed mRNA interactors.

We carried out our investigation in Rhabdomyosarcoma cells for three main reasons: a) circHIPK3 is highly expressed in the skeletal muscle (circATLAS); b) standard treatments for Rhabdomyosarcoma are, in many cases, still not sufficient and can cause important side-effects in children, hence there

is the need to find new molecular mechanisms to be targeted c) we found that circHIPK3 results up-regulated in both Rhabdomyosarcoma cell lines and biopsies (Figure 8B-C)

AMT (4'-aminomethyl-4,5',8-trimethylpsoralen)-crosslinking pulldown represents the gold-standard for the identification of direct RNA-RNA interactions *in vivo*[148,156,157], since the psoralen derived compound intercalates into RNA duplexes and, upon 365 nm UV irradiation, generates inter-strand adducts between juxtaposed pyrimidine bases, crosslinking RNA molecules that are in very close proximity[148]. Through this approach, we found different putative mRNAs interactors of circHIPK3 that we validated in both the Alveolar (RH4) and Embryonal (RD) RMS cell models (Figure 11A-B).

We then decided to carry on our investigation in RD cells since in this cell model only circHIPK3, and not the linear *HIPK3* mRNA, results upregulated compared to myoblasts (Figure 8B), suggesting a specific regulatory role of the circular molecule in the tumoral context. In RD cells, after circHIPK3 knock-down, we observed a deregulation of several of its interactors suggesting a role of the circRNA in their regulation (Figure 12B). Among them, we decided to focus on BRCA1 since it is essential for DNA-damage repair and its deregulation is associated with cancer.
We observed that circHIPK3 regulates both BRCA1 RNA and protein levels (reduced after circHIPK3 knock-down) (Figure 12C) and we showed that the RNA-RNA interaction occurs between a region across the BSJ of circHIPK3 and a sequence on the last coding exon (exon 23) of *BRCA1* mRNA (Figures 16A-B-C). The involvement of the BSJ of circHIPK3 in the regulatory interaction with *BRCA1* mRNA suggests that the regulation is specifically mediated by the circRNA. Notably, the transfection in cells of an LNA antisense oligonucleotide which specifically targets

circHIPK3 BSJ, blocking its interaction with *BRCA1* mRNA, induces a strong downregulation of BRCA1 protein (Figure 17A-B).

An issue to be considered is the possible involvement of *HIPK3* mRNA in the observed BRCA1 regulation. Considering that part of *BRCA1*-interacting site on circHIPK3 is also present in *HIPK3* mRNA and that the pulldown probes for circHIPK3 also targets the second exon of the mRNA, we performed a series of experiments in order to exclude the involvement of the linear counterpart in BRCA1 regulation. First of all, for all the crucial experiments in which we knocked-down circHIPK3, we also used, as a control, a siRNA against the *HIPK3* mRNA and we did not observe neither a reduction of BRCA1 protein (Figure 12C), nor an accumulation of DNA-damage (Figure 23E), indicating that BRCA1 regulation is specifically mediated by the circRNA. Moreover, to exclude any possible interaction between *HIPK3* mRNA and *BRCA1* mRNA, we performed a pulldown of circHIPK3 after the knock-down of the circRNA (Figure14A) and a pulldown of *HIPK3* mRNA (Figure 14B) in RD cells and, in both cases, we didn't observe an enrichment of *BRCA1*, indicating that its presence in circHIPK3 pulldown was caused by the specific interaction with circHIPK3.

Once demonstrated the role of circHIPK3 in regulating BRCA1 expression, we looked for possible RNA-Binding Proteins (RBP) involved in this regulation. The catRAPID v2.122148 algorithm, which computes RNA-protein interaction propensities, predicted FMRP and its paralog FXR2 as BRCA1-binding RBPs with the highest interaction ranking (Figure 18A). By consulting CLIP-seq published data[152,154] (Figure 18B) and by performing different *in vitro* and *in vivo* experiments in our system (Figures 19A, 20A,

20B), we showed that the RBP FMRP interacts with different regions of *BRCA1* mRNA and that circHIPK3, through the interaction with the *BRCA1* exon 23, can prevent the binding of FMRP to this specific site of the mRNA.
We discovered that FMRP acts as an inhibitor of BRCA1 translation (Figures 21C, 22B and 22E) and that circHIPK3, by preventing the binding of the RBP to the transcript, can promote BRCA1 protein production (Figure 22C). Notably, after sucrose-gradient polysome fractionation, we found that most of circHIPK3 is associated to the 40S and 60S ribosome subunits (Figure 22D). This observation suggests that, though it is not associated to polysomes and, so, it is not actively translated, the circRNA is present on the ribosomes, probably with the aim of regulating the translation of other transcripts, such as *BRCA1* mRNA.
How the circRNA can significantly influence BRCA1 translation by occupying only one FMRP binding site on *BRCA1* mRNA has still to be elucidated.
We hypothesize that maybe the proximity to the stop codon could represent an important factor for the FMRP-mediated translational inhibition of BRCA1.

Once identified the molecular mechanism through which circHIPK3 promotes BRCA1 expression, we confirmed that the depletion of the circRNA leads to DNA-damage accumulation (Figure 23C-D) mainly through the impaired BRCA1 activity in the Homologous Recombination repair pathway (Figure 23G).
We validated the circHIPK3-mediated mechanism of BRCA1 regulation also in other cell lines (Figure 25B-C-D-E), suggesting that the circRNA has a role in preventing DNA damage accumulation in different tumoral contexts.

A question that we asked is why cancer cells should up-regulate a circRNA which increases the levels of a protein commonly considered as an oncosuppressor.
By consulting GENT2 (Figure 25A) and TCGA (Figure not shown) databases, we discovered that, in contrast to what is believed, also BRCA1 results up-regulated in many tumours compared to the healthy condition. In RMS cell lines we also experimentally validated BRCA1 protein upregulation in respect to myoblast (Figure 23B).
We hypothesized that, in the tumoral context, cancer cells which up-regulate circHIPK3 and, consequently, BRCA1, could be selected fort their ability to prevent possible lethal DNA damage accumulation.
The observed up-regulation of BRCA1 expression in several tumoral contexts leads to an important consideration. Proteins that are commonly named “oncosuppressors” normally protect cells from tumoral transformation by sensing pro-tumoral alterations and promoting their resolution. Hence, the deregulation of these proteins is linked to higher cancer development probability. However, once that the malignant transformation has occurred, we cannot exclude that, during tumour progression, cancer cells with high levels of “genome guardians”, such as BRCA1, could be selected for their capability to proliferate without accumulating death-promoting alterations. The clonal expansion of these selected cells could explain the upregulation of both circHIPK3 and BRCA1 that occurs in different tumoral contexts.
Accordingly, the balance between DNA damage and DNA repair is important to be maintained by the cell in different stages of its life cycle and the disruption of this balance, to one direction or to another one, could represent a therapeutic strategy. In particular, we hypothesized that both an inhibition of circHIPK3/*BRCA1* interaction, with consequent BRCA1 down-regulation, and the inhibition of

FMRP/*BRCA1* interaction, with consequent BRCA1 up-regulation, could represent therapeutic approaches depending on the context.

In cancer cells with high wild-type levels of BRCA1, RD, A172 (glioblastoma), SKOV3 (ovarian adenocarcinoma) and MCF7 (breast adenocarcinoma), we observed that the depletion of circHIPK3, with consequent BRCA1 downregulation, strengthen the effects of DNA-damage inducing drugs such as cisplatin and doxorubicin (Figures 24A-B, 25B-C-D). Moreover, the absence of the circRNA, or the specific blocking of its interaction with *BRCA1* mRNA through the BSJ-targeting LNA (for RD), makes those BRCA1 wt cancer cells sensible to PARP-inhibitors, inducing synthetic lethality (Figures 24C, 25B-C-D).
Hence, the inhibition of circHIPK3/*BRCA1* interaction opens the possibility to treat BRCA1 wt cells with DNA-damage targeting chemotherapeutics that are generally used for the treatment of BRCA1 mutated tumours.

On the other hand, in the context of breast cells with BRCA1 haploinsufficiency, due to BRCA1 loss-of functions mutations in one gene, the increase of the wild-type BRCA1 levels could allow to prevent cancer-promoting DNA-damage accumulation.
In a breast cell line with a CRISPR/Cas9-induced deletion of one BRCA1 allele, which mimics this BRCA1 haploinsufficiency that occurs in HBOC syndrome (Figure 26A), we observed that the inhibition of FMRP/*BRCA1* mRNA interaction through an LNA (Figure 26B) restores physiological BRCA1 protein levels and reduce DNA-damage accumulation (Figure 26C-D).

Eventually, it is important to underline that in this work we decided to focus only on the specific molecular mechanism

involving circHIPK3, BRCA1 and FMRP. We have restricted the analysis to the effect of circHIPK3 on BRCA1 because of its essential role in the control of the DNA-damage repair, however, we cannot exclude that circHIPK3 could induce the observed phenotypic effects also through other interactors. Two of our experiments suggest that, in fact, circHIPK3 could also regulate DNA-damage repair through other mechanisms. First of all, BRCA1 ectopic expression does not totally rescue the DNA damage accumulation induced by circHIPK3 knockdown (Figure 23C); secondly, circHIPK3 knockdown also seems to affect NHEJ repair pathway independently from BRCA1 (Figure 23H). Other circHIPK3-interactors, such as RNF40 (Figure 11A-B), known to participate to protein recruitment to the site of DSBs, could be involved in circHIPK3-mediated DNA damage regulation. Similarly, we cannot exclude that, besides FMRP, other RNA-binding protein could also be involved in the circHIPK3-mediated regulation of BRCA1 expression.

To conclude, this work shows the importance of identifying specific RNA-RNA interactions to understand tumour-related mechanisms and to develop new targeted therapeutic approaches. The discovery of more circRNA/mRNA interactions could allow to expand the knowledge about the post-transcriptional regulation of cancer-related genes.

MATERIALS AND METHODS

Cell cultures

All cell lines were grown at 37 C and 5% CO2 and tested for mycoplasma contamination.

Wild-type human primary myoblasts (Telethon Biobank, obtained from a skeletal muscle biopsy of a 2-year old male child) were cultured in DMEM supplemented with 10% FBS, 2 mM L-glutamine, insulin 50 mg/ml, FGFb 25 ng/ml, EGF 1 ng/ml and penicillin-streptomycin 1X.

Human RD (embryonal rhabdomyosarcoma cell line), RH4 (alveolar rhabdomyosarcoma cell line), U2OS (osteosarcoma cell line), and modified U2OS DR-GFP and EJ5-GFP, A172 (glioblastoma cell line) and A549 (lung adenocarcinoma cell line) cells were cultured in DMEM high-glucose supplemented with 10% fetal bovine serum (FBS), 2 mM L-glutamine and 1% penicillin-streptomycin.

Human SKOV-3 cells (ovarian serous cystadenocarcinoma cell line) were cultured in RPMI 1640 medium supplemented with 10% fetal bovine serum (FBS), 2 mM L-glutamine and 1% penicillin-streptomycin.

Human MCF7 cells (invasive breast carcinoma cell line) cells were grown and maintained in Minimum Essential Medium Eagle supplemented with 10% fetal bovine serum, 1mM sodium pyruvate, 1x MEM Non-Essential Amino acids, 0.01mg/ml bovine insulin, 2mM L-Glutamine and penicillin/streptomycin.

Patients biopsies

Tumour samples from 8 primary RMS tumours, 3 ARMSs and 5 ERMSs, were obtained at diagnosis before any treatment from children admitted to the Department of Oncology at Alder Hey Children's NHS Foundation Trust, Liverpool, United Kingdom. Control RNA was extracted from normal skeletal muscle biopsies obtained from 3 children undergoing surgery

for non-oncological condi- tions. Institutional written informed consent was obtained from the patient's parents or legal guardians. The study underwent ethical review and approval according to the local institutional guidelines (Alder Hey Children's NHS Foundation Trust Ethics Committee, approval number 09/H1002/88).

RNAse R treatment

RNase R treatment was performed as follows: 1 µg of total RNA was diluted in 20 µL of water with 1u RNase R/µg and 2 µL of enzyme buffer (LGC Biosearch Technologies), then incubated 10 min at 37°C and purified by phenol-chloroform extraction.

Cell transfections

30 nM of siRNA (ON-TARGETplus, Dharmacon), 200 nM of miRNA-blockers LNA, 5 nM (for RD cells) or 20 nM (for MCF7 cells) of LNA (Integrated DNA Technologies) were transfected with Opti-MEM and Lipofectamine RNAiMAX Transfection Reagent (Invitrogen), according to the manufacturer's instructions. Unless differentially specified, the medium was replaced 6 h after transfection and cells were harvested 48 h after transfection. siRNAs and LNAs used are listed in Table1.

Western blot

Cells were detached with Trypsin-EDTA 1X and centrifuged at 1500 rpm for 5 minutes. Pellets were resuspended in Protein Extraction Buffer (100 mM Tris pH 7.5, EDTA 1 mM, SDS 2%) supplemented with PIC 2X (Complete- EDTA free, Roche–Merck), incubated 30 min at 4 C on a rotating wheel and centrifuged at 15000g for 15 min at 4 C. Proteins (20-30 mg for most of the experiments, quantified through Bradford reagent (Bio-Rad Protein Assay)) were heated 50 at 80 C for denaturation, incubated 50 in ice and were loaded

on 4%-12% bis-tris-acrylamide gel or, in case of BRCA1 detection, 3-8% Tris-acetate gel (ThermoFisher Scientific) for a 1-1.5h running process at 150V.Proteins were transferred to a nitrocellulose membrane through a 1-2h blotting process at 400 mA with BioRad blotting apparatus and a 20% methanol buffer. The membrane was blocked in 5% milk and hybridized with the specific primary antibody overnight at
4 C or 1 h at room temperature for HRP antibodies. Membranes hybridized with non-HRP antibodies, were then hybridized the morning after with the appropriate secondary antibody (Invitrogen) for 1-2 h at room temperature. Protein detection was carried out with WesternBright ECL Chemiluminescent HRP Substrate (Advansta) or with WesternBright Sirius Chemiluminescent HRP Substrate
(Advansta). Images were acquired with ChemiDoc MP Imager (Bio-Rad) and the analysis was performed using Image Lab 5.2.1 software (Bio-Rad). Images were linearly adjusted in contrast and brightness when necessary.

RNA isolation and analysis

For most of the experiments, total RNA was extracted with Direct-zol RNA Miniprep kit (Zymo Research) with a 15-minute DNase-I treatment according to the manufacturer's protocol. For IP and RNA pull-down experiments, and polysome fractionation experiments, RNA was precipitated through phenol/chloroform extraction.RNA was subjected to reverse transcription with PrimeScript RT Reagent Kit (Takara Bio), or, in case of RNA pull-down and IP ex-
periments, with SuperScript VILO cDNA Synthesis Kit (ThermoFisher Scientific), both used according to the manufacturer's protocol. For qRT-PCR, PowerUp SYBR Green Master Mix reagent (ThermoFisher Scientific) was used according to the manufacturer's instructions. RNA levels are relative to GAPDH mRNA unless differently specified. Relative RNA quantity was calculated as the fold

change ($2^{\wedge-DDCt}$) with respect to the control sample set as 1, unless differently specified.The efficiency of qRT-PCR primers was calculated based on a standard curve made from serial dilutions of RD cDNA, followed by qPCR with a specific pair of oligonucleotides. Then, the slope of the standard curve was used to calculate the amplification efficiency of each qPCR reaction. Oligonucleotides used are listed in Table1.

RNA pulldown

For native RNA-pull-down protocol, 10-15x10^6 cells for each biological replicate were pelleted and resuspended in 1 ml of cold Lysis Buffer (Tris-HCl pH 7.5 50mM, NaCl 150mM, MgCl2 3mM, NP40 0.5%, EDTA 2mM) supplemented with PIC 1X, RNAse Inhibitor 1:400, DTT 1mM. Cells were passed through a 27 gauge needle 4 times and incubated 30' at 4°C on a rotating wheel to allow nuclear lysis. Lysate was centrifuged 15' at 4 C at 1500g. The same volume of supernatant was taken for target and LacZ (negative control) pull downs and 10% of pull-down volume was saved as input condition. For every pull-down reaction, a double volume of cold Hybridization Buffer (Tris-HCl pH 7.5 1000mM, NaCl 300mM, MgCl2 1mM, NP40 0.5%, EDTA 10mM, SDS 0.2%, Formamide 15%) supplemented with PIC 1X, RNAse Inhibitor 1:400, DTT 1mM was added. 200 pmol of biotinylated probes mix dissolved in 50 µl of Lysis Buffer, heated at 80°C for 30' and then transferred in ice, were added in each pull-down reaction and samples were incubated 4h at 4°C on a rotating wheel. Therefore, 100 µl of pre-washed streptavidin beads (Promega) were added and samples were incubated 2h at 4°C on a rotating wheel.

For RNA pulldown in si-scr or si-circHIPK3 condition, 2x10^6 RD cells were plated in two 10-cm plates, transfected the morning after with 30 nM of si-SCR and si-circHIPK3 respectively, moved to 15-cm plates 24h post-transfection and pelleted for the pulldown 48h after transfection.

For AMT-crosslinked RNA-pull-down protocol, $40x10^6$ RD cells for each biological replicate were pelleted, resuspended in 1 ml of cold PBS supplemented with 0.5 mg/ml of 4'-aminomethyl-4,5',8-trimethylpsoralen (AMT, Cayman Chemical) per $1x10^7$ cells and crosslinked at 365 nm for five 2-minute cycles. 1 volume of Guanidinium Hydrochloride 6M per each volume of AMT was added. The lysate was subdivided into 250µl aliquots. 12,5 µl of a 20mg/mL solution of Proteinase K (Ambion), 6.5 µL of 20% SDS and RNAse Inhibitor 1:250 were added to each aliquot and the samples were incubated at 65 C for 1 h. RNA was precipitated through phenol/ chloroform extraction, subjected to DNAse I treatment and re-extracted. RNA extracted post DNAse treatment was equally divided in three tubes, one per pull down (LacZ, ODD, EVEN) and 10% of every fraction of RNA was taken and considered as input, while the rest was brought to a volume of 500 µL with RNAse free water, incubated 2' at 98°C and put in ice. For every pull down, 500 pmoles of biotinylated probes (4 ODD probes, 4 EVEN probes, 4 LacZ probes, listed in Table 1), 500 µL of 2X binding buffer (Tris-HCl 20mM, NaCl 1M, EDTA 2mM, SDS 0.1%) and 4µL of RNAse Inhibitor were added to RNA. The mixes were heated at 65°C for 30' and then incubated 4h on a rotating wheel at room temperature. Then, 500 µL of Streptavidin beads (Promega), resuspended in 1X binding buffer, and 2µL of RNAse Inhibitor, were added and RNA-probes-beads mixes were incubated 2h on a rotating wheel at 4°C. Finally, beads were washed two times with 1X binding buffer and two times with 1X wash buffer (Tris-HCl 10mM, NaCl 200mM, EDTA 1mM, SDS 0.05%) and 1 mL of TRIzol was added for each sample.

RNA immunoprecipitation (RIP and CLIP)

The RNA-immunoprecipitation (RIP) assays for FMRP, FXR2 and RPL22-FLAG protein were performed in RD cells following the protocol described in Keene *et al*[158].

For RPL22-FLAG immunoprecipitation in si-scr or si-circHIPK3 condition, $2x10^6$ RD cells were plated in two 10-cm plates and transfected the morning after with 10 µg of RPL22 (Myc-DDK-tagged)-Human ribosomal protein L22 plasmid plasmid (Origene, Cat# RC208910). 6 h after transfection, RPL22-FLAG-transfected cells were split into two 10-cm plates and the following morning were transfected with either 30 nM si-scr or 30 nM si-circHIPK3. 48 h after siRNA transfection, cells were harvested and the RIP assay with Dynabeads Protein G was performed. 20% of each lysate was saved as input. Half of the remaining lysate was used to precipitate RPL22-FLAG with 2 µg of FLAG antibody, while for the other half 2 µg of IgG antibody was used as a negative control. 15% of what was immunoprecipitated with each antibody was used to analyze the levels of the flagged protein precipitated, while the remaining 75% was used to examine the RNAs associated to the ribosomal flagged protein.

Cross-linking immunoprecipitation (CLIP) was performed according to Beltran *et al*[159] with the following modifications. A total of $2.5x10^7$ RD cells per CLIP were irradiated with 0.4 J/cm^2 of 254 nm UV light. Cells were lysed and treated for fragmentation with Turbo DNase (4 µL) and RNAse T1 (10 µL of a dilution 1/500) for 3 minutes at 37°C. Lysate was cleared by centrifugation and 5 µg of antibody coupled to Dynabeads Protein G were added. After 4h incubation beads washed 3 times with wash buffer containing 1000 mM NaCl, pelleted and then incubated in 200 µL PK buffer (100 mM Tris-HCl pH 7.4, 50 mM NaCl and 40 mL Proteinase K) for 20 min at 1100 rpm and 37°C. An equal volume of PK buffer containing 7 M urea was added, and a second incubation was performed. Supernatant was collected, and RNA was purified via phenol-

chloroform extraction. 10% of each lysate was saved prior proteinase K treatment to check protein enrichment by western blot. Oligonucleotides used for qRT-PCR are listed in Table1.

Drug treatments

For Cisplatin, Doxorubicin (MedChemExpress) or Talazoparib (SelleckChem) treatment,$1x10^5$ -$1,5x10^5$ cells for well were seeded in 12 well plates. Cells were transfected with siRNAs or LNAs the day after, treated with the drug 24h from transfection and, finally, detached with Trypsin-EDTA 1X and counted 24, 30 or 48h after the treatment with Trypan blue to consider only the living ones. The percentage of survival was calculated by dividing the number of living treated cells with the number of living non- treated cells, transfected with the same siRNA, multiplied by 100. For Cisplatin and Doxorubicin experiments, cells were pelleted after the count and resuspended in Protein Extraction Buffer (100 mM Tris pH 7.5, EDTA 1 mM, SDS 2%) supplemented with PIC 2X (Complete-EDTA free, Roche–Merck) for protein extraction.

For alpha-amanitin treatment (Sigma-Aldrich), $5x10^5$ cells were seeded in each of two 6 cm-plate. Cells of each 6 cm-plate were transfected with siRNAs the day after, split in 3 well (0h,5h,10h) of a 12-well plate 24h from transfection and treated with alpha- amanitin 25 µg/ml (in fresh medium) 48h after transfection. 0h cells were harvested with TRIzol before treatment, while 5h and 10h cells were harvested respectively 5 and 10h after treatment.

Polysome fractionation

Sucrose gradients were prepared the day before cells harvesting by carefully adding in a tube decreasing concentrations of sucrose (50% to 10%) and kept at 4°C over-night. 48h post si-RNAs transfection, $10\text{-}15x10^6$ cells for each condition were treated for 15’ with 100 µg/ml Cycloheximide,

pelleted and resuspended in 430 µl of Polysome Extraction Buffer (Tris-HCl 20mM, KCl 100mM, MgCl2 5mM, NP40 0.5%) supplemented with PIC 1X, RNAse Inhibitor 1:200, 100 µg/ml Cycloheximide. Lysates were kept 10' in ice, centrifuged 10' at 4°C at 12000g and supernatants (cytoplasmatic fractions) were carefully added on the top of sucrose gradients. Tubes were ultra-centrifuged for 2h at 4°C at 37000 rpm. After ultra-centrifugation, each sample was divided in 100 µl fractions and the 260nm absorbance was measured. Absorbance vs density graph was plotted, and fractions were separated according the profile. A spike RNA was added in each fraction. The amount of RNA, detected for qRT-PCR, for each fraction was normalized to spike levels and considered as a percentage of the total amount of RNA, obtained by summing the quantity of RNA present in each fraction.

Immunofluorescence

$8x10^4$ RD cells cultured on pre-coated glass coverslips (0.4 mg/ml Collagen Rat Tail, Corning) were transfected the morning after with 30 nM si-scr or 30 nM si-circHIPK3. 48h post transfection, cells were fixed in 4% paraformaldehyde in warm PBS for 15 min at room temperature, washed three times with warm PBS and then blocked and permeabilized for 60 min at room temperature with a blocking buffer (PBS with 5% BSA, 0.3% Triton X-100).Cells were hybridized overnight with anti-γH2AX Ser139 primary antibody (Santa Cruz Biotechnology) diluted 1:200 in a dilution buffer (PBS with 1% BSA, 0.3% Triton X-100). The morning after, behind five washes in PBS, cells were hybridized with fluorescent goat anti-mouse IgG (H+L) cross-adsorbed secondary antibody (Alexa Fluor 488; ThermoFisher Scientific) and DAPI solution (Sigma- Aldrich), diluted respectively 1:200 and 1:5000 in the same dilution buffer, for 2 h. Cells were, then, washed again three times with PBS and coverslips were mounted on

microscope slides using ProLong Diamond Antifade Mountant (ThermoFischer Scientific). Images were acquired with Zeiss Axio Observer A1 Inverted Microscope and processed only in intensity threshold, contrast, and brightness on ImageJ software.

Flow cytometry

For NHEJ and HR repair reporter assays, $2x10^5$ U2OS EJ5-GFP or U2OS DR-GFP cells were seeded in 6 well plates and transfected with siRNAs (si-scr, si-circHIPK3, si-BRCA1) the day after. 24h post RNA interference, for each siRNA, half of the cells was not transfected, while the other half was transfected with 1µg of plasmid expressing I-SceI nuclease. Cells were harvested 72h after siRNA transfection and resuspended into single cell suspension for flow cytometry experiments performed using Becton Dickinson (BD) instrument LSRFortessa (Becton Dickinson, BD Biosciences, USA) equipped among others with a 488nm Solid Sapphire 488/50 laser (Becton Dickinson, BD Biosciences, USA). Samples were acquired using FACSDiva software (BD Biosciences, version 6.1.3) and analyzed using FlowJo software (BD Biosciences, version 10.10.0). A total of 50,000 events/sample were collected.

In vitro transcription and electrophoresis mobility shift assay

For in vitro transcription, pCDNA 3.1 vectors containing the region of interest downstream of T7 promoter were digested 1h with NotI for linearization and gel purified. 1µg of linearized transcript was used for in vitro transcription using MEGAscript T7 kit (ThermoFisher Cat#AM1334). For biotin-labeled transcripts biotin-16-UTP (ThermoFisher cat#AM8452) was added to the reaction. Reaction was performed 4h at 37°C, followed by DNase treatment and phenol-chloroform purification, correct size and possible degradation was

checked by running samples in a TBE 5% Acrylamide gel 7M Urea. LightShift Chemiluminescent RNA EMSA kit (ThermoScientific cat#20158) was used to perform mobility shift assay. Briefly 5nM of biotinylated oligos, or 0,5-2,5, 25 nM of competing transcripts were mixed in Binding Buffer (10mM HEPES 7.3, 20mM KCl, 1mM MgCl2, 1mM DTT, 1mg/mL tRNA and RNAseOUT). Samples were incubated 2' at 80 and 2' on ice ensure denaturation, and binding reaction was performed for 30 minutes at room temperature. For competition assays with FMRP1 protein, 5nM of biotinylated oligos and 25nM of competing transcripts were incubated as previously described. After denaturation 50nM of recombinant human FMRP protein (Abcam ab132093) was added to the reaction and incubation was carried out for 30 minutes at 4. Non-denaturing RNA loading buffer was added to the reaction and samples were loaded in a 5% TBE gel Acrylamide gel and run in 4 0.5X TBE for 2 hours at 100V. Electro transfer against a nylon membrane was carried out using cold 0.5X TBE at 400mA for 30 minutes, and samples were crosslinked using 480mJ/cm2 254nm UV light. Images were acquired with ChemiDoc MP Imager (Bio-Rad) as previously described.
For control loading images, a part of the reaction was saved and denatured with formamide-containing loading buffer, heated at 80°C 2 minutes and loaded Ethidium bromide agarose gel for imaging.

Absolute copy number quantification

CircHIPK3 and *BRCA1* mRNA copy number per cell was calculated based on a standard curve made from serial dilutions of retrotranscribed RNA fragments ''circHIPK3 BSJ'' and ''BRCA1 ex23+3'UTR''. $4x10^5$ RD cells were harvested in Trizol reagent and RNA isolated according to manufacturer's protocol. Amount of RNA per cell was calculated based on the extraction results. RNA was subjected to reverse transcription with PrimeScript RT Reagent Kit (TakaraBio). qRT-PCR was

performed with 50ng of cDNA, using PowerUp SYBR Green Master Mix reagent (ThermoFisher Scientific).

COMET assay

COMET assay was performed as described in Olive and Banath[160] protocol. Cells were dissolved in low temperature melting agarose and loaded on a frosted-end microscope slide. Cell lysis was performed in alkaline conditions (1.2 M NaCl, 100 mM Na2EDTA, 0.1% sodium lauryl sarcosine, 0.26 M NaOH) and electrophoresis was run in 0.03 M NaOH, 2 mM Na2EDTA solution. Nuclei were stained for 20 minutes at room temperature using Ethidium Bromide solution; then slides were rinsed with distilled water to remove excess stain. Slides were imaged on a Zeiss AXIO Observer A1 microscope. Comet tail moment was measured using the ImageJ Macro ‘‘Comet Assay’’. RD cells were transfected with si-scr or si-circHIPK3 siRNAs; after 6 h, they were transfected with either 4000 ng of empty pcDNA 3.1 (+) plasmid or p-BRCA1. Four independent biological replicates of this experiment were performed at 48 h after siRNAs transfection. Otherwise, MCF7 wt/wt and wt/del cells were transfected with LNA scr or LNAex23. The experiment was performed at 48 h after transfection as well, in four independent biological replicates.

Luciferase assay

$4x10^4$ RD cells were seeded in 24-well plates and cultured until 70% confluency. Afterwards, cells were transfected with si-SCR, si-circHIPK3 or si-linHIPK3. 6 hours after siRNA transfection, cells were transfected with 20 ng of p-luc, p-luc+HIPK3 Ex2 or p-luc+BRCA1 3’-UTR using Lipofectamine 2000 Transfection Reagent (ThermoFisher Scientific, Cat#11668019). After 48 hours, cells were washed twice with 250 µL of fresh PBS, 125 µL of Passive Lysis Buffer (Promega, Cat# E1910) was added and lysis was allowed to

occur in oscillation at 4 C for 15 minutes. Then cells were spun to precipitate biological membranes and 10 mL of sample were plated in a 96-multiwell. Finally, firefly luciferase activity was measured using a dual-luciferase reporter assay system (Promega, Cat# E1910) and normalized to the Renilla value.

circHIPK3 pull-down RNA-seq analysis

Duplicated replicates of circ-HIPK3 pull-down experiment were prepared together with duplicated Input samples (INP). For pull-down samples three distinct sets of probes were used: Even (EVEN), Odd (ODD) and lacZ control (LACZ). RNA library was produced using Stranded Total RNA Prep with Ribo-Zero Plus (Illumina). All samples were sequenced on an Illumina Novaseq 6000 Sequencing system. Cutadapt (v3.2)[161] with parameters: -u 1 -U 1 –nextseq-trim=20 –trim-n and Trimmomatic (v0.39)59 with parameters: -PE ILLUMINACLIP:adapter_path:2:30:10:8:3:true LEADING:3 TRAILING:3 SLIDINGWINDOW:4:20 were used to remove adapter sequences and poor quality bases; for both software the minimum read length after trimming was set to 35. Reads aligning to rRNAs were filtered out; this first alignment was performed using Bowtie2 software (v2.4.2)[162,163]. Then, STAR software (v2.7.7a) was used to align reads to GRCh38 genome using the following parameters: –outSAMstrandField intronMotif –outSAMattrIHstart 0 –outFilterType BySJout –outFilterMultimapNmax 20 –alignSJoverhangMin 8 –alignSJDBoverhangMin 1 –outFilterMismatchNmax 999 –outFilterMismatch- NoverLmax 0.04 –alignIntronMin 20 –alignIntronMax 1000000 –alignMatesGapMax 1000000 –outFilterIntronMotifs RemoveNonca- nonical –peOverlapNbasesMin 50. PCR duplicates were removed from all samples using MarkDuplicates command from Picard suite (v2.24.1) (https://broadinstitute.github.io/picard/) and multi-mapped and un-properly paired reads were filtered out using bamtools (v2.5.1)[164] and samtools (v1.7)[165]

respectively. Gene quantification of RNA fragments was performed using htseq-count software (v0.13.5)[166,167] with the following parameters -s reverse -m union and using Ensembl gene annotation (release 99)[167].
Differential abundance analysis was performed comparing circ-HIPK3 pull down (EVEN, ODD) or control lacZ pull down (LACZ) to Input (INP) through edgeR R package (v3.34.1)[168]. Genes with less than 10 reads in at least 2 samples for each comparison (EVEN vs INP; ODD vs INP and LACZ vs INP) were filtered out. TMM normalization was used to normalize samples between sets while model.
RNA-seq data from RNA pull-down experiments have been deposited at Gene Expression Omnibus GEO: GSE246226.

circHIPK3 pull-down microRNA-seq analysis
QIAseq miRNA library kit (QIAGEN, Hilden, Germany) has been used for library preparation following the manufacturer's instructions. RNA samples were quantified, and quality tested by Agilent 2100 Bioanalyzer RNA assay (Agilent technologies, Santa Clara, CA) or Caliper (PerkinElmer, Waltham, MA). Final libraries were checked with both Qubit 2.0 Fluorometer (Invitrogen, Carlsbad, CA) and Agilent Bioanalyzer DNA assay or Caliper (PerkinElmer, Waltham, MA). Libraries were then prepared for sequencing and sequenced on single-end 150 bp mode on NovaSeq 6000 (Illumina, San Diego, CA). RNA-seq fastq processing and microRNAs quantification from were performed according to Potla *et al.*[169] using miRbase (v22) reference sequences[170].
Differential abundance analysis was performed comparing EVEN, ODD or LACZ pull-down samples to INP sample through edgeR R package (v3.34.1) using exact test
(indicated pipeline without replicates) and NOISeq software (v2.36.0)[171]. CircHIPK3 bound miRNAs were identified as those significantly enriched in the pull-down (EVEN or ODD)

VS Input contrast, but not in the lacZ VS Input comparison. Enriched miRNAs were defined as those with log2 fold-enrichment > 1.5 (pull down vs Input) and FDR < 0.05 in edgeR analysis and probability > 0.95 in NOISeq analysis. In order to obtain more stringent results, log2 fold-enrichment threshold in the lacZ VS Input comparison was set at > 0.
RNA-seq data from RNA pull-down experiments have been deposited at Gene Expression Omnibus GEO: GSE246226.

Quantification and statistical analysis

The distribution and deviation of data are shown in the figures, the exact value of n (e.g., the number of biological replicates of the experiments) are denoted in figure legends. When possible, individual data points from biological replicates were depicted as dots in the graphs. In figure legends, SE stands for standard error and SD stands for standard deviation.
Two-tailed unpaired or paired Student's t test tested the ratio of each sample versus control.
Significance values were depicted in the figures using the following key legend: *: $p < 0.05$, **: $p < 0.01$, ***: $p < 0.001$. The exact p values of statistical confrontations are indicated in the figure legends.

TABLE 1

	Oligonucleotides (sequence 5'-3')
qRT-PCR	Hipk3 FW CGGCCAGTCATGTATCAAAG
	Hipk3 RV_circ CCTGGAATACACAACTGCTTGG
	Hipk3 RV_lin CTGATCATACTCCAAGGCTC
	Gapdh FW CCAAAATCAAGTGGGGCGATG
	Gapdh RV GGCAGAGATGATGACCCTTT
	Brca1 ex21 FW CAACTGGAATGGATGGTACAG
	Brca1 ex22 RV GAAGCCATTGTCCTCTGTCC
	Brca1 ex10 FW GAGTTGGTCTGAGTGACAAGG
	Brca1 ex11 RV CAGAGACGCTTGTTTCACTC
	Brca1 5'-UTR qRT-PCR Fw GCTGTGGGGTTTCTCAGATA
	Brca1 5'-UTR qRT-PCR Rv CGCGAAGAGCAGATAAATCCA
	Brca1 3'-UTR qRT-PCR Fw GCTGAAACCATACAGCTTCAT
	Brca1 3'-UTR qRT-PCR Rv CCTAGTCCTTCCAACAGCTAT
	pre-Brca1 FW CTGCTCTTCGCGTTGAAGAA
	pre-Brca1 RV GCATAGGAGATAATCATAGGAATCCCA
	Rnf40 Fw AGCTTCAACCTCAAGAGGGC
	Rnf40 Rv GTCAACCGCGCCTTGTACT
	Sart1 Fw TTTGAACGGGATGAGGAGCG
	Sart1 Rv TGGAGGAAGCAGAGAAATCCT
	Sart3 Fw GGCTCTCTCGTCTGTTGGTT
	Sart3 Rv GGACTTTCTCAAGCCGAGCA
	Elof1 Fw TTTCGCAGCTGGAGAAGGCTC
	Elof1 Rv GGAGGCGGCTTTCGTTTTG
	Rfx3 Fw CCTCCCCAGCGACAATTGAA
	Rfx3 Rv TGGGAAGGCTCACTCCTTCT
	Snrpa1 Fw AGTCTCGTGGAACTGGGTGA
	Snrpa1 Rv ATCCAGTACTCTGACTTGCGG

Hipk2 Fw GACACAGGCTCAAGATGGCA
Hipk2 Rv CATGTGAGGCCATACCTTCGT
Csrp2 Fw GCCTCCGACTCAAAATGCCT
Csrp2 Rv TCCTGCAAACCATGCAGAGAA
Ipo11 Fw GCTTTCGGCATCAGTAGGC
Ipo11 Rv GATCCATGGAAACCGTTTGG
Bptf Fw TTCAAAGCTAGCAGGTCTCAT
Bptf Rv GCCTGACTAAAAACATCTGGCTC
Akap13 Fw GCTCCATGCGCTCTCTTTCT
Akap13 Rv CCAAGAACTCGCATTGAACTCC
Nfya Fw CAGACCCTCCAGGTAGTCCAAG
Nfya Rv AGCCTGGACCATGATGGGTT
Ywhae Fw CTATCCGCTTCCATCCGTCG
Ywhae Rv TTGACTCCACCATTTCGTCG
Sumo3 Fw CTCCGTGGTGCAGTTCAAGA
Sumo3 Rv TCATTGACAAGCCCTGCCTC
Fxr2 Fw TGAGGGTTCGAGTGGAAGGTGA
Fxr2 Rv GGTGATACTCCAGCAAAGCCTG
Fmr1 Fw GCAGATTCCATTTCATGATGTCA
Fmr1 Rv AACCACCAACAGCAAGGCTCT
Pten Fw TCCAATGTTCAGTGGCGGAA
Pten Rv CGTGTGGGTCCTGAATTGGA
Cdc25a Fw GCTCCTCCGAGTCAACAGAT
Cdc25a Rv ACAGCTTCTGAGGTAGGGAATG
Bcl2 Fw CAACATCGCCCTGTGGATGA
Bcl2 Rv GGGCCGTACAGTTCCACAAA
Timp3 Fw GTGCAACTTCGTGGAGAGGT
Timp3 Rv AGCAAGGCAGGTAGTAGCAG
Cdc34 Fw TCCGTGATGTACAGGAAGTGG
Cdc34 Rv GTCCCCAGGACCTGCTTC
Coil Fw GAGAGACAACGACTGCCTCAG

Coil Rv AAATGCCCGCTTCTTTGCTTT
Anapc1 Fw CACATGGCCCTTGGACTTCT
Anapc1 Rv AAGTGCGGATAAAGGGCACA
Ccnd1 Fw CAGATCATCCGCAAACACGC
Ccnd1 Rv ATGGAGGGCGGATTGGAAAT
Actinin1 Fw ATCAACTTCAACACGCTGCA
Actinin1 RV AGCCTCCGGATCTCATTCAG
spike (IVT mouse Lhx1os) Fw TTCTCTCTGTAGCCCCGACT
spike (IVT mouse Lhx1os) Rv CTCTCCCCTTCTTCACTTTC

siRNAs (sequence 5'-3')

si-circHIPK3 GGUACUACAGGUAUGGCCUUU
si-circHIPK3 II AAUCUCGGUACUACAGGUAUU
si-SCR Cat.# D-001810-10-05
si-HIPK3 Cat.# J-004810-09-0002
si-FXR2 Cat.# J-011955-05-0005
si-FMRP Cat.# J-019631-05-0005
si-BRCA1 Cat.# J-003461-09-0005

Pulldown probes (sequence 5'-3')

circHIPK3 ODD
5'Biotin-GCCATACCTGTAGTACCGAGATTGTAG
5'Biotin-TTGCAACATTGCAGGAAGTATGGAC
5'Biotin-TTGCTGTGCCTGAGCTGCTATGACCTT
5'Biotin-TTGACGGGCATAAGAAGGATGATTC

circHIPK3 EVEN
5'Biotin-ACCCTTAGTGGGAGGATGAGAATTTCC
5'Biotin-GTTGAAGAATGGGCCGAATCACTTTAG
5'Biotin-GCTGTACTAACTGATAGTCACCTTCTC
5'Biotin-GCTGAAAGCATTCATAAGCTCGTACA

HIPK3	5'Biotin-ATCTTGTCCTGGCGGCTGAGAGGAAA
	5'Biotin-CCAATGACCACATGTCTTGGCTTCAC
	5'Biotin-GGTTCAGGGTCTCAGCTGGAGTAATTC
	5'Biotin-GCAGTCAGTGTAGCAGTACTGCTTGAAG
	5'Biotin-CGGCATCACTGAGTTATAATGATTGCTG
	5'Biotin-GTGCTCTGGCAAGCTTCACAATCTAG
	5'Biotin-GCCATATGCTCATCGGCATTTAAGCC
	5'Biotin-TGTAGACGTGTCTTGCACTAGTTAG
LacZ	5'Biotin-AATGTGAGCGAGTAACAACC
	5'Biotin-ATTAAGTTGGGTAACGCCAG
	5'Biotin-AATAATTCGCGTCTGGCCTT
	5'Biotin-AATTCAGACGGCAAACGCT
	5'Biotin-ATCTTCCAGATAACTGCCGT

LNA oligonucleotides (sequence 5'-3')

LNA block 21-5p TCAA+CATC+AGTC+TGAT+
AAGC+TA
LNA block Let7b-5p AACC+ACA+CAAC+CTAC+TACC+TCA
LNA circHIPK3 BSJ +GACC+AAGA+CTTG+TGAG+GCCA
+TACC+TGTAG+T
LNA circHIPK3 ex2 circ +GTG+ACA+GTT+GTG+ACA+GCT
+ACC+ACA+GGA+TCA
LNA ex23 BRCA1 +AAC+ACC+CAC+TCT+CGG+GTC+ACC
+ACA+GGT+GCC
LNA scr (miRCURY LNA miRNA Inhibitor Negative control A)
QIAGEN
LNA ctr (luc_ctr) GCTC+AGAA+TAGA+AGTG+TCGG
+GGAT+GA+T

REFERENCES

1. ENCODE Project Consortium (2004). The ENCODE (ENCyclopedia Of DNA Elements) Project. Science (1979) *306*, 636–640. https://doi.org/10.1126/science.1105136.
2. Anastasiadou, E., Jacob, L.S., and Slack, F.J. (2018). Non-coding RNA networks in cancer. Nat Rev Cancer *18*, 5–18. https://doi.org/10.1038/nrc.2017.99.
3. Liang, D., and Wilusz, J.E. (2014). Short intronic repeat sequences facilitate circular RNA production. Genes Dev *28*, 2233–2247. https://doi.org/10.1101/gad.251926.114.
4. Hsu, M.T.A., and Coca-Prados, M. (1979). Electron microscopic evidence for the circular form of RNA in the cytoplasm of eukaryotic cells [24]. Preprint, https://doi.org/10.1038/280339a0 https://doi.org/10.1038/280339a0.
5. Nigro, J.M., Cho, K.R., Fearon, E.R., Kern, S.E., Ruppert, J.M., Oliner, J.D., Kinzler, K.W., and Vogelstein, B. (1991). Scrambled exons. Cell. https://doi.org/10.1016/0092-8674(91)90244-S.
6. Cocquerelle, C., Daubersies, P., Majérus, M.A., Kerckaert, J.P., and Bailleul, B. (1992). Splicing with inverted order of exons occurs proximal to large introns. EMBO J *11*, 1095–1098. https://doi.org/10.1002/j.1460-2075.1992.tb05148.x.
7. Cocquerelle, C., Mascrez, B., Hétuin, D., and Bailleul, B. (1993). Mis-splicing yields circular RNA molecules. The FASEB Journal *7*, 155–160. https://doi.org/10.1096/fasebj.7.1.7678559.
8. Capel, B., Swain, A., Nicolis, S., Hacker, A., Walter, M., Koopman, P., Goodfellow, P., and Lovell-Badge, R. (1993). Circular transcripts of the testis-determining

gene Sry in adult mouse testis. Cell. https://doi.org/10.1016/0092-8674(93)90279-Y.
9. d'Orval, B.C. (2001). Box C/D RNA guides for the ribose methylation of archaeal tRNAs. The tRNATrp intron guides the formation of two ribose-methylated nucleosides in the mature tRNATrp. Nucleic Acids Res *29*, 4518–4529. https://doi.org/10.1093/nar/29.22.4518.
10. SALGIA, S.R., SINGH, S.K., GURHA, P., and GUPTA, R. (2003). Two reactions of *Haloferax volcanii* RNA splicing enzymes: Joining of exons and circularization of introns. RNA *9*, 319–330. https://doi.org/10.1261/rna.2118203.
11. Singh, S.K., Gurha, P., Tran, E.J., Maxwell, E.S., and Gupta, R. (2004). Sequential 2′-O-Methylation of Archaeal Pre-tRNATrp Nucleotides Is Guided by the Intron-encoded but trans-Acting Box C/D Ribonucleoprotein of Pre-tRNA. Journal of Biological Chemistry *279*, 47661–47671. https://doi.org/10.1074/jbc.M408868200.
12. Salzman, J., Gawad, C., Wang, P.L., Lacayo, N., and Brown, P.O. (2012). Circular RNAs Are the Predominant Transcript Isoform from Hundreds of Human Genes in Diverse Cell Types. PLoS One *7*, e30733. https://doi.org/10.1371/journal.pone.0030733.
13. Jeck, W.R., Sorrentino, J.A., Wang, K., Slevin, M.K., Burd, C.E., Liu, J., Marzluff, W.F., and Sharpless, N.E. (2013). Circular RNAs are abundant, conserved, and associated with ALU repeats. RNA *19*, 141–157. https://doi.org/10.1261/rna.035667.112.
14. Memczak, S., Jens, M., Elefsinioti, A., Torti, F., Krueger, J., Rybak, A., Maier, L., Mackowiak, S.D., Gregersen, L.H., Munschauer, M., et al. (2013). Circular RNAs are a large class of animal RNAs with

regulatory potency. Nature *495*, 333–338. https://doi.org/10.1038/nature11928.
15. Rybak-Wolf, A., Stottmeister, C., Glažar, P., Jens, M., Pino, N., Hanan, M., Behm, M., Bartok, O., Ashwal-Fluss, R., Herzog, M., et al. (2014). Circular RNAs in the Mammalian Brain Are Highly Abundant, Conserved, and Dynamically Expressed. Mol Cell. https://doi.org/10.1016/j.molcel.2015.03.027.
16. Venø, M.T., Hansen, T.B., Venø, S.T., Clausen, B.H., Grebing, M., Finsen, B., Holm, I.E., and Kjems, J. (2015). Spatio-temporal regulation of circular RNA expression during porcine embryonic brain development. Genome Biol. https://doi.org/10.1186/s13059-015-0801-3.
17. Starke, S., Jost, I., Hung, L.-H., Correspondence, A.B., Rossbach, O., Schneider, T., Schreiner, S., and Bindereif, A. (2015). Exon Circularization Requires Canonical Splice Signals. Cell Rep. https://doi.org/10.1016/j.celrep.2014.12.002.
18. Li, X., Yang, L., and Chen, L.-L. (2018). The Biogenesis, Functions, and Challenges of Circular RNAs. Mol Cell *71*, 428–442. https://doi.org/10.1016/j.molcel.2018.06.034.
19. Liang, D., Tatomer, D.C., Luo, Z., Wu, H., Yang, L., Chen, L.-L., Cherry, S., and Wilusz, J.E. (2017). The Output of Protein-Coding Genes Shifts to Circular RNAs When the Pre-mRNA Processing Machinery Is Limiting. Mol Cell *68*, 940-954.e3. https://doi.org/10.1016/j.molcel.2017.10.034.
20. Wang, J., and Wang, L. (2019). Deep learning of the back-splicing code for circular RNA formation. Bioinformatics *35*, 5235–5242. https://doi.org/10.1093/bioinformatics/btz382.
21. Ashwal-Fluss, R., Meyer, M., Pamudurti, N.R., Ivanov, A., Bartok, O., Hanan, M., Evantal, N., Memczak, S.,

Rajewsky, N., and Kadener, S. (2014). CircRNA Biogenesis Competes with Pre-mRNA Splicing. Mol Cell *56*, 55–66. https://doi.org/10.1016/J.MOLCEL.2014.08.019.

22. Zhang, X.-O., Dong, R., Zhang, Y., Zhang, J.-L., Luo, Z., Zhang, J., Chen, L.-L., and Yang, L. (2016). Diverse alternative back-splicing and alternative splicing landscape of circular RNAs. Genome Res *26*, 1277–1287. https://doi.org/10.1101/gr.202895.115.
23. Enuka, Y., Lauriola, M., Feldman, M.E., Sas-Chen, A., Ulitsky, I., and Yarden, Y. (2016). Circular RNAs are long-lived and display only minimal early alterations in response to a growth factor. Nucleic Acids Res *44*, 1370–1383. https://doi.org/10.1093/nar/gkv1367.
24. Westholm, J.O., Miura, P., Olson, S., Shenker, S., Joseph, B., Sanfilippo, P., Celniker, S.E., Graveley, B.R., and Lai, E.C. (2014). Genome-wide Analysis of Drosophila Circular RNAs Reveals Their Structural and Sequence Properties and Age-Dependent Neural Accumulation. Cell Rep *9*, 1966–1980. https://doi.org/10.1016/j.celrep.2014.10.062.
25. Gruner, H., Cortés-López, M., Cooper, D.A., Bauer, M., and Miura, P. (2016). CircRNA accumulation in the aging mouse brain. Sci Rep *6*, 38907. https://doi.org/10.1038/srep38907.
26. Chen, L.-L., and Yang, L. (2015). Regulation of circRNA biogenesis. RNA Biol *12*, 381–388. https://doi.org/10.1080/15476286.2015.1020271.
27. Zhang, X.O., Wang, H. Bin, Zhang, Y., Lu, X., Chen, L.L., and Yang, L. (2014). Complementary sequence-mediated exon circularization. Cell. https://doi.org/10.1016/j.cell.2014.09.001.
28. Ivanov, A., Memczak, S., Wyler, E., Torti, F., Porath, H.T., Orejuela, M.R., Piechotta, M., Levanon, E.Y., Landthaler, M., Dieterich, C., et al. (2015). Analysis of

intron sequences reveals hallmarks of circular RNA biogenesis in animals. Cell Rep. https://doi.org/10.1016/j.celrep.2014.12.019.
29. Liang, D., and Wilusz, J.E. (2014). Short intronic repeat sequences facilitate circular RNA production. Genes Dev *28*, 2233–2247. https://doi.org/10.1101/gad.251926.114.
30. Conn, S.J., Pillman, K.A., Toubia, J., Conn, V.M., Salmanidis, M., Phillips, C.A., Roslan, S., Schreiber, A.W., Gregory, P.A., and Goodall, G.J. (2015). The RNA binding protein quaking regulates formation of circRNAs. Cell. https://doi.org/10.1016/j.cell.2015.02.014.
31. Wen, X., Huang, X., Mok, B.W.-Y., Chen, Y., Zheng, M., Lau, S.-Y., Wang, P., Song, W., Jin, D.-Y., Yuen, K.-Y., et al. (2014). NF90 Exerts Antiviral Activity through Regulation of PKR Phosphorylation and Stress Granules in Infected Cells. The Journal of Immunology *192*, 3753–3764. https://doi.org/10.4049/jimmunol.1302813.
32. Li, F., Zhang, L., Li, W., Deng, J., Zheng, J., An, M., Lu, J., and Zhou, Y. (2015). Circular RNA ITCH has inhibitory effect on ESCC by suppressing the Wnt/β-catenin pathway. Oncotarget *6*, 6001–6013. https://doi.org/10.18632/oncotarget.3469.
33. Errichelli, L., Modigliani, S.D., Laneve, P., Colantoni, A., Legnini, I., Capauto, D., Rosa, A., Santis, R. De, Scarfò, R., Peruzzi, G., et al. (2017). FUS affects circular RNA expression in murine embryonic stem cell-derived motor neurons. Nat Commun. https://doi.org/10.1038/ncomms14741.
34. Fei, T., Chen, Y., Xiao, T., Li, W., Cato, L., Zhang, P., Cotter, M.B., Bowden, M., Lis, R.T., Zhao, S.G., et al. (2017). Genome-wide CRISPR screen identifies HNRNPL as a prostate cancer dependency regulating

RNA splicing. Proceedings of the National Academy of Sciences *114*. https://doi.org/10.1073/pnas.1617467114.

35. Zhou, C., Molinie, B., Daneshvar, K., Pondick, J. V., Wang, J., Van Wittenberghe, N., Xing, Y., Giallourakis, C.C., and Mullen, A.C. (2017). Genome-Wide Maps of m6A circRNAs Identify Widespread and Cell-Type-Specific Methylation Patterns that Are Distinct from mRNAs. Cell Rep *20*, 2262–2276. https://doi.org/10.1016/j.celrep.2017.08.027.
36. Timoteo, G. Di, Dattilo, D., Centrón-Broco, A., Colantoni, A., Guarnacci, M., Rossi, F., Incarnato, D., Oliviero, S., Fatica, A., Morlando, M., et al. (2020). Modulation of circRNA Metabolism by m6A Modification. Cell Rep. https://doi.org/10.1016/j.celrep.2020.107641.
37. Memczak, S., Papavasileiou, P., Peters, O., and Rajewsky, N. (2015). Identification and Characterization of Circular RNAs As a New Class of Putative Biomarkers in Human Blood. PLoS One *10*, e0141214. https://doi.org/10.1371/journal.pone.0141214.
38. Jeck, W.R., and Sharpless, N.E. (2014). Detecting and characterizing circular RNAs. Preprint, https://doi.org/10.1038/nbt.2890 https://doi.org/10.1038/nbt.2890.
39. Li, X., Zhang, J.-L., Lei, Y.-N., Liu, X.-Q., Xue, W., Zhang, Y., Nan, F., Gao, X., Zhang, J., Wei, J., et al. (2021). Linking circular intronic RNA degradation and function in transcription by RNase H1. Sci China Life Sci *64*, 1795–1809. https://doi.org/10.1007/s11427-021-1993-6.
40. Li, Z., Huang, C., Bao, C., Chen, L., Lin, M., Wang, X., Zhong, G., Yu, B., Hu, W., Dai, L., et al. (2015). Exon-intron circular RNAs regulate transcription in the

nucleus. Nat Struct Mol Biol *22*, 256–264. https://doi.org/10.1038/nsmb.2959.
41. Guarnerio, J., Zhang, Y., Cheloni, G., Panella, R., Mae Katon, J., Simpson, M., Matsumoto, A., Papa, A., Loretelli, C., Petri, A., et al. (2019). Intragenic antagonistic roles of protein and circRNA in tumorigenesis. Cell Res *29*, 628–640. https://doi.org/10.1038/s41422-019-0192-1.
42. Gu, X., Zhang, J., Ran, Y., Pan, H., Jia, J., Zhao, Y., Zhao, X., Li, W., Song, S., and Yu, X. (2021). Circular RNA hsa_circ_101555 promotes hepatocellular carcinoma cell proliferation and migration by sponging miR-145-5p and regulating CDCA3 expression. Cell Death Dis *12*, 356. https://doi.org/10.1038/s41419-021-03626-7.
43. Conn, V.M., Hugouvieux, V., Nayak, A., Conos, S.A., Capovilla, G., Cildir, G., Jourdain, A., Tergaonkar, V., Schmid, M., Zubieta, C., et al. (2017). A circRNA from SEPALLATA3 regulates splicing of its cognate mRNA through R-loop formation. Nat Plants *3*, 17053. https://doi.org/10.1038/nplants.2017.53.
44. Holdt, L.M., Stahringer, A., Sass, K., Pichler, G., Kulak, N.A., Wilfert, W., Kohlmaier, A., Herbst, A., Northoff, B.H., Nicolaou, A., et al. (2016). Circular non-coding RNA ANRIL modulates ribosomal RNA maturation and atherosclerosis in humans. Nat Commun *7*, 12429. https://doi.org/10.1038/ncomms12429.
45. Du, W.W., Yang, W., Liu, E., Yang, Z., Dhaliwal, P., and Yang, B.B. (2016). Foxo3 circular RNA retards cell cycle progression via forming ternary complexes with p21 and CDK2. Nucleic Acids Res *44*, 2846–2858. https://doi.org/10.1093/nar/gkw027.
46. Xia, P., Wang, S., Ye, B., Du, Y., Li, C., Xiong, Z., Qu, Y., and Fan, Z. (2018). A Circular RNA Protects Dormant Hematopoietic Stem Cells from DNA Sensor

cGAS-Mediated Exhaustion. Immunity *48*, 688-701.e7. https://doi.org/10.1016/j.immuni.2018.03.016.
47. Liu, C.-X., Li, X., Nan, F., Jiang, S., Gao, X., Guo, S.-K., Xue, W., Cui, Y., Dong, K., Ding, H., et al. (2019). Structure and Degradation of Circular RNAs Regulate PKR Activation in Innate Immunity. Cell *177*, 865-880.e21. https://doi.org/10.1016/j.cell.2019.03.046.
48. Salmena, L., Poliseno, L., Tay, Y., Kats, L., and Pandolfi, P.P. (2011). A ceRNA Hypothesis: The Rosetta Stone of a Hidden RNA Language? Cell *146*, 353–358. https://doi.org/10.1016/J.CELL.2011.07.014.
49. Hansen, T.B., Kjems, J., and Damgaard, C.K. (2013). Circular RNA and miR-7 in Cancer. Preprint, https://doi.org/10.1158/0008-5472.CAN-13-1568 https://doi.org/10.1158/0008-5472.CAN-13-1568.
50. Huang, R., Zhang, Y., Han, B., Bai, Y., Zhou, R., Gan, G., Chao, J., Hu, G., and Yao, H. (2017). Circular RNA *HIPK2* regulates astrocyte activation via cooperation of autophagy and ER stress by targeting *MIR124–2HG*. Autophagy *13*, 1722–1741. https://doi.org/10.1080/15548627.2017.1356975.
51. Yu, C.Y., Li, T.C., Wu, Y.Y., Yeh, C.H., Chiang, W., Chuang, C.Y., and Kuo, H.C. (2017). The circular RNA circBIRC6 participates in the molecular circuitry controlling human pluripotency. Nat Commun *8*. https://doi.org/10.1038/s41467-017-01216-w.
52. Piwecka, M., Glažar, P., Hernandez-Miranda, L.R., Memczak, S., Wolf, S.A., Rybak-Wolf, A., Filipchyk, A., Klironomos, F., Jara, C.A.C., Fenske, P., et al. (2017). Loss of a mammalian circular RNA locus causes miRNA deregulation and affects brain function. Science (1979) *357*, eaam8526. https://doi.org/10.1126/science.aam8526.
53. Legnini, I., Timoteo, G. Di, Rossi, F., Morlando, M., Briganti, F., Sthandier, O., Fatica, A., Santini, T.,

Andronache, A., Wade, M., et al. (2017). Circ-ZNF609 Is a Circular RNA that Can Be Translated and Functions in Myogenesis. Mol Cell *66*, 22-37.e9. https://doi.org/10.1016/j.molcel.2017.02.017.

54. Pamudurti, N.R., Bartok, O., Jens, M., Ashwal-Fluss, R., Stottmeister, C., Ruhe, L., Hanan, M., Wyler, E., Perez-Hernandez, D., Ramberger, E., et al. (2017). Translation of CircRNAs. Mol Cell *66*, 9-21.e7. https://doi.org/10.1016/j.molcel.2017.02.021.
55. Yang, Y., Fan, X., Mao, M., Song, X., Wu, P., Zhang, Y., Jin, Y., Yang, Y., Chen, L.-L., Wang, Y., et al. (2017). Extensive translation of circular RNAs driven by N6-methyladenosine. Cell Res *27*, 626–641. https://doi.org/10.1038/cr.2017.31.
56. Chen, C.-K., Cheng, R., Demeter, J., Chen, J., Weingarten-Gabbay, S., Jiang, L., Snyder, M.P., Weissman, J.S., Segal, E., Jackson, P.K., et al. (2021). Structured elements drive extensive circular RNA translation. Mol Cell *81*, 4300-4318.e13. https://doi.org/10.1016/j.molcel.2021.07.042.
57. Li, Y., Chen, B., Zhao, J., Li, Q., Chen, S., Guo, T., Li, Y., Lai, H., Chen, Z., Meng, Z., et al. (2021). HNRNPL Circularizes ARHGAP35 to Produce an Oncogenic Protein. Advanced Science *8*. https://doi.org/10.1002/advs.202001701.
58. Rossi, F., Beltran, M., Damizia, M., Grelloni, C., Colantoni, A., Setti, A., Timoteo, G. Di, Dattilo, D., Centrón-Broco, A., Nicoletti, C., et al. (2022). Circular RNA ZNF609/CKAP5 mRNA interaction regulates microtubule dynamics and tumorigenicity. Mol Cell *82*, 75-89.e9. https://doi.org/10.1016/j.molcel.2021.11.032.
59. Hafez, A.K., Zimmerman, A.J., Papageorgiou, G., Chandrasekaran, J., Amoah, S.K., Lin, R., Lozano, E., Pierotti, C., Dell'Orco, M., Hartley, B.J., et al. (2022). A bidirectional competitive interaction between

circHomer1 and Homer1b within the orbitofrontal cortex regulates reversal learning. Cell Rep *38*, 110282. https://doi.org/10.1016/j.celrep.2021.110282.

60. Zhang, X., Lu, N., Wang, L., Wang, Y., Li, M., Zhou, Y., Yan, H., Cui, M., Zhang, M., and Zhang, L. (2020). Circular RNAs and esophageal cancer. Cancer Cell Int *20*, 362. https://doi.org/10.1186/s12935-020-01451-0.
61. Guarnerio, J., Bezzi, M., Jeong, J.C., Paffenholz, S.V., Berry, K., Naldini, M.M., Lo-Coco, F., Tay, Y., Beck, A.H., and Pandolfi, P.P. (2016). Oncogenic Role of Fusion-circRNAs Derived from Cancer-Associated Chromosomal Translocations. Cell *165*, 289–302. https://doi.org/10.1016/j.cell.2016.03.020.
62. Patop, I.L., and Kadener, S. (2018). circRNAs in Cancer. Curr Opin Genet Dev *48*, 121–127. https://doi.org/10.1016/J.GDE.2017.11.007.
63. Su, M., Xiao, Y., Ma, J., Tang, Y., Tian, B., Zhang, Y., Li, X., Wu, Z., Yang, D., Zhou, Y., et al. (2019). Circular RNAs in Cancer: Emerging functions in hallmarks, stemness, resistance and roles as potential biomarkers. Preprint, https://doi.org/10.1186/s12943-019-1002-6 https://doi.org/10.1186/s12943-019-1002-6.
64. Cortés-López, M., and Miura, P. (2016). Emerging Functions of Circular RNAs. Yale J Biol Med *89*, 527–537.
65. Wang, F., Wang, J., Cao, X., Xu, L., and Chen, L. (2018). Hsa_circ_0014717 is downregulated in colorectal cancer and inhibits tumor growth by promoting p16 expression. Biomedicine & Pharmacotherapy *98*, 775–782. https://doi.org/10.1016/j.biopha.2018.01.015.
66. Qiu, M., Xia, W., Chen, R., Wang, S., Xu, Y., Ma, Z., Xu, W., Zhang, E., Wang, J., Fang, T., et al. (2018). The Circular RNA circPRKCI Promotes Tumor Growth

in Lung Adenocarcinoma. Cancer Res *78*, 2839–2851. https://doi.org/10.1158/0008-5472.CAN-17-2808.

67. Meng, S., Zhou, H., Feng, Z., Xu, Z., Tang, Y., Li, P., and Wu, M. (2017). CircRNA: Functions and properties of a novel potential biomarker for cancer. Preprint, https://doi.org/10.1186/s12943-017-0663-2 https://doi.org/10.1186/s12943-017-0663-2.
68. Li, Y., Zheng, Q., Bao, C., Li, S., Guo, W., Zhao, J., Chen, D., Gu, J., He, X., and Huang, S. (2015). Circular RNA is enriched and stable in exosomes: a promising biomarker for cancer diagnosis. Cell Res *25*, 981–984. https://doi.org/10.1038/cr.2015.82.
69. Wu, W., Ji, P., and Zhao, F. (2020). CircAtlas: an integrated resource of one million highly accurate circular RNAs from 1070 vertebrate transcriptomes. Genome Biol *21*, 101. https://doi.org/10.1186/s13059-020-02018-y.
70. Zhan, W., Liao, X., Wang, Y., Li, L., Li, J., Chen, Z., Tian, T., and He, J. (2019). circCTIC1 promotes the self-renewal of colon TICs through BPTF-dependent c-Myc expression. Carcinogenesis *40*, 560–568. https://doi.org/10.1093/carcin/bgy144.
71. Ren, X., Yu, J., Guo, L., and Ma, H. (2021). Circular RNA circRHOT1 contributes to pathogenesis of non-small cell lung cancer by epigenetically enhancing C-MYC expression through recruiting KAT5. Aging *13*, 20372–20382. https://doi.org/10.18632/aging.203417.
72. Wang, X., Xing, L., Yang, R., Chen, H., Wang, M., Jiang, R., Zhang, L., and Chen, J. (2021). The circACTN4 interacts with FUBP1 to promote tumorigenesis and progression of breast cancer by regulating the expression of proto-oncogene MYC. Mol Cancer *20*, 91. https://doi.org/10.1186/s12943-021-01383-x.

73. Barbagallo, D., Caponnetto, A., Brex, D., Mirabella, F., Barbagallo, C., Lauretta, G., Morrone, A., Certo, F., Broggi, G., Caltabiano, R., et al. (2019). CircSMARCA5 Regulates VEGFA mRNA Splicing and Angiogenesis in Glioblastoma Multiforme Through the Binding of SRSF1. Cancers (Basel) *11*, 194. https://doi.org/10.3390/cancers11020194.
74. Conn, V.M., Gabryelska, M., Toubia, J., Kirk, K., Gantley, L., Powell, J.A., Cildir, G., Marri, S., Liu, R., Stringer, B.W., et al. (2023). Circular RNAs drive oncogenic chromosomal translocations within the MLL recombinome in leukemia. Cancer Cell *41*, 1309-1326.e10. https://doi.org/10.1016/j.ccell.2023.05.002.
75. Jackson, S.P., and Bartek, J. (2009). The DNA-damage response in human biology and disease. Nature *461*, 1071–1078. https://doi.org/10.1038/nature08467.
76. Carusillo, A., and Mussolino, C. (2020). DNA Damage: From Threat to Treatment. Cells *9*, 1665. https://doi.org/10.3390/cells9071665.
77. Bartkova, J., Hořejší, Z., Koed, K., Krämer, A., Tort, F., Zieger, K., Guldberg, P., Sehested, M., Nesland, J.M., Lukas, C., et al. (2005). DNA damage response as a candidate anti-cancer barrier in early human tumorigenesis. Nature *434*, 864–870. https://doi.org/10.1038/nature03482.
78. Gorgoulis, V.G., Vassiliou, L.-V.F., Karakaidos, P., Zacharatos, P., Kotsinas, A., Liloglou, T., Venere, M., DiTullio, R.A., Kastrinakis, N.G., Levy, B., et al. (2005). Activation of the DNA damage checkpoint and genomic instability in human precancerous lesions. Nature *434*, 907–913. https://doi.org/10.1038/nature03485.
79. Lieber, M.R. (2008). The Mechanism of Human Nonhomologous DNA End Joining. Journal of

Biological Chemistry *283*, 1–5. https://doi.org/10.1074/jbc.R700039200.
80. Thompson, L.H., and Schild, D. (1999). The contribution of homologous recombination in preserving genome integrity in mammalian cells. Biochimie *81*, 87–105. https://doi.org/10.1016/S0300-9084(99)80042-X.
81. Li, X., and Heyer, W.-D. (2008). Homologous recombination in DNA repair and DNA damage tolerance. Cell Res *18*, 99–113. https://doi.org/10.1038/cr.2008.1.
82. Miki, Y., Swensen, J., Shattuck-Eidens, D., Futreal, P.A., Harshman, K., Tavtigian, S., Liu, Q., Cochran, C., Bennett, L.M., Ding, W., et al. (1994). A Strong Candidate for the Breast and Ovarian Cancer Susceptibility Gene *BRCA1*. Science (1979) *266*, 66–71. https://doi.org/10.1126/science.7545954.
83. Li, M.L., and Greenberg, R.A. (2012). Links between genome integrity and BRCA1 tumor suppression. Trends Biochem Sci *37*, 418–424. https://doi.org/10.1016/j.tibs.2012.06.007.
84. Rogakou, E.P., Pilch, D.R., Orr, A.H., Ivanova, V.S., and Bonner, W.M. (1998). DNA Double-stranded Breaks Induce Histone H2AX Phosphorylation on Serine 139. Journal of Biological Chemistry *273*, 5858–5868. https://doi.org/10.1074/jbc.273.10.5858.
85. Scully, R., and Xie, A. (2013). Double strand break repair functions of histone H2AX. Mutation Research/Fundamental and Molecular Mechanisms of Mutagenesis *750*, 5–14. https://doi.org/10.1016/j.mrfmmm.2013.07.007.
86. Chen, B.-R., Quinet, A., Byrum, A.K., Jackson, J., Berti, M., Thangavel, S., Bredemeyer, A.L., Hindi, I., Mosammaparast, N., Tyler, J.K., et al. (2019). XLF and H2AX function in series to promote replication fork

stability. Journal of Cell Biology *218*, 2113–2123. https://doi.org/10.1083/jcb.201808134.

87. Mailand, N., Bekker-Jensen, S., Faustrup, H., Melander, F., Bartek, J., Lukas, C., and Lukas, J. (2007). RNF8 Ubiquitylates Histones at DNA Double-Strand Breaks and Promotes Assembly of Repair Proteins. Cell *131*, 887–900. https://doi.org/10.1016/j.cell.2007.09.040.
88. Kolas, N.K., Chapman, J.R., Nakada, S., Ylanko, J., Chahwan, R., Sweeney, F.D., Panier, S., Mendez, M., Wildenhain, J., Thomson, T.M., et al. (2007). Orchestration of the DNA-Damage Response by the RNF8 Ubiquitin Ligase. Science (1979) *318*, 1637–1640. https://doi.org/10.1126/science.1150034.
89. Kim, H., Chen, J., and Yu, X. (2007). Ubiquitin-Binding Protein RAP80 Mediates BRCA1-Dependent DNA Damage Response. Science (1979) *316*, 1202–1205. https://doi.org/10.1126/science.1139621.
90. Sobhian, B., Shao, G., Lilli, D.R., Culhane, A.C., Moreau, L.A., Xia, B., Livingston, D.M., and Greenberg, R.A. (2007). RAP80 Targets BRCA1 to Specific Ubiquitin Structures at DNA Damage Sites. Science (1979) *316*, 1198–1202. https://doi.org/10.1126/science.1139516.
91. Wang, B., Matsuoka, S., Ballif, B.A., Zhang, D., Smogorzewska, A., Gygi, S.P., and Elledge, S.J. (2007). Abraxas and RAP80 Form a BRCA1 Protein Complex Required for the DNA Damage Response. Science (1979) *316*, 1194–1198. https://doi.org/10.1126/science.1139476.
92. Li, S., Chen, P.-L., Subramanian, T., Chinnadurai, G., Tomlinson, G., Osborne, C.K., Sharp, Z.D., and Lee, W.-H. (1999). Binding of CtIP to the BRCT Repeats of BRCA1 Involved in the Transcription Regulation of p21 Is Disrupted Upon DNA Damage. Journal of Biological

Chemistry *274*, 11334–11338. https://doi.org/10.1074/jbc.274.16.11334.
93. Yu, X., Wu, L.C., Bowcock, A.M., Aronheim, A., and Baer, R. (1998). The C-terminal (BRCT) Domains of BRCA1 Interact in Vivo with CtIP, a Protein Implicated in the CtBP Pathway of Transcriptional Repression. Journal of Biological Chemistry *273*, 25388–25392. https://doi.org/10.1074/jbc.273.39.25388.
94. Wong, A.K., Ormonde, P.A., Pero, R., Chen, Y., Lian, L., Salada, G., Berry, S., Lawrence, Q., Dayananth, P., Ha, P., et al. (1998). Characterization of a carboxy-terminal BRCA1 interacting protein. Oncogene *17*, 2279–2285. https://doi.org/10.1038/sj.onc.1202150.
95. Sartori, A.A., Lukas, C., Coates, J., Mistrik, M., Fu, S., Bartek, J., Baer, R., Lukas, J., and Jackson, S.P. (2007). Human CtIP promotes DNA end resection. Nature *450*, 509–514. https://doi.org/10.1038/nature06337.
96. Zhang, J., Willers, H., Feng, Z., Ghosh, J.C., Kim, S., Weaver, D.T., Chung, J.H., Powell, S.N., and Xia, F. (2004). Chk2 Phosphorylation of BRCA1 Regulates DNA Double-Strand Break Repair. Mol Cell Biol *24*, 708–718. https://doi.org/10.1128/MCB.24.2.708-718.2004.
97. Xia, B., Sheng, Q., Nakanishi, K., Ohashi, A., Wu, J., Christ, N., Liu, X., Jasin, M., Couch, F.J., and Livingston, D.M. (2006). Control of BRCA2 Cellular and Clinical Functions by a Nuclear Partner, PALB2. Mol Cell *22*, 719–729. https://doi.org/10.1016/j.molcel.2006.05.022.
98. Sy, S.M.H., Huen, M.S.Y., and Chen, J. (2009). PALB2 is an integral component of the BRCA complex required for homologous recombination repair. Proceedings of the National Academy of Sciences

106, 7155–7160. https://doi.org/10.1073/pnas.0811159106.
99. Davies, A.A., Masson, J.-Y., McIlwraith, M.J., Stasiak, A.Z., Stasiak, A., Venkitaraman, A.R., and West, S.C. (2001). Role of BRCA2 in Control of the RAD51 Recombination and DNA Repair Protein. Mol Cell *7*, 273–282. https://doi.org/10.1016/S1097-2765(01)00175-7.
100. Morrical, S.W. (2015). DNA-Pairing and Annealing Processes in Homologous Recombination and Homology-Directed Repair. Cold Spring Harb Perspect Biol *7*, a016444. https://doi.org/10.1101/cshperspect.a016444.
101. Huen, M.S.Y., Sy, S.M.H., and Chen, J. (2010). BRCA1 and its toolbox for the maintenance of genome integrity. Nat Rev Mol Cell Biol *11*, 138–148. https://doi.org/10.1038/nrm2831.
102. Wu-Baer, F., Lagrazon, K., Yuan, W., and Baer, R. (2003). The BRCA1/BARD1 Heterodimer Assembles Polyubiquitin Chains through an Unconventional Linkage Involving Lysine Residue K6 of Ubiquitin. Journal of Biological Chemistry *278*, 34743–34746. https://doi.org/10.1074/jbc.C300249200.
103. Reid, L.J., Shakya, R., Modi, A.P., Lokshin, M., Cheng, J.-T., Jasin, M., Baer, R., and Ludwig, T. (2008). E3 ligase activity of BRCA1 is not essential for mammalian cell viability or homology-directed repair of double-strand DNA breaks. Proceedings of the National Academy of Sciences *105*, 20876–20881. https://doi.org/10.1073/pnas.0811203106.
104. Nishikawa, H., Wu, W., Koike, A., Kojima, R., Gomi, H., Fukuda, M., and Ohta, T. (2009). BRCA1-Associated Protein 1 Interferes with BRCA1/BARD1 RING Heterodimer Activity. Cancer Res *69*, 111–119. https://doi.org/10.1158/0008-5472.CAN-08-3355.

105. Fabbro, M., Schuechner, S., Au, W.W.Y., and Henderson, B.R. (2004). BARD1 regulates BRCA1 apoptotic function by a mechanism involving nuclear retention. Exp Cell Res *298*, 661–673. https://doi.org/10.1016/j.yexcr.2004.05.004.
106. Cantor, S.B., Bell, D.W., Ganesan, S., Kass, E.M., Drapkin, R., Grossman, S., Wahrer, D.C.R., Sgroi, D.C., Lane, W.S., Haber, D.A., et al. (2001). BACH1, a Novel Helicase-like Protein, Interacts Directly with BRCA1 and Contributes to Its DNA Repair Function. Cell *105*, 149–160. https://doi.org/10.1016/S0092-8674(01)00304-X.
107. Litman, R., Peng, M., Jin, Z., Zhang, F., Zhang, J., Powell, S., Andreassen, P.R., and Cantor, S.B. (2005). BACH1 is critical for homologous recombination and appears to be the Fanconi anemia gene product FANCJ. Cancer Cell *8*, 255–265. https://doi.org/10.1016/j.ccr.2005.08.004.
108. Zhong, Q., Chen, C.-F., Chen, P.-L., and Lee, W.-H. (2002). BRCA1 Facilitates Microhomology-mediated End Joining of DNA Double Strand Breaks. Journal of Biological Chemistry *277*, 28641–28647. https://doi.org/10.1074/jbc.M200748200.
109. Jiang, G., Plo, I., Wang, T., Rahman, M., Cho, J.H., Yang, E., Lopez, B.S., and Xia, F. (2013). BRCA1-Ku80 Protein Interaction Enhances End-joining Fidelity of Chromosomal Double-strand Breaks in the G1 Phase of the Cell Cycle. Journal of Biological Chemistry *288*, 8966–8976. https://doi.org/10.1074/jbc.M112.412650.
110. Moynahan, M.E., Chiu, J.W., Koller, B.H., and Jasin, M. (1999). Brca1 Controls Homology-Directed DNA Repair. Mol Cell *4*, 511–518. https://doi.org/10.1016/S1097-2765(00)80202-6.

111. Snouwaert, J.N., Gowen, L.C., Latour, A.M., Mohn, A.R., Xiao, A., DiBiase, L., and Koller, B.H. (1999). BRCA1 deficient embryonic stem cells display a decreased homologous recombination frequency and an increased frequency of non-homologous recombination that is corrected by expression of a Brca1 transgene. Oncogene *18*, 7900–7907. https://doi.org/10.1038/sj.onc.1203334.
112. Wang, H., Zeng, Z.C., Bui, T.A., DiBiase, S.J., Qin, W., Xia, F., Powell, S.N., and Iliakis, G. (2001). Nonhomologous end-joining of ionizing radiation-induced DNA double-stranded breaks in human tumor cells deficient in BRCA1 or BRCA2. Cancer Res *61*, 270–277.
113. Roy, R., Chun, J., and Powell, S.N. (2012). BRCA1 and BRCA2: different roles in a common pathway of genome protection. Nat Rev Cancer *12*, 68–78. https://doi.org/10.1038/nrc3181.
114. Futreal, P.A., Liu, Q., Shattuck-Eidens, D., Cochran, C., Harshman, K., Tavtigian, S., Bennett, L.M., Haugen-Strano, A., Swensen, J., Miki, Y., et al. (1994). *BRCA1* Mutations in Primary Breast and Ovarian Carcinomas. Science (1979) *266*, 120–122. https://doi.org/10.1126/science.7939630.
115. King, M.-C., Marks, J.H., and Mandell, J.B. (2003). Breast and Ovarian Cancer Risks Due to Inherited Mutations in *BRCA1* and *BRCA2*. Science (1979) *302*, 643–646. https://doi.org/10.1126/science.1088759.
116. Metcalfe, K.A., Poll, A., Royer, R., Llacuachaqui, M., Tulman, A., Sun, P., and Narod, S.A. (2010). Screening for Founder Mutations in *BRCA1* and *BRCA2* in Unselected Jewish Women. Journal of Clinical Oncology *28*, 387–391. https://doi.org/10.1200/JCO.2009.25.0712.

117. Han, S.-A., and Kim, S.-W. (2021). BRCA and Breast Cancer-Related High-Penetrance Genes. In, pp. 473–490. https://doi.org/10.1007/978-981-32-9620-6_25.
118. Thompson, D., and Easton, D. (2004). The Genetic Epidemiology of Breast Cancer Genes. J Mammary Gland Biol Neoplasia *9*, 221–236. https://doi.org/10.1023/B:JOMG.0000048770.90334.3b.
119. Karami, F., and Mehdipour, P. (2013). A Comprehensive Focus on Global Spectrum of *BRCA1* and *BRCA2* Mutations in Breast Cancer. Biomed Res Int *2013*, 1–21. https://doi.org/10.1155/2013/928562.
120. Venkitaraman, A.R. (2002). Cancer Susceptibility and the Functions of BRCA1 and BRCA2. Cell *108*, 171–182. https://doi.org/10.1016/S0092-8674(02)00615-3.
121. Farmer, H., McCabe, N., Lord, C.J., Tutt, A.N.J., Johnson, D.A., Richardson, T.B., Santarosa, M., Dillon, K.J., Hickson, I., Knights, C., et al. (2005). Targeting the DNA repair defect in BRCA mutant cells as a therapeutic strategy. Nature *434*, 917–921. https://doi.org/10.1038/nature03445.
122. Dedes, K.J., Wilkerson, P.M., Wetterskog, D., Weigelt, B., Ashworth, A., and Reis-Filho, J.S. (2011). Synthetic lethality of PARP inhibition in cancers lacking *BRCA1* and *BRCA2* mutations. Cell Cycle *10*, 1192–1199. https://doi.org/10.4161/cc.10.8.15273.
123. Satoh, M.S., and Lindahl, T. (1992). Role of poly(ADP-ribose) formation in DNA repair. Nature *356*, 356–358. https://doi.org/10.1038/356356a0.
124. Bryant, H.E., Schultz, N., Thomas, H.D., Parker, K.M., Flower, D., Lopez, E., Kyle, S., Meuth, M., Curtin, N.J., and Helleday, T. (2005). Specific killing of BRCA2-deficient tumours with inhibitors of poly(ADP-ribose) polymerase. Nature *434*, 913–917. https://doi.org/10.1038/nature03443.

125. Shen, Y., Rehman, F.L., Feng, Y., Boshuizen, J., Bajrami, I., Elliott, R., Wang, B., Lord, C.J., Post, L.E., and Ashworth, A. (2013). BMN 673, a Novel and Highly Potent PARP1/2 Inhibitor for the Treatment of Human Cancers with DNA Repair Deficiency. Clinical Cancer Research *19*, 5003–5015. https://doi.org/10.1158/1078-0432.CCR-13-1391.
126. Lord, C.J., and Ashworth, A. (2017). PARP inhibitors: Synthetic lethality in the clinic. Science (1979) *355*, 1152–1158. https://doi.org/10.1126/science.aam7344.
127. Sun, M., Huang, F., Yu, D., Zhang, Y., Xu, H., Zhang, L., Li, L., Dong, L., Guo, L., and Wang, S. (2015). Autoregulatory loop between TGF-β1/miR-411-5p/SPRY4 and MAPK pathway in rhabdomyosarcoma modulates proliferation and differentiation. Cell Death Dis *6*, e1859–e1859. https://doi.org/10.1038/cddis.2015.225.
128. Egas-Bejar, D., and Huh, W.W. (2014). Rhabdomyosarcoma in adolescent and young adult patients: current perspectives. Adolesc Health Med Ther *5*, 115–125. https://doi.org/10.2147/AHMT.S44582.
129. Skapek, S.X., Ferrari, A., Gupta, A.A., Lupo, P.J., Butler, E., Shipley, J., Barr, F.G., and Hawkins, D.S. (2019). Rhabdomyosarcoma. Nat Rev Dis Primers *5*, 1. https://doi.org/10.1038/s41572-018-0051-2.
130. Hartley, A.L., Birch, J.M., Marsden, H.B., Harris, M., and Blair, V. (1988). Neurofibromatosis in children with soft tissue sarcoma. Pediatr Hematol Oncol *5*. https://doi.org/10.3109/08880018809031246.
131. Li, F.P., and Fraumeni, J.F. (1969). Soft-tissue sarcomas, breast cancer, and other neoplasms. A familial syndrome? Ann Intern Med *71*, 747–752. https://doi.org/10.7326/0003-4819-71-4-747.

132. Breneman, J.C., Lyden, E., Pappo, A.S., Link, M.P., Anderson, J.R., Parham, D.M., Qualman, S.J., Wharam, M.D., Donaldson, S.S., Maurer, H.M., et al. (2003). Prognostic factors and clinical outcomes in children and adolescents with metastatic rhabdomyosarcoma-a report from the intergroup rhabdomyosarcoma study IV. Journal of Clinical Oncology. https://doi.org/10.1200/JCO.2003.06.129.
133. Kashi, V.P., Hatley, M.E., and Galindo, R.L. (2015). Probing for a deeper understanding of rhabdomyosarcoma: Insights from complementary model systems. Preprint, https://doi.org/10.1038/nrc3961 https://doi.org/10.1038/nrc3961.
134. Xia, S.J., Pressey, J.G., and Barr, F.G. (2002). Molecular Pathogenesis of Rhabdomyosarcoma. Cancer Biol Ther *1*, 97–104. https://doi.org/10.4161/cbt.51.
135. Bajard, L., Relaix, F., Lagha, M., Rocancourt, D., Daubas, P., and Buckingham, M.E. (2006). A novel genetic hierarchy functions during hypaxial myogenesis: Pax3 directly activates Myf5 in muscle progenitor cells in the limb. Genes Dev. https://doi.org/10.1101/gad.382806.
136. O-Sullivan, I., Zhang, W., Wasserman, D.H., Liew, C.W., Liu, J., Paik, J., Depinho, R.A., Stolz, D.B., Kahn, C.R., Schwartz, M.W., et al. (2015). FoxO1 integrates direct and indirect effects of insulin on hepatic glucose production and glucose utilization. Nat Commun *6*, 7079. https://doi.org/10.1038/ncomms8079.
137. Barr, F.G. (2001). Gene fusions involving PAX and FOX family members in alveolar rhabdomyosarcoma. Preprint, https://doi.org/10.1038/sj.onc.1204599 https://doi.org/10.1038/sj.onc.1204599.

138. Sun, X., Guo, W., Shen, J.K., Mankin, H.J., Hornicek, F.J., and Duan, Z. (2015). Rhabdomyosarcoma: Advances in Molecular and Cellular Biology. Sarcoma *2015*, 1–14. https://doi.org/10.1155/2015/232010.
139. Panda, S.P., Chinnaswamy, G., Vora, T., Prasad, M., Bansal, D., Kapoor, G., Radhakrishnan, V., Agarwala, S., Laskar, S., Arora, B., et al. (2017). Diagnosis and Management of Rhabdomyosarcoma in Children and Adolescents: ICMR Consensus Document. The Indian Journal of Pediatrics *84*. https://doi.org/10.1007/s12098-017-2315-3.
140. Zarrabi, A., Perrin, D., Kavoosi, M., Sommer, M., Sezen, S., Mehrbod, P., Bhushan, B., Machaj, F., Rosik, J., Kawalec, P., et al. (2023). Rhabdomyosarcoma: Current Therapy, Challenges, and Future Approaches to Treatment Strategies. Cancers (Basel) *15*, 5269. https://doi.org/10.3390/cancers15215269.
141. van der Graaf, W.T.A., Orbach, D., Judson, I.R., and Ferrari, A. (2017). Soft tissue sarcomas in adolescents and young adults: a comparison with their paediatric and adult counterparts. Lancet Oncol *18*, e166–e175. https://doi.org/10.1016/S1470-2045(17)30099-2.
142. El Demellawy, D., McGowan-Jordan, J., de Nanassy, J., Chernetsova, E., and Nasr, A. (2017). Update on molecular findings in rhabdomyosarcoma. Pathology *49*, 238–246. https://doi.org/10.1016/j.pathol.2016.12.345.
143. Erp, A.E.M. Van, Versleijen-Jonkers, Y.M.H., Graaf, W.T.A. Van Der, and Fleuren, E.D.G. (2018). Targeted therapy-based combination treatment in rhabdomyosarcoma. Preprint, https://doi.org/10.1158/1535-7163.MCT-17-1131 https://doi.org/10.1158/1535-7163.MCT-17-1131.

144. Zheng, Q., Bao, C., Guo, W., Li, S., Chen, J., Chen, B., Luo, Y., Lyu, D., Li, Y., Shi, G., et al. (2016). Circular RNA profiling reveals an abundant circHIPK3 that regulates cell growth by sponging multiple miRNAs. Nat Commun *7*, 11215. https://doi.org/10.1038/ncomms11215.
145. Li, Y., Zheng, F., Xiao, X., Xie, F., Tao, D., Huang, C., Liu, D., Wang, M., Wang, L., Zeng, F., et al. (2017). Circ <scp>HIPK</scp> 3 sponges miR-558 to suppress heparanase expression in bladder cancer cells. EMBO Rep *18*, 1646–1659. https://doi.org/10.15252/embr.201643581.
146. Chen, G., Shi, Y., Liu, M., and Sun, J. (2018). circHIPK3 regulates cell proliferation and migration by sponging miR-124 and regulating AQP3 expression in hepatocellular carcinoma. Cell Death Dis *9*, 175. https://doi.org/10.1038/s41419-017-0204-3.
147. Dattilo, D., Timoteo, G. Di, Setti, A., Giuliani, A., Peruzzi, G., Nebot, M.B., Centrón-Broco, A., Mariani, D., Mozzetta, C., and Bozzoni, I. (2023). The m6A reader YTHDC1 and the RNA helicase DDX5 control the production of rhabdomyosarcoma-enriched circRNAs. Nat Commun *14*, 1898. https://doi.org/10.1038/s41467-023-37578-7.
148. Calvet, J.P., and Pederson, T. (1981). Base-pairing interactions between small nuclear RNAs and nuclear RNA precursors as revealed by psoralen cross-linking in vivo. Cell *26*, 363–370. https://doi.org/10.1016/0092-8674(81)90205-1.
149. Mann, M., Wright, P.R., and Backofen, R. (2017). IntaRNA 2.0: Enhanced and customizable prediction of RNA-RNA interactions. Nucleic Acids Res. https://doi.org/10.1093/nar/gkx279.
150. Bellucci, M., Agostini, F., Masin, M., and Tartaglia, G.G. (2011). Predicting protein associations with long

noncoding RNAs. Nat Methods *8*, 444–445. https://doi.org/10.1038/nmeth.1611.
151. Li, Z. (2001). The fragile X mental retardation protein inhibits translation via interacting with mRNA. Nucleic Acids Res *29*, 2276–2283. https://doi.org/10.1093/nar/29.11.2276.
152. Ascano, M., Mukherjee, N., Bandaru, P., Miller, J.B., Nusbaum, J.D., Corcoran, D.L., Langlois, C., Munschauer, M., Dewell, S., Hafner, M., et al. (2012). FMRP targets distinct mRNA sequence elements to regulate protein expression. Nature *492*, 382–386. https://doi.org/10.1038/nature11737.
153. Liu, X.S., Wu, H., Krzisch, M., Wu, X., Graef, J., Muffat, J., Hnisz, D., Li, C.H., Yuan, B., Xu, C., et al. (2018). Rescue of Fragile X Syndrome Neurons by DNA Methylation Editing of the FMR1 Gene. Cell *172*, 979-992.e6. https://doi.org/10.1016/j.cell.2018.01.012.
154. Nostrand, E.L. Van, Freese, P., Pratt, G.A., Wang, X., Wei, X., Xiao, R., Blue, S.M., Chen, J.-Y., Cody, N.A.L., Dominguez, D., et al. (2020). A large-scale binding and functional map of human RNA-binding proteins. Nature *583*, 711–719. https://doi.org/10.1038/s41586-020-2077-3.
155. Liu, C.-X., Guo, S.-K., Nan, F., Xu, Y.-F., Yang, L., and Chen, L.-L. (2022). RNA circles with minimized immunogenicity as potent PKR inhibitors. Mol Cell *82*, 420-434.e6. https://doi.org/10.1016/j.molcel.2021.11.019.
156. Lu, Z., Gong, J., and Zhang, Q.C. (2018). PARIS: Psoralen Analysis of RNA Interactions and Structures with High Throughput and Resolution. In, pp. 59–84. https://doi.org/10.1007/978-1-4939-7213-5_4.
157. Ziv, O., Gabryelska, M.M., Lun, A.T.L., Gebert, L.F.R., Sheu-Gruttadauria, J., Meredith, L.W., Liu, Z.-Y., Kwok, C.K., Qin, C.-F., MacRae, I.J., et al. (2018).

COMRADES determines in vivo RNA structures and interactions. Nat Methods *15*, 785–788. https://doi.org/10.1038/s41592-018-0121-0.
158. Keene, J.D., Komisarow, J.M., and Friedersdorf, M.B. (2006). RIP-Chip: The isolation and identification of mRNAs, microRNAs and protein components of ribonucleoprotein complexes from cell extracts. Nat Protoc *1*, 302–307. https://doi.org/10.1038/nprot.2006.47.
159. Beltran, M., Tavares, M., Justin, N., Khandelwal, G., Ambrose, J., Foster, B.M., Worlock, K.B., Tvardovskiy, A., Kunzelmann, S., Herrero, J., et al. (2019). G-tract RNA removes Polycomb repressive complex 2 from genes. Nat Struct Mol Biol *26*. https://doi.org/10.1038/s41594-019-0293-z.
160. Olive, P.L., and Banáth, J.P. (2006). The comet assay: A method to measure DNA damage in individual cells. Nat Protoc *1*, 23–29. https://doi.org/10.1038/nprot.2006.5.
161. Martin, M. (2011). Cutadapt removes adapter sequences from high-throughput sequencing reads. EMBnet J *17*, 10. https://doi.org/10.14806/ej.17.1.200.
162. Langmead, B., and Salzberg, S.L. (2012). Fast gapped-read alignment with Bowtie 2. Nat Methods *9*, 357–359. https://doi.org/10.1038/nmeth.1923.
163. Dobin, A., Davis, C.A., Schlesinger, F., Drenkow, J., Zaleski, C., Jha, S., Batut, P., Chaisson, M., and Gingeras, T.R. (2013). STAR: ultrafast universal RNA-seq aligner. Bioinformatics *29*, 15–21. https://doi.org/10.1093/bioinformatics/bts635.
164. Barnett, D.W., Garrison, E.K., Quinlan, A.R., Strömberg, M.P., and Marth, G.T. (2011). BamTools: a C++ API and toolkit for analyzing and managing BAM files. Bioinformatics *27*, 1691–1692. https://doi.org/10.1093/bioinformatics/btr174.

165. Li, H., Handsaker, B., Wysoker, A., Fennell, T., Ruan, J., Homer, N., Marth, G., Abecasis, G., and Durbin, R. (2009). The Sequence Alignment/Map format and SAMtools. Bioinformatics *25*, 2078–2079. https://doi.org/10.1093/bioinformatics/btp352.
166. Anders, S., Pyl, P.T., and Huber, W. (2015). HTSeq—a Python framework to work with high-throughput sequencing data. Bioinformatics *31*, 166–169. https://doi.org/10.1093/bioinformatics/btu638.
167. Yates, A.D., Achuthan, P., Akanni, W., Allen, J., Allen, J., Alvarez-Jarreta, J., Amode, M.R., Armean, I.M., Azov, A.G., Bennett, R., et al. (2019). Ensembl 2020. Nucleic Acids Res. https://doi.org/10.1093/nar/gkz966.
168. Robinson, M.D., McCarthy, D.J., and Smyth, G.K. (2009). edgeR: A Bioconductor package for differential expression analysis of digital gene expression data. Bioinformatics *26*, 139–140. https://doi.org/10.1093/bioinformatics/btp616.
169. Potla, P., Ali, S.A., and Kapoor, M. (2021). A bioinformatics approach to microRNA-sequencing analysis. Osteoarthr Cartil Open *3*, 100131. https://doi.org/10.1016/j.ocarto.2020.100131.
170. Kozomara, A., Birgaoanu, M., and Griffiths-Jones, S. (2019). miRBase: from microRNA sequences to function. Nucleic Acids Res *47*, D155–D162. https://doi.org/10.1093/nar/gky1141.
171. Tarazona, S., Furió-Tarí, P., Turrà, D., Pietro, A. Di, Nueda, M.J., Ferrer, A., and Conesa, A. (2015). Data quality aware analysis of differential expression in RNA-seq with NOISeq R/Bioc package. Nucleic Acids Res, gkv711. https://doi.org/10.1093/nar/gkv711.

LIST OF PUBLICATIONS

BRCA1 levels and DNA damage response are controlled by the competitive binding of circHIPK3 or FMRP to the BRCA1 mRNA – Molecular Cell, 2024
Chiara Grelloni, Raffaele Garraffo, Adriano Setti, Francesca Rossi, Giovanna Peruzzi, Mario Cinquanta, Maria Carmela Di Rosa, Marco Alessandro Pierotti, Manuel Beltran Nebot †, Irene Bozzoni †.

CircAFF1 is a Circular RNA with a role in alveolar rhabdomyosarcoma cell migration – Biomedicines, 2023
Alvaro Centron Broco †, Francesca Rossi †, Chiara Grelloni, Raffaele Garraffo, DarioDattilo, Andrea Giuliani, Gaia di Timoteo, Alessio Colantoni, Irene Bozzoni, Manuel Beltran Nebot

Circular RNA ZNF609/CKAP5 mRNA interaction regulates microtubule dynamics and tumorigenicity - Molecular Cell, 2022
Francesca Rossi †, Manuel Beltran Nebot †, Michela Damizia, Chiara Grelloni, Adriano Setti, Gaia di Timoteo, Dario Dattilo, Alvaro Centron Broco, Carmine Nicoletti, Irene Bozzoni